

An Investigation of Hadron Mass Calculations in Lattice QCD

Sara Collins

Doctor of Philosophy
University of Edinburgh
1993



To my family and friends

Abstract

In this thesis I study Quantum Chromodynamics on the lattice. This formulation of QCD allows for a first-principles calculation of the hadron mass spectrum. Comprehensive agreement with experiment has yet to be achieved, and this is due in part to the difficulties of isolating the ground state mass from the spectrum of excited states created using an interpolating field on the lattice.

In the first chapter, after briefly introducing the standard Wilson action for lattice QCD, and the improved clover action with reduced discretisations errors, the standard techniques for extracting hadron masses are reviewed. In the second chapter I present two new methods for the extraction of hadron masses using a combination of two operators with the same quantum numbers to isolate the ground and first excited states. I apply these two methods to the low-lying hadron states and compare the results with existing methods for extracting the first excited state.

Conventionally the Wilson and clover actions are assumed to be inappropriate for the simulation of hadrons containing one or more quarks with Compton wavelengths shorter than twice the lattice spacing. The discretisation errors for both actions are expected to diverge in this limit. In chapter three I discuss a proposal that actions of this type are suitable for non-relativistic QCD. This proposal suggests a continuum non-relativistic dispersion relation for hadrons containing heavy quarks, parameterised by two mass scales. A dispersion relation of this form is tested against the finite-momentum behaviour of the pseudoscalar mesons containing one or more heavy quarks. The effects of using the different mass parameters to fix the physical quark mass on the predictions for the pseudoscalar and vector decay constants are studied, and this analysis is extended to the mass splittings in the mesons containing one or more heavy quarks in chapter four.

Declaration

This thesis has been wholly composed by me and contains my own work carried out as a member of the UKQCD Collaboration. The study in Chapter 2 was performed with the initial guidance of David Richards, while Jim Simone and Richard Kenway provided guidance in the work presented in Chapter 3. The codes written by Jim Simone formed the foundations of the analysis routines used throughout this thesis.

Some of the material in Chapter 2 has been published in

- UKQCD Collaboration, C. R. Allton et al. Phys. Rev. **D47** (1993) 5128
- S. Collins, Nuc. Phys. **B(Proc. Suppl.)30** (1993) 393

Other related work to which I have contributed includes

- UKQCD Collaboration, C. R. Allton et al. Phys. Lett. **B284** (1992) 377
- UKQCD Collaboration, C. R. Allton et al. Nucl. Phys. **B(Proc. Suppl.)26** (1992) 211
- UKQCD Collaboration, C. R. Allton et al. Nucl. Phys. **B** to be published

Sara Collins

Acknowledgements

First of all I would like to thank Ken Bowler, Richard Kenway and Brian Pendleton for their encouragement and guidance, particularly in the final panic stricken stages of finishing this thesis. I am grateful to David Richards, David Henty and Jim Simone for many invaluable discussions and careful reading of this thesis. I have also enjoyed sharing an office with Barry Wilkes and Robert Baxter over the past three years.

I am indebted to Miles Bader for chiseling away at my prose style until it reached a semi-respectable form, and to my friends Almuth, David, Emily, Gerry, Neeraj, Rachel and Zöe for their good company and support, which gave me the courage to finish this thesis.

Finally, my deepest thanks must go to my family for their patience and understanding over the last few months.

*There is no mark on the wall with
which to measure the height of women.*

Virginia Woolf, 1950

Contents

Abstract	ii
Declaration	iii
Acknowledgements	iv
1 Lattice QCD	1
1.1 Introduction	1
1.2 The Lattice Formulation of QCD	2
1.2.1 The Wilson Action	3
1.2.2 The Clover Action	4
1.2.3 Mean-Field Improvement	5
1.3 Numerical Simulation	7
1.4 Hadron Operators	9

1.5	Correlation Functions and Masses	10
1.6	Extracting Mass Estimates	11
1.6.1	Effective Mass	12
1.6.2	Correlated fits	13
1.6.3	Error Estimation	14
1.6.4	Fitting Procedure	15
2	Multistate Techniques Applied to the Light Hadron Spectrum	16
2.1	Motivation	17
2.2	Multistate Methods	19
2.2.1	Transfer Matrix	20
2.2.2	Matrix of Correlators	21
2.3	Propagators and Smearing	22
2.4	Results for Smeared Correlators	24
2.4.1	Results for the First Excited State from $C(t)$	25
2.4.2	Results for the Ground State	27
2.5	Subtraction Fit	30

2.5.1	Obtaining estimates for A and m from $c_{ij}(t)$	32
2.5.2	Results from the Subtraction Fit Method	35
2.6	Multiple Local Operators on the Lattice	40
2.7	Results for Local-Local Correlators	40
2.7.1	Results for the Ground and First Excited State from $C(t)$	41
2.8	Results from the Subtraction Fit Method	41
2.8.1	Extracting the Masses and Amplitudes of the Ground States	42
2.8.2	Results for the clover action	43
2.9	Summary of Results for the Ground State	46
2.10	Summary of Results for the First Excited State	48
3	Heavy Quark Physics at Finite Momentum	52
3.1	Motivation	53
3.2	Theoretical Toys for Non-Zero Momentum	54
3.3	Computational Details	58
3.4	Fitting Ranges	60
3.5	Results	62

3.5.1	A Comparison with the Continuum Dispersion Relation . .	62
3.5.2	Estimating the Dynamical Mass	64
3.5.3	A Comparison with the Nonrelativistic Dispersion Relation	69
3.6	Summary	75
3.7	Determination of the Quark Masses	76
3.8	Renormalisation Constants: Z_A and Z_V	79
3.9	Setting the Physical Scale	80
3.10	Decay Constants From Zero- and Finite-Momentum Propagators .	82
3.10.1	Pseudoscalar Decay Constant	82
3.10.2	Results for the Pseudoscalar Decay Constant	84
3.10.3	Summary of Pseudoscalar Decay Constant Results	95
3.10.4	Vector Decay Constant	96
3.10.5	Results for the Vector Decay Constant	99
3.11	Conclusions	103
4	Mass Splittings in Heavy-Quark Systems	107
4.1	Theoretical Predictions	108

4.1.1	Heavy-Light Mesons: Chiral Heavy Quark Effective Theory	108
4.1.2	Heavy-Heavy Mesons: Potential Models	113
4.1.3	The Effect of Quenching on the Hyperfine Splitting	116
4.2	Computational Details and Fitting Procedure	117
4.3	Results for the Hyperfine Splitting in Heavy-Heavy Mesons	119
4.4	Results for Heavy-Light Mesons	126
4.4.1	The Hyperfine Splitting	126
4.4.2	The s-d Splittings	132
4.4.3	The $s - d$ Hyperfine Splitting	134
4.5	Conclusions	136
5	Summary, Conclusions and Future Prospects	139
	Bibliography	142

Chapter 1

Lattice QCD

This chapter presents a brief overview of the lattice formulation of Quantum Chromodynamics (QCD), leading from the discretisation of the QCD action to the extraction of physical quantities.

1.1 Introduction

QCD is the gauge theory of the interactions of quarks and gluons, the constituents of hadronic matter. The asymptotic freedom property of QCD, which means that the coupling between quarks and gluons is small for small quark separations, has led to highly successful quantitative perturbative calculations of high energy phenomena. However, at intermediate and low energy scales the coupling is $O(1)$, and hence many of the fundamental properties of hadrons, such as the mass spectrum, are inaccessible in perturbation theory. Thus, a non-perturbative treatment of QCD is required and lattice QCD provides the only possible framework at present.

In lattice QCD, the gauge theory is formulated on a discrete lattice of points in Euclidean space-time. Regularising QCD in this manner, quantum averages are

given by mathematically well-defined expressions, at all values of the coupling. In addition, this approach allows for a closer analogy with a statistical mechanics system, and the use of all the calculational techniques developed therein, such as the powerful Monte Carlo technique. Considerable freedom exists in the choice of lattice action, since, a priori, the only requirement is that it reproduces the correct classical expression in the naïve continuum limit. Thus, the lattice action can be systematically improved through the addition of extra terms proportional to powers of the lattice spacing.

In recent years, lattice QCD has begun to enter the mainstream of particle physics and I shall only present elements of the subject here. More detailed reviews are contained in references [1, 2, 3]

1.2 The Lattice Formulation of QCD

The action for QCD in the continuum is

$$S = \int d^4x \frac{1}{4} F_{\nu\mu} F_{\nu\mu} + \bar{\psi}(\not{D} + m)\psi \quad (1.1)$$

where ψ , $\bar{\psi}$ are the fermionic quark fields and $F_{\nu\mu}$ is the gluon field strength tensor.

In a lattice formulation of QCD, the fermion fields are only defined on the lattice sites. The representation chosen for the gauge fields, $A_\mu(x)$, is determined by the requirement that gauge invariance be preserved. In the continuum, in order to construct a gauge-invariant scalar product from fields $\bar{\psi}(y)$ and $\psi(z)$, the field $\psi(z)$ must undergo parallel transport from point z to point y using the operator,

$$U_\mu(y) = \mathcal{P} e^{ig \int_y^z A_\mu dx_\mu} \quad (1.2)$$

Thus, the quantity

$$\bar{\psi}(y) U_\mu(y) \psi(z) \quad (1.3)$$

is gauge-invariant. This suggests that on the lattice the gauge fields should be associated with the links between neighbouring lattice sites, and thus the gauge variable,

$$U_\mu(x) = \exp(iagA_\mu(x + \frac{\hat{\mu}}{2})) \in SU(3) \quad (1.4)$$

is used to represent the link from site x in direction μ .

There are two types of gauge-invariant object which can be constructed on the lattice: a product of gauge links connecting a fermion and an antifermion, the simplest of which is (1.3), and a product of links around a closed loop, the smallest of which is the plaquette

$$U_\mu^{\square} = U_\mu(x)U_\nu(x + \hat{\mu})U_\mu^\dagger(x + \hat{\nu})U_\nu^\dagger(x), \quad (1.5)$$

where a is set to 1.

1.2.1 The Wilson Action

Thus, using these building blocks, it is possible to construct a lattice QCD action. The gluonic term in the lattice action poses no problems and is defined as [4]

$$S_G = -\beta \sum_x \sum_{\nu, \mu > \nu} \text{ReTr} [U_{\mu\nu}^{\square}(x)] \quad (1.6)$$

where $\beta \equiv 6/g^2$. For the fermionic part, however, the naïve choice of

$$S_F = \sum_x \left\{ \sum_\mu \frac{1}{2} (\bar{\psi}(x) \gamma_\mu(x) U_\mu(x - \hat{\mu}) \psi(x - \hat{\mu}) - \bar{\psi}(x) U_\mu(x) \gamma_\mu \psi(x + \hat{\mu})) \right. \\ \left. + m \bar{\psi}(x) \psi(x) \right\} \quad (1.7)$$

obtained by replacing the covariant derivative in (1.1) by a finite difference, defines a theory whose continuum limit contains 2^4 fermions; this is known as species doubling. As noted above the lattice action is not unique, and an extra term can

be added which gives $2^4 - 1$ of the fermions, masses proportional to a^{-1} ; this was the approach suggested by Wilson [5]. The resulting action is

$$S_{WF} = \sum_x \left\{ \sum_{\mu=0}^3 \bar{\psi}(x) \frac{1}{2} \left[U_{\mu}(x)(r - \gamma_{\mu})\psi(x + \hat{\mu}) + U_{\mu}^{\dagger}(x - \hat{\mu})(r + \gamma_{\mu})\psi(x - \hat{\mu}) \right] + (m + 4r)\bar{\psi}(x)\psi(x) \right\}. \quad (1.8)$$

r is now set to 1.

A more common parameterisation of the Wilson fermion action is in terms of the hopping parameter, κ ,

$$S_{WF} = \frac{1}{2\kappa} \bar{\psi}(x) \mathcal{M}_{WF}(x, y) \psi(y) \quad (1.9)$$

where the Wilson fermion matrix $\mathcal{M}_{WF}(x, y)$ is defined as

$$\mathcal{M}_{WF}(x, y) = \delta(x, y) - \kappa \mathcal{D}(x, y) \quad (1.10)$$

and

$$\mathcal{D}(x, y) \equiv \sum_{\mu} \left(U_{\mu}(x)(1 - \gamma_{\mu})\delta(x + \hat{\mu}, y) + U_{\mu}^{\dagger}(x - \hat{\mu})(1 + \gamma_{\mu})\delta(x - \hat{\mu}, y) \right). \quad (1.11)$$

The bare quark mass is defined as

$$m = \frac{1}{2} \left(\frac{1}{\kappa} - \frac{1}{\kappa_{crit}} \right), \quad (1.12)$$

where κ_{crit} is the value of the hopping parameter corresponding to zero quark mass. In the limit where the fermions are asymptotically free $\kappa_{crit} = 1/(8r)$.

1.2.2 The Clover Action

For lattice spacing a , S_{WF} differs from the fermionic term in the continuum action by a term of $O(a)$, while S_G differs by terms of $O(a^2)$. Although in the continuum

limit these corrections should not matter, from current numerical simulations there is some evidence that it affects the results. Since the major discretisation error comes from the fermions, attempts to reduce this error have concentrated on improving the fermion action. The prescription for removing $O(a)$ effects proposed by Heatlie [6] is considered here. The fermion fields are rotated:

$$\begin{aligned}\psi &\rightarrow \psi' = \left(1 - \frac{1}{4}(\gamma \cdot \vec{D} - m)\right) \psi \\ \bar{\psi} &\rightarrow \bar{\psi}' = \bar{\psi} \left(1 - \frac{1}{4}(\gamma \cdot \vec{D} + m)\right) \psi\end{aligned}\quad (1.13)$$

and an extra term, ΔS , originally proposed by Sheikholeslami and Wohlert [7],

$$\Delta S = -ic \frac{g}{2} \sum_x \sum_{\mu, \nu} \bar{\psi}(x) F_{\mu\nu} \sigma_{\mu\nu} \psi(x) \quad (1.14)$$

is added to the fermion action (dubbed the clover or S-W action):

$$S_C = S_F + \Delta S \quad (1.15)$$

In equation (1.14) $F_{\mu\nu}$ is the lattice definition of the field strength tensor,

$$F_{\mu\nu} = \frac{1}{4} \sum_j \frac{1}{2gi} [U_j^\square - U_j^{\square\dagger}] \quad (1.16)$$

and the sum is over the 4-plaquettes in the $\mu\nu$ -plane around site x . In the following, the term ‘the general Wilson action’ will be used when referring to both the clover and Wilson actions. Heatlie et al. demonstrated the absence of leading logarithmic terms at n^{th} order in perturbation theory, in matrix elements of operators rotated according to (1.13). These terms are of the form $g^{2n} a \ln^n a$, and hence effectively $O(a)$ in the weak coupling regime.

1.2.3 Mean-Field Improvement

Lepage and Mackenzie [8] have suggested that, without rotating the operators, loop $O(a)$ effects can be removed by a suitable choice of c and a rescaling of the

fermion fields. These authors have attempted to calculate the value of c using mean field theory. They observed that in lattice perturbation theory, tadpole graphs spoil the relation between the lattice and continuum gauge field:

$$U_\mu = e^{igaA_\mu(x)} \rightarrow 1 + igaA_\mu(x) \quad (1.17)$$

The average link is considerably smaller than one, and this suggests an alternative expansion

$$U_\mu \rightarrow u_0(1 + igaA_\mu(x)) \quad (1.18)$$

about the average link, u_0 . Lepage and Mackenzie argue that U_μ/u_0 is a better approximation to the continuum field, and hence the lattice action,

$$\tilde{S}_G = \sum \frac{1}{\tilde{g}^2 u_0^4} \text{Tr} U^\square \quad (1.19)$$

will approximate continuum behaviour more closely than S_G . It is only necessary to rescale the coupling,

$$g \rightarrow \tilde{g} = g^2/u_0^4 \quad (1.20)$$

in order to obtain \tilde{S}_G from S_G . The same consideration of the fermion action leads to

$$c \rightarrow \tilde{c} = c/u_0^3, \quad \kappa \rightarrow \tilde{\kappa} = \kappa u_0 \quad (1.21)$$

u_0 can be defined in a number of ways; most commonly, either $u_0 = (\frac{1}{3}\langle U^\square \rangle)^{\frac{1}{4}}$ or $u_0 = 1/(8\kappa_{crit})$ is used.

Furthermore, these authors assert that the correct normalisation of the fermion fields for κ away from κ_{crit} , i.e. for heavy quark masses, is $\sqrt{1 - 6\kappa}$ rather than the conventional $\sqrt{2\kappa}$ [8, 9, 10]. Combined with the mean-field improvement, this becomes $\sqrt{1 - 6\tilde{\kappa}}$ (referred to here as the mean-field heavy-quark normalisation).

1.3 Numerical Simulation

Having defined QCD on a lattice, we can proceed to the calculation of physical quantities. In lattice QCD, as in any field theory, this involves the calculation of the expectation value of some operator. In the path integral formalism the expectation value of an operator, \mathcal{O} , is

$$\langle \mathcal{O} \rangle = \frac{1}{Z} \int \mathcal{D}\bar{\psi} \mathcal{D}\psi \mathcal{D}U \mathcal{O} e^{-\bar{\psi} \mathcal{M} \psi - S_G} \quad (1.22)$$

where Z is the partition function and \mathcal{M} represents the fermion matrix. The most fundamental quantity to consider is quark propagator, $G(x, y)$, for which $\mathcal{O} = \psi(x)\bar{\psi}(y)$ and

$$G(x, y) = \langle \psi(x)\bar{\psi}(y) \rangle \quad (1.23)$$

$$= \frac{1}{Z} \int \mathcal{D}\bar{\psi} \mathcal{D}\psi U \psi(x)\bar{\psi}(y) e^{-\bar{\psi} \mathcal{M} \psi - S_G} \quad (1.24)$$

The integration over the fermion fields can be done analytically to give

$$G(x, y) = \frac{1}{Z} \int \mathcal{D}\bar{\psi} \mathcal{D}\psi \mathcal{D}U \mathcal{M}^{-1}(x, y) \det \mathcal{M} e^{-S_G} \quad (1.25)$$

In order to evaluate this numerically, a method of generating a representative ensemble of field configurations, $\{U^{(i)}, i = 1 \dots N_{conf}\}$ where N_{conf} is the number of configurations, is required. This is done using importance sampling, where the configurations are generated with the probability

$$\mathcal{D}U \det \mathcal{M} e^{-S_G}; \quad (1.26)$$

$G(x, y)$ is then approximated by

$$\frac{1}{N_{conf}} \sum_{i=1}^{N_{conf}} G(x, y; U^{(i)}) \quad (1.27)$$

where $G(x, y; U^{(i)})$ is the quark propagator evaluated on the i 'th configuration. Since the fermion matrix is a highly non-local object, the generation of gauge configurations using (1.26) is prohibitively expensive for the computational resources

available for most lattice QCD calculations. The simplest way to overcome this problem, and the one used here, is to set $\det \mathcal{M} = 1$. This is known as the quenched approximation and corresponds to the omission of internal fermion loops. There is little physical justification for this approximation, and it may introduce a significant systematic error in the predictions for physical quantities, and in particular, those quantities which are sensitive to short distance effects; this is discussed in Chapter 4.

From (1.25), in order to obtain $G(x, y; U^{(i)})$ it is necessary to invert the fermion matrix, and this can be done by solving equations of the form,

$$\mathcal{M}(x, y)G(y, 0) = \eta(x, 0), \quad (1.28)$$

where $\eta(x, 0)$ is a source function. In this work, both point and spatially-extended functions are used; the latter are called “smeared” sources and will be discussed in Chapter 2.

The gauge configurations and quark propagators used in this thesis were produced as part of the UKQCD project on the 64-node i860 Meiko Computing Surface at the University of Edinburgh. The $SU(3)$ gauge fields were generated using the Hybrid Over-Relaxed algorithm, detailed in reference [13]. The Over-Relaxed Minimal Residual algorithm with red-black preconditioning was used to solve (1.28); a detailed study of this algorithm is contained in reference [14].

The following sections will show that by computing the quark propagator it is possible to construct the correlators of hadron operators, and hence investigate the properties of lattice hadrons.

1.4 Hadron Operators

Consider the hadron correlator

$$c(\vec{x}, t) = \langle 0 | \mathcal{O}(x) \mathcal{O}^\dagger(0) | 0 \rangle \quad (1.29)$$

where \mathcal{O} is the generic hadron operator. For mesons this operator has the form

$$\mathcal{O}_M(x) = \bar{\psi}(x) \Gamma \psi(x) \quad (1.30)$$

and Γ can be any one of the 16 linearly independent γ -matrix combinations. By inserting (1.30), the correlator becomes

$$c(\vec{x}, t) = \langle 0 | \bar{\psi}_\alpha^i(x) \Gamma^{ij} \psi_\alpha^j(x) \bar{\psi}_\beta^k(0) \Gamma^{\dagger kl} \psi_\beta^l(0) | 0 \rangle \quad (1.31)$$

where i, j are spin indices and α, β are colour indices. Performing the Wick decomposition gives

$$c(\vec{x}, t) = \Gamma^{ij} \Gamma^{\dagger kl} \langle 0 | \bar{\psi}_\alpha^i(x) \psi_\beta^l(0) | 0 \rangle \langle 0 | \psi_\alpha^j(x) \bar{\psi}_\beta^k(0) | 0 \rangle \quad (1.32)$$

$$= \Gamma^{ij} \Gamma^{\dagger kl} G_{\beta\alpha}^{li}(0, x) G_{\alpha\beta}^{jk}(x, 0) \quad (1.33)$$

From the lattice Dirac equation

$$G_{\beta\alpha}^{li}(0, x) = (\gamma_5)^{lm} G_{\beta\alpha}^{\dagger mn}(0, x) (\gamma_5)^{ni} \quad (1.34)$$

and hence

$$c(\vec{x}, t) = \text{Tr} \left[G(x, 0) \Gamma^\dagger \gamma_5 G^\dagger(0, x) \gamma_5 \Gamma \right] \quad (1.35)$$

A similar analysis is possible for the baryons, where the generic operator has the form

$$\mathcal{O}_B = \epsilon_{\alpha\beta\omega} (\psi_1^\alpha(x) C \Gamma \psi_2^\beta(x)) \psi_3^\omega(x) \quad (1.36)$$

for quark flavours 1, 2, 3 and colours α, β, ω . C is the charge conjugation matrix. Thus, any hadron correlator can be obtained by constructing an operator with

meson operators			baryon operators		
operator	J^{PC}	channel	operator	$I(J)$	channel
$\bar{\psi}\gamma_5\psi$	0^{-+}	PS	$(\psi_1 C\psi_2)\psi_3$	$1/2(1/2)$	N
$\bar{\psi}\gamma_i\psi$	1^{--}	V	$(\psi_1 C\gamma_i\psi_2)\psi_3$	$3/2(3/2)$	Δ

Table 1.1: The meson and baryon operators.

the correct quantum numbers, through an appropriate choice of Γ , and calculating the quark propagator.

Table 1.1 lists the hadron operators used in this thesis, where PS and V denote the pseudoscalar and vector meson channels respectively. Note that there is not a unique choice of operator. For example, $\bar{\psi}\gamma_4\gamma_5\psi$ and $\bar{\psi}\gamma_4\gamma_i\psi$ also have the same quantum numbers as the pseudoscalar and vector mesons respectively; However, for each channel the operators appearing in table 1.1 were found to provide the best signal. It is also interesting to note that for the pseudoscalar meson, for which $\Gamma = \gamma_5$

$$c(\vec{x}, t) = \left| G_{\alpha\beta}^{ij}(x, 0) \right|^2 \quad (1.37)$$

the correlator is absolute value of the quark propagator squared.

1.5 Correlation Functions and Masses

Returning to equation (1.29), and inserting a complete set of states, labelled by spatial momentum \vec{p} and particle X_n , and using translational invariance,

$$c(\vec{x}, t) = \sum_n \int \frac{d^3\vec{p}}{16\pi^3 E_n(\vec{p})} \langle 0 | \mathcal{O}(0) | X_n, \vec{p} \rangle \langle X_n, \vec{p} | \mathcal{O}^\dagger(0) | 0 \rangle e^{i\vec{p}\cdot\vec{x}} \quad (1.38)$$

The correlator at momentum \vec{q} can be obtained by weighting the operators with the phase factor $e^{-i\vec{q}\cdot\vec{x}}$ and summing over the lattice:

$$c(\vec{q}, t) = \sum_{\vec{x}} c(\vec{x}, t) e^{-i\vec{q}\cdot\vec{x}} \quad (1.39)$$

$$= \sum_n \frac{1}{2E_n(\vec{q})} \langle 0 | \mathcal{O}(0) | X_n, \vec{q} \rangle \langle X_n, \vec{q} | \mathcal{O}^\dagger(0) | 0 \rangle e^{iE_n(\vec{q})t} \quad (1.40)$$

Working in Euclidean space with a lattice periodic in time, T ,

$$c(\vec{q}, t) = \sum_n \left(A_n(\vec{q}) e^{-E_n(\vec{q})t} + B_n(\vec{q}) e^{-E_n^*(\vec{q})(T-t)} \right) \quad (1.41)$$

where,

$$A_n(\vec{q}) = \frac{1}{2E_n(\vec{q})} |\langle 0 | \mathcal{O}(0) | X_n, \vec{q} \rangle|^2 \quad (1.42)$$

$$B_n(\vec{q}) = \frac{1}{2E_n^*(\vec{q})} |\langle 0 | \mathcal{O}(0) | X_n^*, \vec{q} \rangle|^2 \quad (1.43)$$

and * indicates the backwardly propagating particle. At large times,

$$c(\vec{q}, t) \sim \left(A_0(\vec{q}) e^{-E_0(\vec{q})t} + B_0(\vec{q}) e^{-E_0^*(\vec{q})(T-t)} \right) \quad (1.44)$$

For mesons, the forwardly and backwardly propagating particles are identical, and equation (1.44) becomes

$$c(\vec{q}, t) = 2A_0(\vec{q}) e^{-E_0(\vec{q})T/2} \cosh E_0(\vec{q}) \left(\frac{T}{2} - t \right) \quad (1.45)$$

However, the backwardly propagating state created with a forwardly propagating baryon is the baryon parity partner; $A_0(\vec{q}) \neq B_0(\vec{q})$ and $E_0(\vec{q}) \neq E_0^*(\vec{q})$.

Thus, from equation (1.44) the energy of the lightest state can be extracted from the exponential decay of the correlation function.

1.6 Extracting Mass Estimates

With the knowledge of how to construct hadron correlators using combinations of the quark propagator, and the asymptotic form of these correlators, it is possible to extract the ground-state hadron masses.

The primary difficulty in this final stage is one of reliably identifying the region of timeslices where the correlator takes the asymptotic form in equation (1.44), or in terms of some estimator of the ground state energy, identifying the plateau region. Strictly speaking this only occurs in the limit $t \rightarrow \infty$, and excited states always contribute to $c(\vec{q}, t)$ for finite t . However, for finite statistics, equation (1.44) approximates the correlator at timeslices where the excited state contribution is far less than the statistical errors in the correlator.

The statistical errors can, over a few timeslices, conspire to give the impression that the asymptotic region has been reached, while the excited state contributions to the correlator are still significant. If the temporal length of the lattice is restricted (a particular problem when periodic boundary conditions are imposed since the effective propagation time is $T/2$) this may lead to the misidentification of the plateau region. Thus, the plateau region must extend over at least 5 or 6 timeslices in order to provide confidence in the estimate of the ground state energy extracted. This difficulty is given further consideration in the next chapter.

1.6.1 Effective Mass

A useful diagnostic tool for determining the region of timeslices where the correlator takes the asymptotic form in equation (1.44) is the effective mass, $m^{eff}(t)$. The effective mass is calculated using the values of the correlator from adjacent timeslices. The definition,

$$m^{eff}(t) = F \left(\frac{c(\vec{q}, t)}{c(\vec{q}, t+1)} \right) \quad (1.46)$$

is used here, where the function F is \cosh^{-1} for the meson correlators and \ln for the baryons. In the meson case, this definition has the advantage that it properly deals with interference between the contributions to $c(\vec{q}, t)$ from the forward and backwardly propagating states [15], and thus remains valid close to $t = T/2$.

From (1.44) and (1.45), as t increases and the contributions to $c(\vec{q}, t)$ from the excited states become less significant, the effective mass tends to the value of the ground state energy.

1.6.2 Correlated fits

The effective mass can be used as an estimate of the ground state energy, but the values of the correlator at only two timeslices are used. A more reliable estimate is obtained from fitting to the correlator over as many timeslices as possible. Equations (1.44) and (1.45) suggest fitting functions of the form

$$c(\vec{q}, t) = A(\vec{q})F(E(\vec{q}), t, T) \quad (1.47)$$

$$= A(\vec{q}) \cosh E(\vec{q})(T/2 - t) \quad \text{mesons} \quad (1.48)$$

$$= A(\vec{q})e^{-E(\vec{q})t} \quad \text{baryons} \quad (1.49)$$

where $A(\vec{q})$ is the amplitude of the ground state.

The standard way to fit data to a functional form is to minimise a measure of the goodness of fit as a function of the fit parameters, $\vec{a} = (A(\vec{q}), E(\vec{q}))$. If the procedure is to be a meaningful test of the fitting function, such a measure must take into account the correlations existing between the values of $c(\vec{q}, t)$ at different timeslices. If correlators at different values of the hopping parameter are fitted simultaneously then, ideally, the correlations between the data at different κ values should also be included. In this work, the correlated- χ^2 is used, where

$$\chi_{corr}^2(\vec{a}) = \sum_{t_i} \sum_{t_j} \text{Cov}(t_i, t_j)^{-1} (c(\vec{q}, t_i) - c(\vec{q}, t_i; \vec{a})) (c(\vec{q}, t_j) - c(\vec{q}, t_j; \vec{a})). \quad (1.50)$$

and $c(\vec{q}, t_j; \vec{a})$ is the theoretical value for the correlator at timeslice t_j derived from the parameters \vec{a} . The data covariance matrix is

$$\text{Cov}(t_i, t_j) = \frac{1}{N(N-1)} \sum_{k=1}^N (c_k(\vec{q}, t_i) - \langle c(\vec{q}, t_i) \rangle) (c_k(\vec{q}, t_j) - \langle c(\vec{q}, t_j) \rangle). \quad (1.51)$$

The sum is over N configurations, and $c_k(\vec{q}, t_i)$ is the value of the correlator at timeslice t_i from configuration k .

Equation (1.50) does not include the κ correlations. For a correlator fitted over n_t timeslices, (1.51) is an $n_t \times n_t$ matrix. The number of configurations must be at least as large as n_t otherwise the covariance matrix contains repeated rows, and is singular. If the correlator is also being fitted at n_k values of the hopping parameter, the minimum value of N required rises to $n_k n_t$. The number of configurations available for the various studies in this work are not sufficient to include the κ correlations. Nevertheless, these correlations still exist in the data and N should not fall too far below $n_k n_t$.

A “good” fit to the correlator is indicated by a value of χ^2 close to the number of degrees of freedom, n , where $n = n_t - n_a$, and n_a is the number of fit parameters. There is no clear minimum value of χ^2 , above which the fit function is not considered a good functional representation of the data, however $\chi^2/n < 3$ is reasonable cut-off [16, 17]. In the following χ^2 will be used to denote χ^2 per degree of freedom.

1.6.3 Error Estimation

Except where explicitly stated otherwise, the errors quoted for the fit parameters are purely statistical and are calculated according to the prescription [18]:

- create 1000 bootstrap samples from the original dataset of N configurations by randomly choosing, with replacement, N configurations per sample;
- for each bootstrap sample, perform all the mass fits and extrapolations as for the original data;

- obtain the errors on a given quantity from the 68% confidence limits of the corresponding bootstrap distribution.

1.6.4 Fitting Procedure

Following the reasoning of [19] we adopt the procedure of fitting to the correlator over as many timeslices as possible as far out as possible, in the hope of reducing contamination from excited states. The region of timeslices where the effective mass is constant within statistical errors, indicates an appropriate fitting range. t_{max} is fixed to be as large as possible, by choosing the timeslice within the plateau region which is furthest from the source, before the region when statistical errors dominate. t_{min} is chosen to be 3 or 4 timeslices less than t_{max} , and then reduced until the χ^2 shows a significant increase.

Chapter 2

Multistate Techniques Applied to the Light Hadron Spectrum

This chapter addresses the problem of extracting hadron masses in the context of the light hadron spectrum. A brief motivation for studying new methods for the extraction of hadron masses, is given in §(2.1). §(2.2) outlines two methods, each using a combination of two operators with the same quantum numbers to isolate the ground and first excited states. Possible candidates for these operators are the smeared and local operators, and an overview of the chosen smearing technique is given in §(2.3). §(2.4) presents the results obtained using the Wilson action at $\beta = 6.2$. The subtraction fit method is then outlined, and used as an independent check on these results. Next, all three methods are applied to data involving local operators and the clover action at $\beta = 6.2$. The chapter closes with a summary of the analysis.

2.1 Motivation

The pioneering work in lattice QCD during the early 1980s [19, 20, 21, 22], centered on a reproduction of the hadron spectrum in the light sector. To date this validation of the lattice approach remains a fundamental goal. Although much progress has been made from the low statistics, small lattice beginnings, a definitive calculation is still out of reach. With statistical errors now of the order of a few percent, there is a need to re-analyse and quantify the magnitude of the systematic errors involved in calculating hadron masses.

The main sources of error can be identified as the use of the quenched approximation, finite lattice size, finite lattice spacing, and the techniques used for extraction of hadron masses. The work in this chapter is concerned with the latter. A review of the current status of the other sources of error is contained within reference [23].

The results for hadron masses at the same β values often differ beyond quoted errors even among simulations with quite high statistics, and this points towards possible systematic errors in the extraction of masses from correlators. For example, the discrepancy between the values obtained by APE [24] and QCDPAX [25] for the mass of the vector meson is three times larger than the statistical error of 1%. APE found $m_V = 0.429(4)$ compared to $0.417(5)$ obtained by QCDPAX, where both groups used $\beta = 6.0$ with Wilson fermions at $\kappa = 0.155$ on the same spatial lattice size of 24^3 .

This discrepancy may be due to the fitting range used by APE corresponding to a region where excited state contributions to the correlator are significant. A fit to the correlator was performed between $t = 9$ and 15 , where $T/2 = 16$. In contrast, QCDPAX used $t = 15$ to 26 , where $T/2 = 27$. This group found the effective mass decreased by approximately 3% from $t = 10$ to $t = 16$, consistent with the discrepancy between the results of the two investigations.

This disagreement is particularly worrying considering that the APE results were derived using quark propagators “smeared” at the source. Such sources are spatially extended and are expected to have a larger overlap with the ground state wavefunction than the conventional point source. Hence, the contamination from excited states is expected to be less for smeared correlators, and the ground state isolated closer to the source compared to using correlators local at both the source and sink (LL).

The results of the two groups illustrate that use of a systematic fitting procedure, such as the one outlined in §(1.6.4), will provide a fitting range which corresponds to a plateau region in the effective masses; however, if the lattice size and statistics are limited, and hence the plateau is over a short time interval, this may be a misidentification of the true asymptotic region. Furthermore, smearing may reduce the contributions of excited states but not to the extent of isolating the ground state closer to the source. The increase in statistical noise in the correlator, accompanying the use of smeared sources, means that limited statistics are a particular problem; the plateau region in the effective masses may begin at earlier timeslices but it is still over a short time interval and it is difficult to obtain confidence in the fitting ranges chosen.

More information is needed about the excited-state contributions for a clearer picture to emerge. A first step is to calculate the mass and amplitude of the first excited state; however, the ultimate goal is an improvement in the isolation of the ground state and the corresponding mass estimate. Two methods which attempt to achieve both through the combining of the correlators representing the same particle channel are studied in the following sections.

2.2 Multistate Methods

Consider a set of m independent operators, $\{\mathcal{O}_i, i = 1, \dots, m\}$, with the same quantum numbers, and a basis of hadron states,

$$|h_n(\vec{p})\rangle, n = 0, 1, 2, \dots \quad (2.1)$$

Using all combinations of \mathcal{O}_i to create and annihilate the particle, an $m \times m$ matrix $C(t)$ of timesliced correlators can be constructed:

$$C(t) = \begin{pmatrix} c_{11}(t) & \dots & c_{1m}(t) \\ \vdots & \ddots & \vdots \\ c_{m1}(t) & \dots & c_{mm}(t) \end{pmatrix}$$

where

$$c_{ij}(t) = \omega_i \omega_j \sum_{\vec{x}} \langle 0 | \mathcal{O}_i(\vec{x}, t) \mathcal{O}_j^\dagger(\vec{0}, 0) | 0 \rangle e^{-i\vec{p} \cdot \vec{x}}, \quad (2.2)$$

and ω_i is an arbitrary normalisation factor for the operator \mathcal{O}_i . Inserting a complete set of states in equation (2.2), $C(t)$ has the form:

$$C(t) = \sum_{n \geq 0} e^{-E_n(\vec{p})t} \begin{pmatrix} |a_n^1|^2 \omega_1^2 & \dots & a_n^{1*} a_n^m \omega_1 \omega_m \\ \vdots & \ddots & \vdots \\ a_n^{m*} a_n^1 \omega_m \omega_1 & \dots & |a_n^m|^2 \omega_m^2 \end{pmatrix} \quad (2.3)$$

where

$$a_n^i = \frac{1}{\sqrt{2E_n(\vec{p})}} \langle 0 | \mathcal{O}_i | h_n(\vec{p}) \rangle. \quad (2.4)$$

There is in general an infinite number of excited states that contribute to the correlators $c_{ij}(t)$. However if only m of those states make a significant contribution then the set of m operators will effectively span the space of physical states. The isolation of each state can be sought, therefore, by considering various manipulations of the matrix $C(t)$. In the following sections two such methods will be discussed, both based on the work of Lüscher et al [26]. As the analysis is restricted to two operators, only the separation of the ground state and first excited

state can be attempted. Note, only a single, relative, normalisation factor (ω) need be used in this case.

2.2.1 Transfer Matrix

Consider the eigenvalue equation

$$C(t)u = \lambda(t, t_0)C(t_0)u, \quad (2.5)$$

for fixed $t_0 < t$. This is the transfer matrix equation for a particle travelling from time t_0 to t . If the system contains only two independent states, then the eigenvalues, $\lambda_{+/-}^{TS}(t, t_0)$, of the transfer matrix are

$$\begin{aligned} \lambda_+^{TS}(t, t_0) &= e^{-(t-t_0)E_0(\vec{p})} \\ \lambda_-^{TS}(t, t_0) &= e^{-(t-t_0)E_1(\vec{p})}, \end{aligned} \quad (2.6)$$

and the ground state and first excited state are separated exactly. In the general case, where there are more than two states, the further excited states introduce corrections to equation (2.6) and the eigenvalues have the form:

$$\begin{aligned} \lambda_+(t, t_0) &= e^{-(t-t_0)E_0(\vec{p})} + c_+(t_0)e^{-E_1(\vec{p})t} + O(e^{-E_2(\vec{p})t}) \\ \lambda_-(t, t_0) &= e^{-(t-t_0)E_1(\vec{p})} + c_-(t_0)e^{-E_2(\vec{p})t} + \dots \end{aligned} \quad (2.7)$$

At sufficiently large times, the first two states are dominant, and equation (2.7) shows that $\lambda_+(t, t_0)$ will have a contribution from the first excited state. In this limit, the only difference between (2.7) and (2.6) is that the two states form a complete set in the ideal two-state case but not in the general case, where $(a_0^1)^2 + (a_1^1)^2 \neq 1$ and $(a_0^2)^2 + (a_1^2)^2 \neq 1$. However, even if the two states do not form a complete set in the ideal case, the two states are separated. Hence $\lambda_+(t, t_0)$ must be approximately equal to $\lambda_+^{TS}(t, t_0)$ - i.e. the contribution from the first excited state to $\lambda_+(t, t_0)$ must be suppressed. This suggests the coefficient $c_+(t_0)$ does not grow exponentially with t_0 . The first excited state contribution to $\lambda_+(t, t_0)$

is expected, therefore, to be further suppressed relative to the leading behaviour, for large t_0 , and it is desirable to study $\lambda_+(t, t_0)$ for t_0 as large as possible. As the corrections to the leading behaviour of $\lambda_-(t, t_0)$ are from the second excited state, it is unclear whether these corrections are small, or suppressed for large t_0 .

2.2.2 Matrix of Correlators

An alternative approach to §(2.2.1) is to find the eigenvalues $\chi_{+/-}(t, \omega)$ of $C(t)$ directly. At large times,

$$\begin{aligned}\chi_+(t, \omega) &= f_+(\omega, a_i^1, a_i^2) e^{-E_0(\vec{p})t} \{1 + g_+(\omega, a_i^1, a_i^2) O(e^{-\Delta E_1(\vec{p})t})\} \\ \chi_-(t, \omega) &= f_-(\omega, a_i^1, a_i^2) e^{-E_1(\vec{p})t} \{1 + g_-(\omega, a_i^1, a_i^2) O(e^{-\Delta \tilde{E}(\vec{p})t})\},\end{aligned}\quad (2.8)$$

where

$$\begin{aligned}\Delta E_n(\vec{p}) &= E_n(\vec{p}) - E_0(\vec{p}) \\ \Delta \tilde{E}(\vec{p}) &= \min[E_1(\vec{p}) - E_0(\vec{p}), E_2(\vec{p}) - E_1(\vec{p})].\end{aligned}\quad (2.9)$$

$\chi_+(t, \omega)$ and $\chi_-(t, \omega)$ are dominated by the ground and first excited state respectively. In the case of only two states, however, specific conditions are necessary to obtain separation. The eigenvalues take the form,

$$\begin{aligned}\chi_{-/+}(t, \omega) &= \frac{1}{2}(Ae^{-E_0(\vec{p})t} + Be^{-E_1(\vec{p})t}) \pm \\ &\quad \left\{ \frac{1}{4}[Ae^{-E_0(\vec{p})t} - Be^{-E_1(\vec{p})t}]^2 + Ce^{-(E_0(\vec{p})+E_1(\vec{p}))t} \right\}^{\frac{1}{2}}\end{aligned}\quad (2.10)$$

where,

$$A = (a_0^1)^2 + \omega^2(a_0^2)^2 \quad B = (a_1^1)^2 + \omega^2(a_1^2)^2 \quad C = a_0^1 a_1^1 + \omega^2 a_0^2 a_1^2 \quad (2.11)$$

Only if the states $|\mathcal{O}_1\rangle$ and $|\mathcal{O}_2\rangle$ are orthogonal and form a complete set, i.e.

$$(a_0^1)^2 + (a_1^1)^2 = 1 \quad (a_0^2)^2 + (a_1^2)^2 = 1 \quad a_0^1 a_0^2 + a_1^1 a_1^2 = 0, \quad (2.12)$$

and $\omega^2 = 1$ does $C = 0$, and a separation of the ground state and first excited state is achieved. In the general case, at timeslices when all but the first two states make a significant contribution to $c_{ij}(t)$, the requirement that the two states form a complete set, prevents a separation of the ground state and first excited state. Hence, in contrast to $\lambda_+(t, t_0)$, the contribution of the first excited state to $\chi_+(t, \omega)$ cannot be assumed to be small.

The usefulness of this method derives from the dependence on ω of the corrections to the leading behaviour of the eigenvalues. At each timeslice, $C(t)$ is diagonalised, which means that a different operator is chosen to create and destroy the particle. Thus, the corrections to the leading behaviour of the eigenvalues are real but not positive definite. Cancellation of the contributions from excited states can be sought by varying ω , isolating the ground and first excited states at timeslices close to the source. Any resulting uncertainty in the onset of the plateau region in the effective masses can be reduced by observing that for sufficiently large times the excited state contributions to equation (2.8) will be negligible. Consequently the effective masses derived from $\chi_{+/-}(t, \omega)$ must be insensitive to ω , at large times.

2.3 Propagators and Smearing

Possible candidates for \mathcal{O}_1 and \mathcal{O}_2 are the local (\mathcal{O}_L) and smeared (\mathcal{O}_S) interpolating fields respectively. As outlined in §(2.1), smeared sources (or sinks) are introduced with the aim of reducing the contributions of excited states to the correlator. Such a source, $S(\vec{x}', \vec{0})$, proposed by the Wuppertal group [27], can be obtained by solving the 3-dimensional Klein-Gordon equation

$$\sum_{\vec{x}'} K(\vec{x}, \vec{x}') S(\vec{x}', \vec{0}) = \delta_{\vec{x}, \vec{0}}, \quad (2.13)$$

where

$$K(\vec{x}, \vec{x}') = \delta_{\vec{x}, \vec{x}'} - \kappa_S \Delta_{\vec{x}, \vec{x}'} \quad (2.14)$$

and

$$\Delta_{\vec{x}, \vec{x}'} = \sum_{\mu=1}^3 U_{\mu}(\vec{x}) \delta_{\vec{x}', \vec{x}+\vec{\mu}} + U_{\mu}^{\dagger}(\vec{x}-\vec{\mu}) \delta_{\vec{x}', \vec{x}-\vec{\mu}} \quad (2.15)$$

Each quark is localised at the origin with an rms radius controlled by the scalar hopping parameter, κ_S . The rms radius r is defined by

$$r^2 = \frac{\sum_{\vec{x}} |\vec{x}|^2 |S(\vec{x}, \vec{0})|^2}{\sum_{\vec{x}} |S(\vec{x}, \vec{0})|^2}. \quad (2.16)$$

For each ground state, an optimal radius is expected, corresponding to the smeared source which best approximates the lattice ground-state wavefunction. As the radius is increased towards this value the contributions of excited states decrease. A radius greater than this leads to an increase in noise without any improvement in the overlap of the source function with the ground state wavefunction.

In the continuum, the 3-dimensional Klein-Gordon equation formally represents a scalar particle of mass m . On the lattice, m is a function of κ_S in the parameterisation used in equation (2.14). Large radii are derived from a κ_S close to a critical value (κ_S^{crit}), that corresponds to zero mass for the scalar particle. The long-range correlations present when κ is close to the critical point cause the inversion of $K(\vec{x}, \vec{x}')$ to be prohibitively expensive in terms of computer time. Hence there is plenty of evidence in support of smeared sources of this type, reducing the contributions of excited states to correlators [27, 28, 29], but little to suggest a maximum smearing radius.

A less expensive gauge-invariant smeared source can be obtained by solving equation (2.13) as a power series in κ_S , stopping at some finite power N . Using the Jacobi iteration to obtain this series results in the smearing function, $J(\vec{x})$:

$$J(\vec{x}) = \sum_{p=0}^N \kappa_S^p \Delta_{\vec{x}, \vec{x}'}^p \delta_{\vec{x}', \vec{0}} \quad (2.17)$$

For κ_S greater than κ_C^{crit} , the series diverges. Nevertheless, $J(\vec{x})$ still provides a valid smeared source, for any choice of N and the shorter the power series, the greater the savings in computer time. Conversely, with κ_S below κ_C^{crit} , the Jacobi iteration is method of inverting $K(\vec{x}', \vec{0})$, although rather inefficient.

The smearing is still characterised purely by the rms smearing radius [28], and the same radius can be obtained from various choices of $\{N, \kappa_S\}$. Each successive iteration of the Jacobi procedure extends the smearing function along each axis by one link, and thus a minimum value of N exists for a particular radius.

The smeared correlators used to obtain the results in this chapter were derived from quark propagators smeared using Jacobi iteration with $\{N = 50, \kappa_S = 0.125\}$ (corresponding to an rms radius of approximately four¹). In terms of radius size this choice balances the reduction in excited state contribution against the corresponding increase in statistical noise, while $N = 50$ is close to the minimum value of N that can produce this radius. This choice of N provides a reduction in computer time of a factor of 10, compared to inverting $K(\vec{x}, \vec{x}')$ using the most efficient inversion procedure found by UKQCD [14] (the minimal residual inversion procedure with red-black preconditioning).

2.4 Results for Smeared Correlators

The results in this section were obtained on a $24^3 \times 48$ lattice at $\beta = 6.2$. Wilson fermions were used with a quark hopping parameter $\kappa = 0.152$, corresponding to a pseudoscalar mass of approximately 600 MeV, if the scale is set using m_p ($a^{-1} \sim 2.7(1)$ GeV [13]). The quark propagators were obtained using all smeared-local, source-sink combinations on 30 configurations, and the matrix $C(t)$ was

¹In the case of a correlator with more than one smeared propagator the average separation of the quarks may be larger.

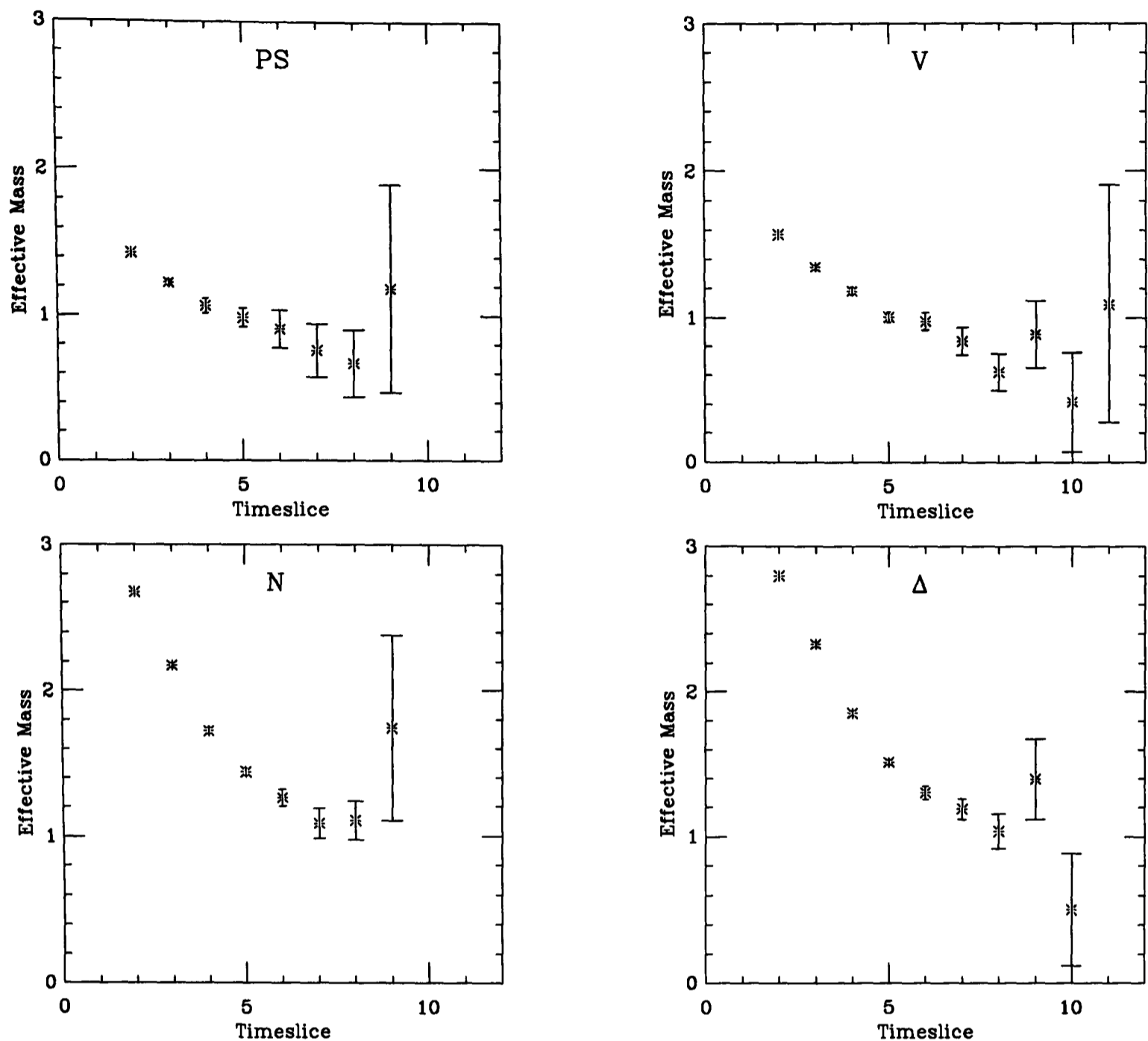


Figure 2.1: The effective masses of the first excited states in the pseudoscalar, vector, nucleon and Δ channels, obtained from $\lambda_-(t, t_0)$ for $t_0 = 1$ (bursts).

computed at zero spatial momentum.

2.4.1 Results for the First Excited State from $C(t)$

Shown in figure 2.1 are the effective masses obtained from the eigenvalues $\lambda_-(t, t_0)$ for the pseudoscalar, vector, nucleon and Δ channels, with $t_0 = 1$. There is a suggestion that the effective mass may be beginning to stabilise after $t = 7$

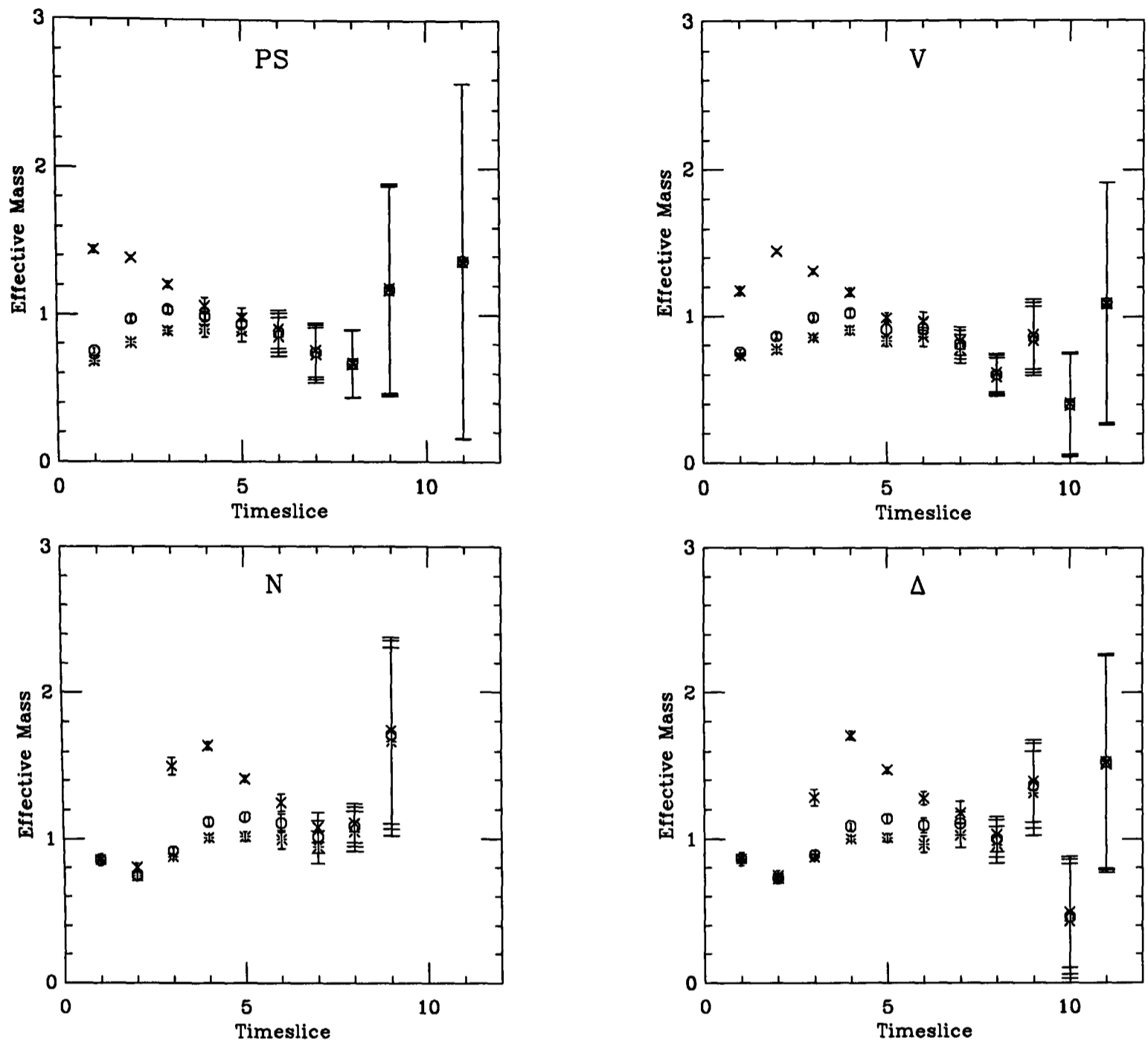


Figure 2.2: The effective masses of the first excited states in the pseudoscalar, vector, nucleon and Δ channels, derived from $\chi_-(t, \omega)$, for $\omega = 10\omega_0$ (crosses), $\omega = \omega_0$ (circles) and $\omega = 0.1\omega_0$ (bursts).

for all channels. However statistical noise dominates 2 timeslices later, and it is impossible to identify this unambiguously as the beginning of a plateau. No improvement can be obtained by increasing t_0 , only an increase in the statistical errors. Nevertheless the transfer method provides an upper bound for the first excited state of approximately 0.6 for the pseudoscalar, 0.8 for the vector and 1.0 for the nucleon and Δ .

The effective masses calculated from $\chi_-(t, \omega)$ are shown in figure 2.2 for the same hadron channels, with $\omega = 10\omega_0$, ω_0 and $0.1\omega_0$; ω_0 is defined as,

$$\omega_0 = \sqrt{\frac{c_{LL}(t=12)}{c_{SS}(t=12)}}. \quad (2.18)$$

For all channels there is a region where effective masses coincide for the different values of ω ; as mentioned in §(2.2.2) this can be taken as signal for the first excited state. At timeslices close to the source, varying ω from $10\omega_0$ to $0.1\omega_0$ causes a decrease in the effective masses as the states above the first excited state change from making a positive contribution to a negative one. For the two meson channels, figure 2.2 shows that this decrease is not to the extent of producing effective masses consistent with those at $t \geq 6$, where the effective masses for all values of ω agree. For the nucleon and Δ channels, there is a plateau consistent with the effective masses at later times, between timeslices $t = 5$ and 8. A stable value for the effective mass over four timeslices is the first evidence that varying ω can lead to cancellation of further excited states.

Figure 2.3 shows the effective masses obtained using the transfer matrix method, and the matrix of correlators method at a roughly optimal value of ω . The two methods yield consistent results for the effective masses close to timeslice 7. The estimates for the masses (\tilde{m}) and amplitudes (\tilde{A}) of the first excited states obtained using the matrix of correlators method are shown in table 2.1. The systematic errors in these results can be estimated by looking at the fluctuations in the central values of the mass as ω is varied about the optimal value, keeping the fitting range fixed. These additional errors were found to be of the order of 5%.

2.4.2 Results for the Ground State

Both the methods explored above fail to improve on the mass estimates for the ground state obtained from the individual correlators $c_{LL}(t)$, $c_{LS}(t)$, $c_{SL}(t)$ and

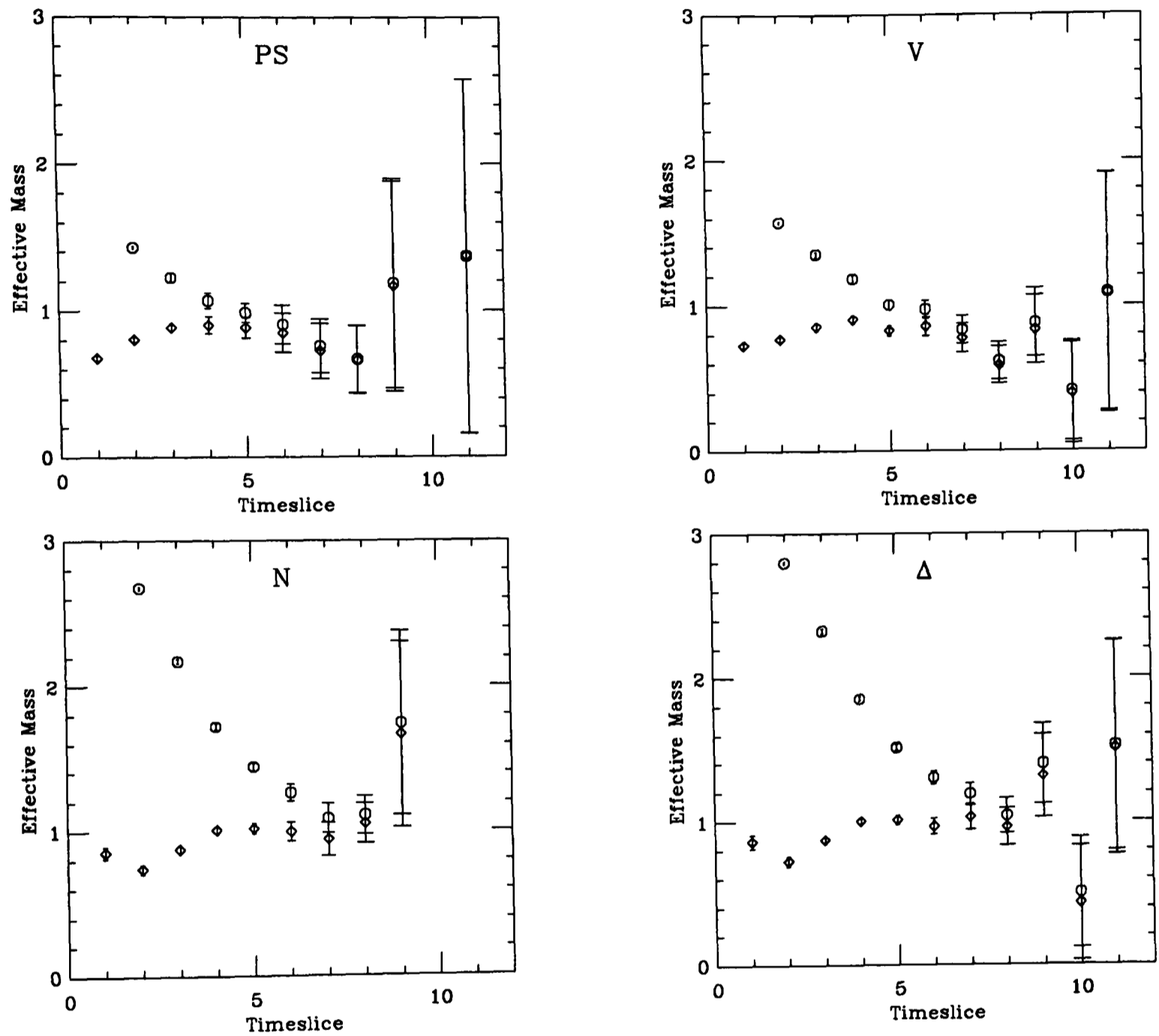


Figure 2.3: The effective masses of the first excited states in the pseudoscalar, vector, nucleon and Δ channel, derived from $\lambda_-(t, t_0)$ with $t_0 = 1$ (circles) and $\chi_-(t, \omega)$ with $\omega = 0.1\omega_0$ (diamonds).

	\tilde{m}_{PS}	\tilde{m}_V	\tilde{m}_N	\tilde{m}_Δ
\tilde{m}	0.67^{+10}_{-6}	0.71^{+9}_{-7}	0.95^{+5}_{-3}	1.00^{+3}_{-1}
\tilde{A}	$1.0^{+10}_{-4} \times 10^{-3}$	$1.1^{+10}_{-4} \times 10^{-3}$	$5^{+1}_{-1} \times 10^{-6}$	$2.4^{+3}_{-3} \times 10^{-5}$
χ^2	1.06/2	1.2/2	5.4/3	2.0/5
fit range	7-10	7-10	6-10	4-10

Table 2.1: The estimates of the first excited state masses in the meson and baryon channels, derived from $\chi_-(t, \omega)$ with $\omega = 0.1 \omega_0$.

$c_{SS}(t)$. In the case of the transfer matrix method, effective masses derived from $\lambda_+(t, t_0 = 1)$ are consistent with those obtained from $c_{SS}(t)$ for all timeslices; no improvement is obtained by using larger values of t_0 . Without knowledge of the masses and amplitudes of the excited states contributing to $c_{ij}(t)$, it is unclear why this is the case and any explanation is delayed until the discussion of the results obtained using the subtraction fit method.

Using the matrix of correlators method results in effective masses consistent with those extracted from the $c_{LL}(t)$ and $c_{SS}(t)$ correlators for $\omega = 0.1 \omega_0$ and $\omega = 10 \omega_0$ respectively. As discussed in §(2.2.2), the contributions of excited states to $\lambda_+(t, t_0)$ are not expected to be small. However, in the same way that varying ω reduces the contribution of the excited states to $\chi_-(t, \omega)$, an optimal value of ω is expected which isolates the ground state closer to the source than the $c_{SS}(t)$ correlator.

To gain some insight into this problem consider the way ω is chosen. When $\omega = \omega_0$ the diagonal elements of $C(t)$ are forced to be identical at $t = 12$. In figure 2.4 the effective masses derived from the individual correlators are shown, for the hadron channels of interest; the effective masses have reached a plateau by timeslice 12, for all channels. The results obtained using $c_{SL}(t)$ are not shown since

they are consistent with the $c_{LS}(t)$ results, only noisier. Figure 2.4 shows that the $c_{LL}(t)$ correlators have a much larger contribution from excited states for $t < 12$ compared to the smeared correlators. Therefore choosing $\omega = \omega_0$ gives $c_{LL}(t)$ a large weighting relative to the smeared correlators in $C(t)$ and correspondingly a large weighting for the excited states relative to the ground state for $t < 12$. This contribution to $\chi_+(t, \omega)$ from the excited states need not be positive; however, in practice it appears to be so. If ω is decreased, the weighting of $c_{LL}(t)$ increases and $\chi_+(t, \omega)$ tends towards the $c_{LL}(t)$ correlator.

Conversely, increasing ω increases the weighting of $c_{LS}(t)$, $c_{SL}(t)$ and $c_{SS}(t)$ compared to $c_{LL}(t)$. The smeared correlators contribute only a small correction from excited states to the leading behaviour of $\chi_+(t, \omega)$. Decreasing the weighting of the excited states stemming from $c_{LL}(t)$ is more likely to provide cancellation with the excited state contributions from the smeared correlators. Here again the amplitudes and masses of the excited states present in this study are such that this is not seen in the data, and as ω increases, $\chi_+(t, \omega)$ tends towards $c_{SS}(t)$.

2.5 Subtraction Fit

An independent method of estimating the amplitude and mass of the first excited state is needed to provide a check on the results of §(2.4.1). The simplest possibility is to extend the fitting function of equation (1.49) to include the contribution of the first excited state. The fitting function becomes

$$c_{ij}(t) = AF(m, t, T) + \tilde{A}F(\tilde{m}, t, T). \quad (2.19)$$

where F has the form given in equation (1.49), and A and m are the mass and amplitude of the ground state. This procedure is notoriously unstable and previous attempts to obtain an estimate for the first excited state using this method have produced results with unacceptably large errors [30]. Alternatively the sub-

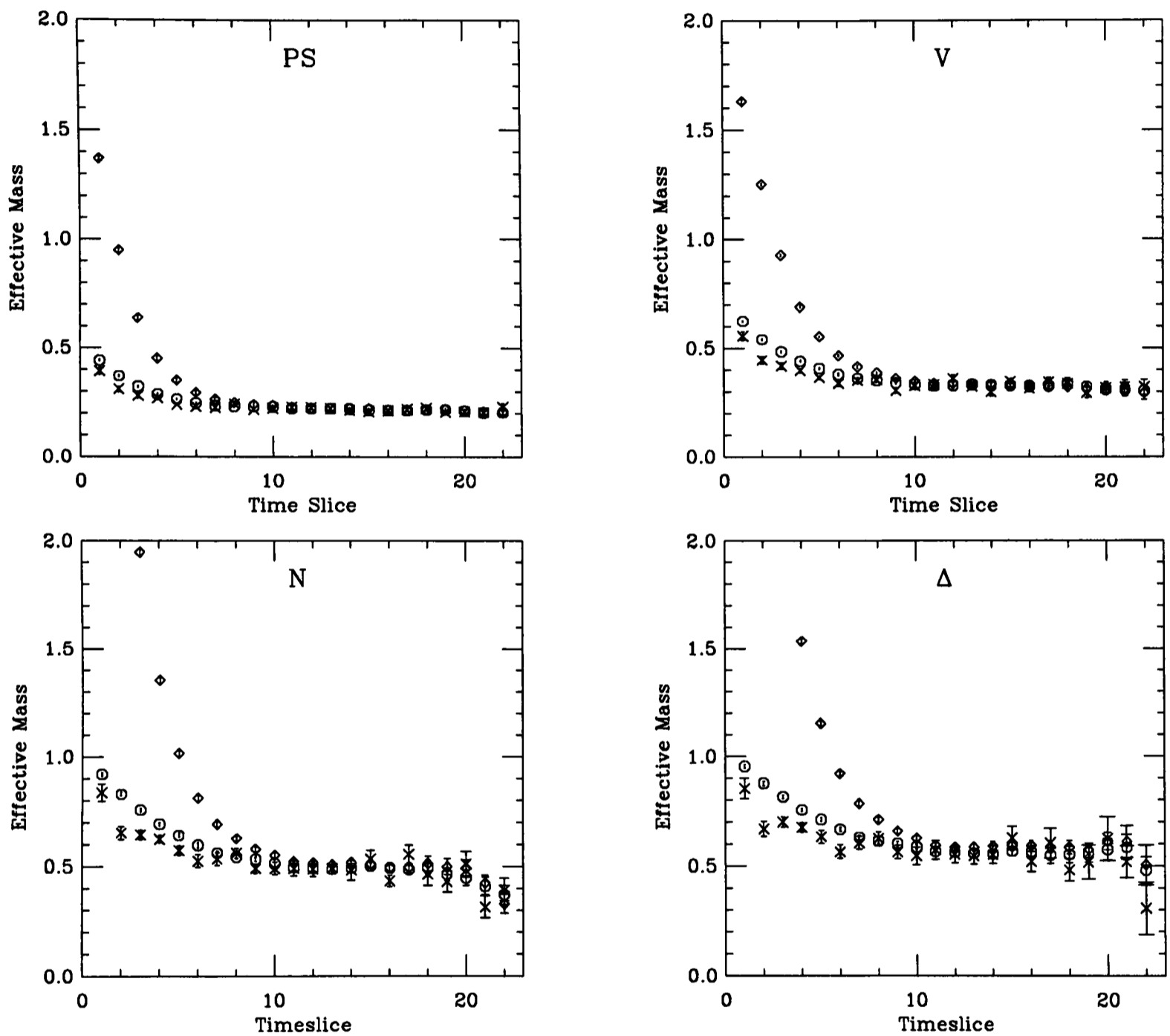


Figure 2.4: The effective masses of the pseudoscalar, vector, nucleon and Δ , computed using LL (diamonds), LS (octagons) and SS (crosses) correlators.

traction method can be used. This procedure utilises the mass and amplitude of the ground state to subtract the ground state contribution from the correlator. The excited state correlator, $c'_{ij}(t)$, is defined as

$$c'_{ij}(t) = c_{ij}(t) - A \times F(m, t, T), \quad (2.20)$$

and a single mass fit is performed on $c'_{ij}(t)$. At large times, when only the ground state is contributing, $c'_{ij}(t)$ must be consistent with zero. This provides a further check on whether A and m are good estimates of the ground state mass and amplitude.

2.5.1 Obtaining estimates for A and m from $c_{ij}(t)$

Figure 2.5 shows the variation in the propagator mass estimates obtained from $c_{ij}(t)$, with the position of the first timeslice in the fitting range, t_{min} , in a variable window, fixing $t_{max} = 18$. For the two meson channels the mass estimates obtained from fitting to the correlators $c_{LL}(t)$ and $c_{LS}(t)$ begin to stabilise by $t_{min} = 12$, compared to $t_{min} = 9$ using $c_{SS}(t)$. The behaviour of the χ^2 supports this, becoming stable and close to 1 for these fitting ranges. The mass estimates obtained from $c_{LS}(t)$ and $c_{SS}(t)$ are consistent, while those derived from $c_{LL}(t)$ are systematically higher. Although the discrepancy is approximately 1σ , a systematic difference suggests there are still excited states contributing to $c_{LL}(t)$ in the region chosen to extract the ground state mass.

Since smearing at both the source and sink reduces the contamination of excited states further than merely smearing at the source, the consistency between estimates for the ground state derived from $c_{LS}(t)$ and $c_{SS}(t)$ implies there is no significant contamination from excited states. Similar behaviour is seen in the nucleon and Δ channels; however the discrepancy between the values obtained from $c_{LL}(t)$ and the smeared correlators is statistically less significant. The best

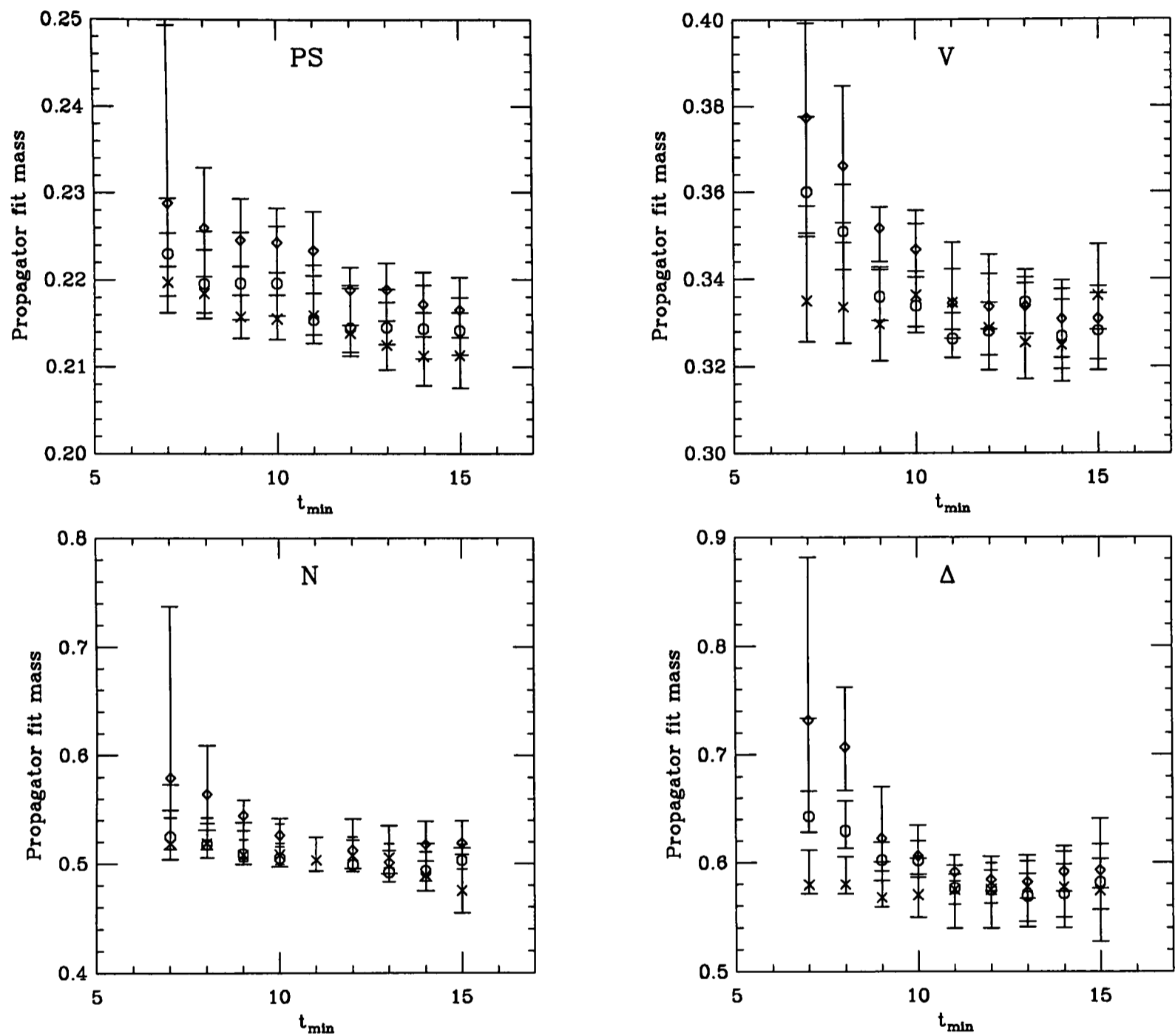


Figure 2.5: Fit stability plots for the pseudoscalar, vector, nucleon and Δ obtained using the LL (diamonds), LS (octagons) and SS (crosses) quark propagators. The variation of fit mass with t_{min} is shown with t_{max} fixed to be equal to 18.

	LL	LS	SL	SS
m_{PS}	0.219^{+4}_{-5}	0.215^{+7}_{-3}	0.217^{+5}_{-4}	0.216^{+5}_{-2}
A_{PS}	0.0118^{+5}_{-11}	4.2^{+2}_{-5}	4.1^{+3}_{-3}	$1.5^{+1}_{-1} \times 10^3$
χ^2	6.8/5	7.9/6	5.7/6	7.6/8
fit range	12-18	11-18	11-18	9-18
m_V	0.335^{+8}_{-8}	0.326^{+6}_{-5}	0.342^{+11}_{-11}	0.330^{+13}_{-9}
A_V	0.0108^{+8}_{-8}	4.4^{+3}_{-4}	5.6^{+7}_{-7}	$2.3^{+3}_{-4} \times 10^3$
χ^2	1.4/6	6.8/6	17.8/6	21.7/8
fit range	11-18	11-18	11-18	9-18
m_N	0.51^{+1}_{-1}	0.50^{+2}_{-1}	0.53^{+2}_{-2}	0.51^{+3}_{-1}
A_N	$1.2^{+2}_{-2} \times 10^{-5}$	$6.0^{+9}_{-10} \times 10^{-2}$	0.079^{+10}_{-9}	0.11^{+3}_{-3}
χ^2	6.9/5	6.6/5	5.4/5	12.2/8
fit range	12-18	12-18	12-18	9-18
m_Δ	0.59^{+2}_{-1}	0.58^{+1}_{-2}	0.58^{+2}_{-2}	0.57^{+2}_{-1}
A_Δ	$6.1^{+9}_{-8} \times 10^{-5}$	0.37^{+3}_{-9}	0.47^{+11}_{-10}	$3.4^{+6}_{-9} \times 10^3$
χ^2	2.2/6	4.1/6	5.4/6	5.1/8
fit range	11-18	11-18	11-18	9-18

Table 2.2: The estimates of baryon and meson masses using LL, SL, LS and SS propagators.

estimates of the mass (m) and amplitude (A) of the ground state obtained from the fits to the correlators are detailed in table 2.2.

	PS	V	N	Δ
\tilde{A}_{LL}/A_{LL}	1.2	10	60	50
\tilde{A}_{LS}/A_{LS}	1.2	2	7	5

Table 2.3: The ratio of the amplitude of the first excited state to that of the ground state, for the LL and LS correlators. Note that the values are only approximate.

2.5.2 Results from the Subtraction Fit Method

Shown in figure 2.6 are the effective masses obtained from $c'_{LL}(t)$ and $c'_{LS}(t)$, for the hadron channels of interest. The corresponding results for $c'_{SS}(t)$ are dominated by statistical noise, even at timeslices close to the source, and are omitted. Three general features are apparent. Firstly, the effective masses derived from $c'_{LL}(t)$ have large contributions from excited states until at least timeslice 7, when the errors become uncontrolled. Secondly, the values obtained from $c'_{LL}(t)$ for $t \geq 7$ lie above those from $c'_{LS}(t)$. This is consistent with the estimates A and m used to obtain $c'_{LL}(t)$ being contaminated by excited states, and hence producing an underestimate of the ground state contribution to $c_{LL}(t)$. Lastly, using $c'_{LS}(t)$ produces a plateau in the effective mass that begins almost at the second timeslice; the pseudoscalar is possibly an exception, the errors are too large to determine whether the decrease in the effective mass at timeslice 7 is significant. This clearly shows that using smeared sources with $r \sim 4$ removes the contributions of the second excited states and above from the correlator, but the contribution of the first excited state remains significant.

Table 2.3 details the approximate values obtained for the ratios \tilde{A}_{LS}/A_{LS} . The overlap of the first excited state with the source function is of the same order of magnitude as that of the ground state. The dramatic reduction in the contribution from higher excited states suggests that the mass of the first excited state lies

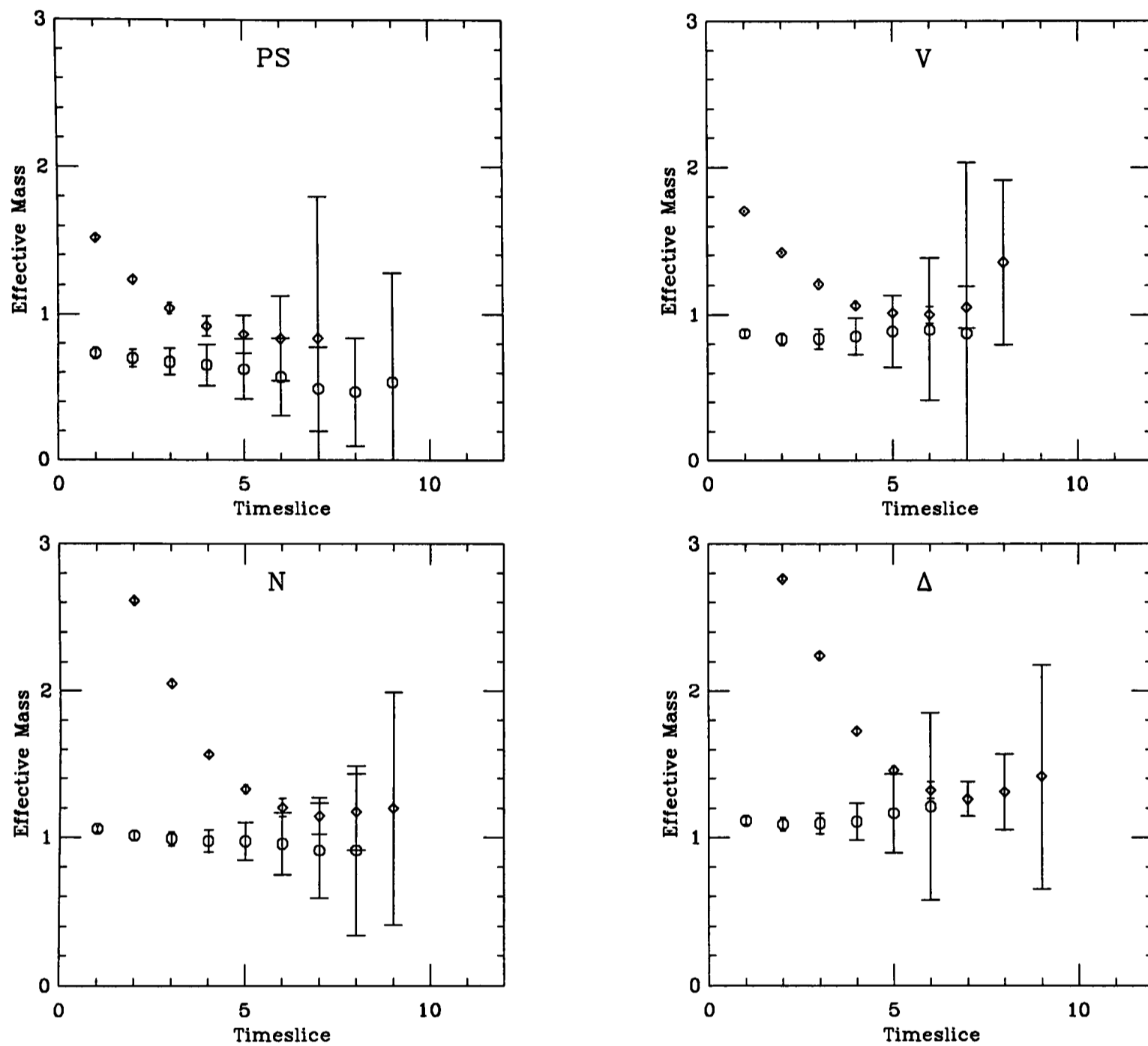


Figure 2.6: The effective masses of the first excited states in the pseudoscalar, vector, nucleon and Δ channels, derived from $c_{LL}(t)$ (diamonds) and $c_{LS}(t)$ (octagons).

much closer to the ground state than the second excited state. It is not obvious why this is the case. A hopping parameter of $\kappa = 0.152$, corresponds to a quark mass slightly less than the strange quark, and experimental measurements have only been made of the first excited states of hadrons containing strange quarks. Theoretically, excited states are most clearly understood in terms of potential models, where S -wave states correspond to radial excitations. In this essentially hydrogen-like picture, the splitting between the energy states decreases for successively higher excited states. However the underlying assumption that the quarks behave non-relativistically is not particularly valid for light quarks.

The ratios \tilde{A}_{LL}/A_{LL} are also shown in table 2.3. A comparison with the values obtained from $c_{LS}(t)$ suggests that although smearing at the source does not remove the contributions from the first excited state, these contributions are reduced. However, combining the systematic uncertainty in the ground and first excited state amplitudes, of the order of 15% and 20% (see below) respectively, with the statistical errors, the values of \tilde{A}_{LL}/A_{LL} are consistent with those for $c_{LS}(t)$.

These results add support to the comments made in the previous section, on the choice of ground-state fitting ranges. From table 2.2, the results from $c_{LS}(t)$ appear disappointing; the same fitting range is used for these correlators as for $c_{LL}(t)$. However, the results from $c'_{LL}(t)$ suggest that the ground state is isolated much further from the source than indicated by the choice of fitting range, while the significant contribution found from the first excited state to $c_{LS}(t)$ explains the need to choose t_{min} as far from the source as timeslice 11 or 12 for this correlator. In addition, the consistency between the estimates of the ground state masses from $c_{SS}(t)$ and $c_{LS}(t)$, provides confidence that the contributions from the first excited state to $c_{LS}(t)$ are not significant for $t \geq 11$.

Figure 2.6 also sheds light on the failure of the transfer matrix method to improve on the results of $c_{SS}(t)$ for the ground state mass estimate. This method will

separate the ground state and first excited states when there are only effectively two states contributing to all $c_{ij}(t)$ in $C(t)$. As noted above the effective masses derived from $c'_{LL}(t)$, and hence $c_{LL}(t)$, do not lose the contributions of further excited states until at least timeslice 7, only two timeslices before the ground state is isolated using $c_{SS}(t)$.

Table 2.4 shows the estimates obtained for the masses and amplitudes of the first excited states obtained from $c'_{LS}(t)$ and $c'_{LL}(t)$. Increasing t_{min} above the values given in the table, with t_{max} fixed, the central values of \tilde{m} and \tilde{A} , extracted from $c_{LS}(t)$, fluctuate by $\sim 3\%$ and $\sim 15\%$ respectively. This is comparable to the stability of the one-mass fits to the $c_{ij}(t)$ correlators. For $c_{LL}(t)$ the stability of the results cannot be checked since the fitting range is too small. The results for $c'_{LS}(t)$ compare favourably with those obtained using the matrix methods, only the mass of the first excited state in the Δ channel differing by more than 1σ .

Table 2.4 shows that different time ranges have been used to obtain the estimates for m and A from $c_{LS}(t)$ to those detailed in table 2.2. For the vector and Δ channels, the restriction $c'_{ij}(t) = 0$ at large times is not satisfied unless t_{min} for the ground state fitting range is moved from $t = 11$, to $t = 13$ and 15 respectively. This is possibly due to the reliance of the subtraction fit method on an accurate determination of the value of the ground state amplitude. A is the less well determined of the two parameters in the fitting function. If $t_{min} > 11$ is used for the vector and Δ channel $c_{LS}(t)$ correlators with t_{max} fixed, A fluctuates by 16% and 15% respectively, compared to 4% and 5% in m . Hence, a different t_{min} may be necessary to provide a better estimate of the ground state amplitude compared to that needed for a reasonable estimate of the mass. However, the results for $c'_{LL}(t)$ suggest this “better” estimate may still contain significant excited state contamination. Although for the fitting range shown in table 2.4, $c'_{LL}(t)$ is consistent with zero at large times, figures 2.5 and 2.6 indicate contributions from excited states to A and m may be significant.

	\tilde{m}_{PS}	\tilde{m}_V	\tilde{m}_N	\tilde{m}_Δ
\tilde{m} (LS)	0.69^{+2}_{-2}	0.81^{+1}_{-2}	1.03^{+1}_{-1}	1.08^{+2}_{-2}
\tilde{A}	6.4^{+3}_{-2}	12.2^{+7}_{-4}	0.50^{+3}_{-3}	2.3^{+2}_{-2}
χ^2	2.0/5	8.6/6	5.0/7	7.7/8
fit range	3-9	3-10	2-10	2-11
m	0.215	0.335	0.499	0.582
A	4.23	5.05	0.079	0.456
fit range	11-18	13-18	12-18	15-18
\tilde{m} (LL)	0.6^{+1}_{-2}	0.92^{+6}_{-4}	1.17^{+6}_{-4}	1.22^{+6}_{-4}
\tilde{A}	0.021^{+7}_{-1}	0.12^{+5}_{-3}	$6^{+3}_{-1} \times 10^{-4}$	$3^{+1}_{-1} \times 10^{-3}$
χ^2	0.7/1	6.1/2	0.7/2	0.04/2
fit range	9-11	7-10	7-10	7-10
m	0.223	0.334	0.523	0.584
A	0.013	0.011	1.4×10^{-5}	5.5×10^{-5}
fit range	11-18	12-18	11-18	12-18

Table 2.4: The estimates of the first excited state masses in the meson and baryon channels, obtained from $c'_{LS}(t)$ (top) and $c'_{LL}(t)$.

The uncertainty in A and m is a source of systematic error in the first excited state mass and amplitude. The magnitude of this error can be estimated by varying t_{min} for the ground state fit above the minimum values, keeping t_{max} and the first excited state fitting range fixed. The resulting $c'_{ij}(t)$ correlators must also be consistent with zero for later times. Applying this procedure to $c'_{LS}(t)$ the systematic errors are found to be of order 3% and 10% for \tilde{m} and \tilde{A} respectively, while for $c'_{LL}(t)$ the errors rise to $> 10\%$ and $> 20\%$ respectively. Considering the statistical and systematic errors in this and the matrix of correlators methods, the discrepancy between the results for the first excited state masses in the Δ channel is not significant.

2.6 Multiple Local Operators on the Lattice

Instead of resorting to smearing, operators having an overlap with the same particle can be constructed from different combinations of gamma matrices, as noted in §(1.4). For the pseudoscalar channel, candidates for \mathcal{O}_1 and \mathcal{O}_2 are $\bar{\psi}\gamma_5\psi$ and $\bar{\psi}\gamma_4\gamma_5\psi$ respectively, while for the vector channel, $\bar{\psi}\gamma_i\psi$ and $\bar{\psi}\gamma_i\gamma_5\psi$ are used. The nucleon channel will not be discussed below except in the subtraction fit analysis; three operators are available and the resulting nine correlators forming $C(t)$ are too computationally expensive to produce. The Δ channel is also omitted because unfortunately only one operator was computed for this analysis.

2.7 Results for Local-Local Correlators

To enable a comparison with the Wilson action analysis, the results for this section were obtained on a lattice size of $24^3 \times 48$ with $\beta = 6.2$. In addition, the hopping parameter, $\kappa = 0.14226$, was chosen so that the pseudoscalar meson mass was

roughly consistent with that from the Wilson data. The quark propagators were obtained using local sources and sinks on 60 configurations. The matrix $C(t)$ formed from the resulting correlators was computed at zero spatial momentum.

2.7.1 Results for the Ground and First Excited State from $C(t)$

The results for the ground and first excited states for both the pseudoscalar and vector channels are disappointing. For the pseudoscalar channel the correlators in $C(t)$ are well behaved and produce good estimates for the pseudoscalar ground state mass. The effective masses obtained from $\lambda_+(t, t_0 = 1)$ and $\chi_+(t, \omega = 1)$ are consistent with those obtained from $c_{11}(t)$. The eigenvalues $\lambda_-(t, t_0 = 1)$ and $\chi_-(t, \omega = 1)$ also produce consistent effective masses, but statistical noise dominates after timeslice 4, before there is any indication of the first excited state being isolated. There is no improvement in the results obtained using $\chi_-(t, \omega)$ if different values of ω are used. The presence of large statistical errors may be due to the fact that the operator $\bar{\psi}\gamma_4\gamma_5\psi$, unlike $\bar{\psi}\gamma_5\psi$, does not give rise to a correlator which is the sum of positive definite terms for each configuration. In the vector case, the diagonal correlators are well behaved but the off-diagonal correlators are dominated at all timeslices by statistical noise. It is impossible to invert $C(t)$ under these circumstances and no results can be obtained.

2.8 Results from the Subtraction Fit Method

Estimates of the first excited state masses for the pseudoscalar, vector, nucleon and Δ channels can be obtained using the subtraction fit method. Only the local operators used in §(2.5.2) are studied; the others produce consistent results but

	m_{PS}	m_V	m_N	m_Δ
m	0.214^{+2}_{-3}	0.343^{+9}_{-7}	0.46^{+2}_{-1}	0.58^{+3}_{-2}
A	0.013^{+0}_{-1}	0.0072^{+8}_{-7}	$4.9^{+2}_{-1} \times 10^{-6}$	$2.9^{+2}_{-1} \times 10^{-5}$
χ^2	6.9/7	7.8/9	5.9/5	1.1/4
fit range	14-22	13-23	16-22	16-21

Table 2.5: The estimates of the ground state masses in the meson and baryon channels, obtained from $c_{LL}(t)$ and using the clover action, with $\kappa = 0.14226$.

with larger statistical errors.

2.8.1 Extracting the Masses and Amplitudes of the Ground States

The extraction of ground state masses from the correlators obtained using the clover action has been extensively studied by UKQCD [31]. Table 2.5 summarises the masses and amplitudes of the ground state for the hadron channels of interest.

An investigation involving limited statistics, of only 18 configurations [47], found the difference between the Wilson ($\kappa = 0.152$) and clover action ($\kappa = 0.14226$) LL ground-state mass estimates to be less than 1σ for the pseudoscalar, vector, nucleon and Δ channels. The fitting ranges chosen were between timeslices 12 and 16 for both actions. For the clover action, this should be compared with the fitting ranges given in table 2.5. Tripling the number of configurations has reduced the statistical errors sufficiently to enable a t_{max} of 22 or 23. This allows larger values of t_{min} to be explored, and thus contributions from excited states are

exposed in the ground state mass estimates obtained using the fitting ranges from the 18 configuration analysis. This results in t_{min} moving from 12 to 14, 13 and 16 for the pseudoscalar, vector and baryon channels. The consistency between the ground state masses using the Wilson and clover actions on 18 configurations suggests similar changes in fitting ranges for an analysis of the Wilson action with 60 configurations. Since t_{min} is equal to 11/12 using the Wilson action and 30 configurations, this supports the suggestion from §(2.5.2) that the $c_{LL}(t)$ ground state mass estimates contain contributions from the excited states.

The ability to investigate fitting ranges close to the limits of the lattice allows greater confidence in the ground state fitting ranges for the pseudoscalar, nucleon and Δ channels. Fitting to the correlator in the vector channel, however, is problematic. If t_{min} is increased above timeslice 13, t_{max} fixed at 23, a monotonic decrease is seen in the propagator fit mass. There is no significant variation in χ^2 for $t_{min} > 13$, and the mass estimates agree within statistical errors. Without a larger lattice in the temporal direction it is impossible to tell whether this effect is due to contamination from excited states, or statistical fluctuations.

2.8.2 Results for the clover action

The effective masses obtained from the $c'_{LL}(t)$ correlators are shown in figure 2.7. For the pseudoscalar channel the effective mass is consistent with the ground state mass at timeslice 13, indicating a bad estimate for A or m has been used. Using a different fitting range for the ground state does not provide any improvement, since A varies by approximately $\sim 1\%$ as t_{min} is moved to timeslices later than 14, with t_{max} fixed at 22. The nucleon and vector channels show clear plateaus in the effective mass for the first excited state, beginning at timeslice 9 and 7 respectively. The effective mass of the Δ channel suggests timeslice 9 is close to the region in which the first excited state is isolated.

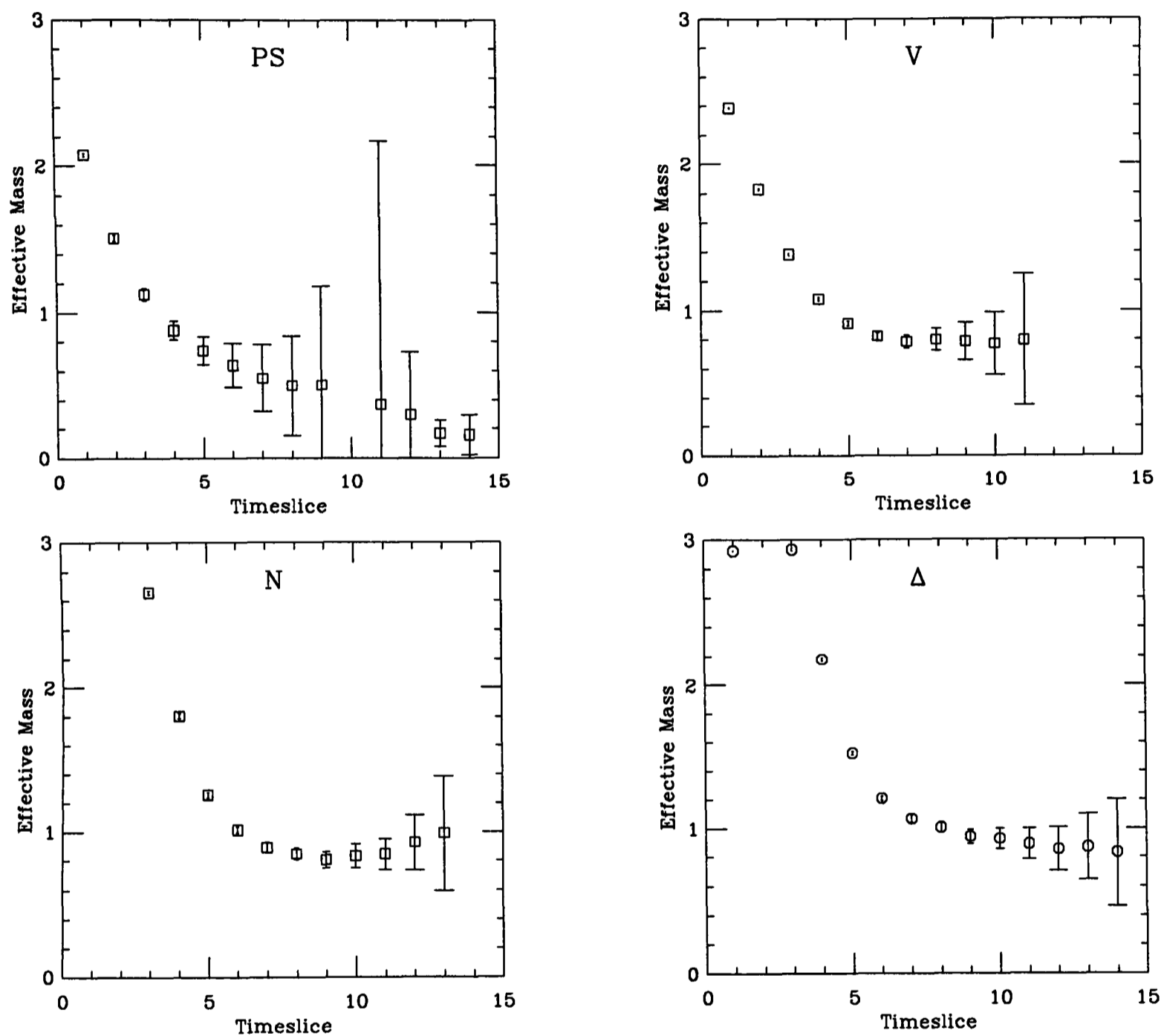


Figure 2.7: The effective masses of the first excited states for the pseudoscalar, vector, nucleon and Δ channels, derived from $c'_{LL}(t)$ with $\kappa = 0.14226$.

	\tilde{m}_V	\tilde{m}_N	\tilde{m}_Δ
\tilde{m}	0.78^{+3}_{-3}	0.79^{+7}_{-2}	0.97^{+4}_{-4}
\tilde{A}	0.054^{+12}_{-8}	$6^{+3}_{-1} \times 10^{-5}$	$4^{+2}_{-1} \times 10^{-4}$
χ^2	4.1/5	3.9/4	0.8/5
fit range	7-13	9-14	9-15
m	0.334	0.462	0.565
A	6.3×10^{-3}	4.9×10^{-6}	2.2×10^{-5}
fit range	16-23	16-22	19-21

Table 2.6: The estimates of the first excited state masses in the meson and baryon channels, obtained from $c'_{LL}(t)$ and using the clover action, with $\kappa = 0.14226$.

The first excited state mass estimates obtained from fitting to $c'_{LL}(t)$ are shown in table 2.6. The stability of the results can be checked in the same way as in §(2.5.2), by varying the fitting range for $c'_{ij}(t)$ while keeping A and m fixed. \tilde{A} and \tilde{m} fluctuate by $\sim 25\%$ and $\sim 5\%$ respectively for the nucleon and vector channels, and $\sim 50\%$ and $\sim 7\%$ for the Δ channel. Similarly, varying the ground state fitting range while keeping the fitting range for $c'_{ij}(t)$ fixed, the systematic errors in the first excited-state mass estimate are found to be $\sim 6\%$ and $\sim 30\%$ for the nucleon and vector channels respectively. The large systematic error for the vector channel arises out of the uncertainty in the ground state mass and amplitudes mentioned previously. Since the propagator fit to $c_{LL}(t)$ in the Δ channel uses $t_{min} = 19$ the systematic errors cannot be estimated.

2.9 Summary of Results for the Ground State

The analysis of the data obtained using the Wilson action has shown some success. The use of smeared sources was found effectively to remove the contribution of all the excited states to the correlators, except for the first excited state. If smeared sinks are also used, the ground state was found to be isolated closer to the source. Thus, the consistency found between the results obtained from the LS and SS correlators provides confidence in the fitting regions chosen to extract the ground state masses from the LS correlators. The discrepancy between these results and those from the LL correlator, is consistent with the LL correlators being contaminated by excited states for the fitting regions chosen.

For the clover data, a comparison can be made with the ground-state fitting ranges used by QCDPAX, in an investigation of LL correlators. The value of the hopping parameter used by this collaboration corresponds to a pseudoscalar meson mass of approximately 600 MeV (using the nominal scale of 2 GeV at $\beta = 6.0$), comparable to the pseudoscalar meson masses obtained from the Wilson and clover data in this study. In addition to the vector channel, discussed in §(2.1), the nucleon channel was also studied. The plateau region in the effective masses was found to begin at timeslice 12 at $\beta = 6.0$, compared to 15 at $\beta = 5.85$. In physical units, timeslice 15 at $\beta = 5.85$ is much further from the source compared to timeslice 12 at $\beta = 6.0$. This motivates QCDPAX to identify the asymptotic region in the effective mass as a region where the contributions from excited states are still significant.

A plateau beginning at timeslices 15 for the vector channel and 12 for the nucleon at $\beta = 6.0$ corresponds to isolating the ground state at timeslice 20 and 16 respectively at $\beta = 6.2$, where the ratio $a^{-1}(\beta = 6.2)/a^{-1}(\beta = 6.0) = 2.7/2.0$ has been used to convert from $\beta = 6.0$ to $\beta = 6.2$. With an effective temporal

lattice extension of 24, fitting ranges for the vector channel with t_{min} around 20 cannot be explored. However, the results for this channel from the clover action are consistent with excited states contributing to the ground-state propagator fit masses, for all possible fitting ranges on this lattice. For the nucleon channel, a stable plateau in the effective mass is found over 7 timeslices [31], and the statistical errors in the ground state mass estimates are of order 5% (compared to 2% for the vector channel). Thus, it is unclear whether an increase in statistics and a larger lattice would lead to a change in the mass estimates greater than the present statistical uncertainty.

The ground-state fitting ranges used for the Wilson data can be compared to those chosen by APE, detailed in §(2.1). The quark propagators were smeared at the source only, using a cube source of size 7^3 at $\beta = 6.0$; from equation (2.16) this corresponds to $r \sim 4$ at $\beta = 6.2$ comparable to the smearing radius used in this investigation. A fitting range beginning at timeslice 9 was chosen for the vector channel, which is equivalent to approximately timeslice 12 at $\beta = 6.2$. The suggestion that there are significant excited-state contributions to the ground-state mass estimate obtained by APE, conflicts with the evidence of a reliable ground state mass estimate from the $c_{LS}(t)$ correlators with a similar fitting range, found in this investigation. However, a difference in the overlap with the excited states is quite possible from such different smearing functions.

This highlights the problem of increased statistical noise in the correlators with the use of smearing, mentioned in §(2.1). Although, there is evidence that the ground state is isolated closer to the source using smeared correlators, confidence in the fitting ranges chosen cannot be improved, since fitting ranges comparable to those used for the clover analysis cannot be explored. Thus, it is difficult to determine the significance of possible discrepancies between the results from different smearing functions.

Attempts to isolate the ground state closer to the source using the transfer matrix and matrix of correlators method were unsuccessful. The best results for the ground state effective masses were consistent with those obtained from the SS correlators. The contributions to the LL correlators from states above the first excited state become negligible close to the timeslice when the SS correlator was found to isolate the ground state. Since using a basis of two operators can only lead to a separation of the ground and first excited states if effectively only those two states are present, a larger basis is needed in order to gain any improvement on the SS correlator results.

2.10 Summary of Results for the First Excited State

For the Wilson data, the matrix of correlators method was found to successfully isolate the first excited state in the hadron channels of interest. The dependence of the eigenvalues on the normalisation factor ω allowed the contributions of the further excited states to be varied. Cancellation of these contributions enabled the first excited state to be isolated close to the source in the nucleon and Δ channels. Although only an upper bound on the first excited states was obtained using the transfer matrix method, this method used in conjunction with a larger basis of operators should separate the states close to the source, without relying on accidental cancellation. The subtraction fit method was found to be another stable method of extracting the first excited-state masses. However this method is dependent on an unambiguous determination of the ground-state masses and amplitudes, which, as discussed in the previous section, has yet to be obtained.

Table 2.7 summarises the results for the first excited state in the pseudoscalar, vector, nucleon and Δ channels. The results for the ground-state masses from the

Wilson				
	\tilde{m}_{PS}	\tilde{m}_V	\tilde{m}_N	\tilde{m}_Δ
matrix	0.67^{+10+3}_{-6-3}	0.71^{+9+4}_{-7-4}	0.95^{+5+5}_{-3-5}	1.00^{+3+5}_{-1-5}
sub. fit	0.69^{+2+5}_{-2-5}	0.81^{+1+6}_{-2-6}	1.03^{+1+8}_{-1-8}	1.08^{+2+8}_{-2-8}
	m_{PS}	m_V	m_N	m_Δ
<i>LS</i>	0.215^{+7}_{-3}	0.326^{+6}_{-5}	0.50^{+2}_{-1}	0.58^{+1}_{-2}

clover				
	\tilde{m}_{PS}	\tilde{m}_V	\tilde{m}_N	\tilde{m}_Δ
sub. fit	-	0.78^{+3+27}_{-3-27}	0.79^{+7+9}_{-2-9}	0.97^{+4+12}_{-4-12}
	m_{PS}	m_V	m_N	m_Δ
<i>LL</i>	0.214^{+1}_{-1}	0.343^{+9}_{-7}	0.46^{+2}_{-1}	0.56^{+3}_{-2}

Table 2.7: A summary of estimates of the first excited state masses in the meson and baryon channels. The first error quoted is statistical, while the second is an estimate of the systematic errors. Also shown are the values obtained for the ground state masses.

\tilde{m}/m	Wilson		clover	expt	
	matrix	sub. fit.	sub. fit.		
PS	3.1^{+5+3}_{-3-3}	3.2^{+2+4}_{-2-4}	-	η'/η	1.8
V	2.2^{+3+2}_{-3-2}	2.5^{+1+3}_{-1-3}	2.3^{+1+8}_{-2-8}	$\phi(1680)/\phi(1020)$	1.7
N	1.9^{+1+2}_{-1-2}	2.1^{+1+2}_{-1-3}	1.7^{+2+3}_{-1-2}	-	-
Δ	1.7^{+1+2}_{-1-1}	1.9^{+1+2}_{-1-2}	1.7^{+2+3}_{-1-2}	$\Omega(2250)^{-}/\Omega^{-}$	1.4

Table 2.8: The ratios of the first excited state mass to the ground state mass in the meson and baryon channels from the Wilson and Clover actions, compared to the experimental results for hadrons containing strange quarks. The first error quoted is statistical, while the second is an estimate of the systematic errors.

Wilson and clover action, also detailed in the table, are consistent to within 1σ for the pseudoscalar and Δ channels, and 2σ for the vector and nucleon channels. This enables a comparison of the first excited-state masses. The first excited-state masses are all of $O(1)$, and discretisation errors are expected to be significant. The combined statistical and systematic errors provide consistency between the clover and Wilson results; however, considering the magnitude of these errors it is possible that the dependence of the first excited-state masses on a is not small.

The pseudoscalar mass in physical units is approximately 600 Mev for both actions. This corresponds to using a quark mass somewhat less than that of the strange quark. The ratio, \tilde{m}/m , is likely to have less dependence on small changes in the quark mass, and thus a rough comparison can be made between the results and experimental values for the hadrons containing strange quarks, shown in table 2.8. The ratios for all channels are too high, although, again, the combined statistical and systematic errors are large enough to provide consistency within 2σ .

This feature is also seen in the results for the first excited states obtained by QCDPAX and APE using the subtraction fit method as part of the investigations detailed in §(2.1). On chirally extrapolating the excited state masses, QCDPAX obtained $\tilde{m}_\rho/m_\rho = 2.3$ and $\tilde{m}_N/m_N = 2.6$, well above the experimental values of 1.9 and 1.5 [32] for the ρ and nucleon respectively. In contrast, APE found the ratio \tilde{m}/m to be approximately 2.6 for the ρ and 2.8 for the nucleon. The previous suggestion of contamination from excited states in the QCDPAX ground state estimate for the nucleon may account for a significant part of the discrepancy of \tilde{m}_N/m_N with experiment. Similarly, the disagreement between the values of \tilde{m}_ρ/m_ρ from the two groups is consistent with the discrepancy between the ground state vector masses.

These results lend further support to using a method for extracting \tilde{m} which does not depend on a determination of the ground state mass and amplitude. However, table 2.8 shows that using the matrix of correlators method does not provide a significant improvement in the estimates of the first excited state; increased statistics and a larger lattice are needed in order for the use of a matrix method to be advantageous.



Chapter 3

Heavy Quark Physics at Finite Momentum

This chapter analyses the viability of using the general Wilson action with quark masses of $O(1)$ and above. Following a brief motivation, §(3.2) outlines a proposal by Kronfeld et al. [9, 10, 33] for reinterpreting the general Wilson action as a non-relativistic effective action in this limit. This suggests a continuum non-relativistic form for the dispersion relation of hadrons containing one or more heavy quarks, and a dispersion relation of this type, parameterised by two mass scales, is applied to the finite-momentum behaviour of the heavy-light and heavy-heavy pseudoscalar mesons in §(3.5). The success of this dispersion relation is compared with the performance of the continuum relativistic dispersion relation and the free scalar lattice dispersion relation.

Having established the form of the dispersion relation of the pseudoscalar mesons for $1 \lesssim m_Q$, §(3.10) analyses the effects of using the different mass scales to fix the physical quark mass on the predictions for the pseudoscalar and vector decay constants. The experimental measurements of the latter in the charmonium system allow for a concrete test of which of the mass parameters corresponds to the physical quark mass.

3.1 Motivation

Current simulations have lattice spacings which place the charm and bottom quarks in a region where $1 \lesssim m_Q$ and the finite lattice spacing errors of the Wilson action are expected to diverge. However, the considerable theoretical and experimental interest in the properties of hadrons containing one or more heavy quarks, means that this is an area where lattice calculations can have a real impact.

The experimental interest in the heavy-light ($\bar{q}Q$) mesons in particular, centres on the decay constants and the $B\bar{B}$ mixing amplitude, the determination of which allows predictions for the elements of the CKM matrix which are still uncertain. The theoretical interest stems from the additional spin-flavour symmetry manifest in the heavy-quark limit, which enables QCD to be replaced by the heavy-quark effective theory (HQET) (for a review see [34]). For the decay constant of the pseudoscalar meson, this theory predicts the scaling law $f_{PS}\sqrt{M_{PS}} \sim \text{constant}$. Thus, a simple test of the utility of HQET is a determination of the size of the $1/m_Q$ corrections to this scaling law.

Several lattice calculations of f_{PS} have been made [12, 35, 36], but with the c and b quark masses, for example, corresponding to $m_Q \sim 1$ and ~ 2 respectively at $\beta = 6.2$, calculations which used the general Wilson action are forced to extrapolate to the b quark mass from the results around the charm quark mass. An interpolation is possible if the results from calculations in the static limit [37, 38] are included. However, thus far, this has been considered unreliable due to the significant discrepancies between the static limit and the extrapolations to $1/m_Q = 0$ obtained from the results of the propagating theory, with $m_Q \sim 1$.

Thus, a study of the viability of the general Wilson action for $m_Q \gg 1$ is of considerable importance in the calculation of leptonic decay constants. Quarkonia ($\bar{Q}Q$) are ideal for such an analysis. The properties of the charmonium system

have been extensively studied experimentally, and this provides a testing ground for the predictions from the general Wilson action in a region where $1 \lesssim m_Q$.

3.2 Theoretical Toys for Non-Zero Momentum

Free field theory provides an initial testing ground for the proposal that the general Wilson action remains valid in the limit $m_Q \gg 1$. In the absence of gauge fields the Wilson and clover actions have the same form, and a fermion matrix in momentum space of

$$M(p) = m_0 + \sum_{\mu=1}^4 [i\gamma_{\mu} \sin p_{\mu} + (1 - \cos p_{\mu})]. \quad (3.1)$$

Using the condition

$$0 = M(p)M^{\dagger}(p), \quad (3.2)$$

where the 4-momentum in Euclidean space is $p_{\mu} = (E(\vec{p}), \vec{p})$, the following dispersion relation is obtained:

$$\cosh E(\vec{p}) = 1 + \frac{1}{2} \frac{\sum_{i=1}^3 \sin^2 p_i + (m_0 + 2 \sum_{i=1}^3 \sin^2 \frac{p_i}{2})^2}{1 + m_0 + 2 \sum_{i=1}^3 \sin^2 \frac{p_i}{2}}. \quad (3.3)$$

Expanding equation (3.3) in the limit $|\vec{p}|a \ll 1$, the dispersion relation becomes

$$E(p) = M_1 + \frac{|\vec{p}|^2}{2M_2} + \dots \quad (3.4)$$

if M_1 and M_2 are identified as

$$M_1 = \log(1 + m_0) \quad (3.5)$$

$$(M_2)^{-1} = \frac{2 + 4m_0 + (m_0)^2}{m_0(1 + m_0)(2 + m_0)}. \quad (3.6)$$

The zero-momentum energy or “static” mass, M_1 , can be interpreted as counting quarks and anti-quarks, while the “dynamical” mass M_2 determines $\partial E(\vec{p})/\partial |\vec{p}|^2$. The dispersion relation is now in a non-relativistic form and remains valid while

$M_2 \gg |\vec{p}|$. The crucial point is that there is no restriction on M_2 , and this expansion of equation (3.3) does not break down for $M_2 \gg 1$.

An equivalent approach is to use the Foldy-Wouthuysen transformation [39] to decouple the quark and antiquark fields, and then to expand the general Wilson action in the non-relativistic limit. With the inclusion of gauge fields, this expansion takes the form [9, 10, 33]

$$S_{NR} = \phi^\dagger \left[M_1 + D_0 + \frac{1}{2M_2} \vec{D}^2 + \frac{\vec{\sigma} \cdot \vec{B}}{2M_3} + \dots \right] \phi + \text{anti-quark terms}, \quad (3.7)$$

where ϕ is a two-component Pauli spinor representing the quark. Relativistic corrections are suppressed by powers of the heavy-quark velocity, v , and the hyperfine $\vec{\sigma} \cdot \vec{B}$ term in (3.7) corresponds to an $O(v^3)$ correction for heavy-light mesons and $O(v^4)$ for quarkonia [10]. The mass parameter, M_3 , associated with the hyperfine term is given to tree-level by [33]

$$(M_3)^{-1} = (M_2)^{-1} - \frac{1-c}{m_0(1+m_0)}, \quad (3.8)$$

where c corresponds to the coefficient of the $O(a)$ -correction term in the clover action. Note that using the mean field theory approach discussed in §(1.2.3), the higher order corrections to (3.5), (3.6) and (3.8) are estimated to have the effect of changing m_0 to \tilde{m} , where $\tilde{m} = \ln(1/(2\tilde{\kappa}) - 3)$.

By re-expressing M_2 and M_3 in terms of M_1 ,

$$M_2 = e^{M_1} \frac{\sinh M_1}{\sinh M_1 + 1}, \quad (3.9)$$

$$(M_3)^{-1} = (M_2)^{-1} - \frac{1-c}{e^{M_1}(e^{M_1} - 1)}, \quad (3.10)$$

it can be seen that for $M_1 \gg 1$ the ratios M_2/M_1 and M_3/M_1 diverge, and the dynamical, hyperfine and static masses are no longer equal. However, since the static mass appears in (3.7) as a constant term, it is not relevant to the calculation of transition amplitudes and most mass splittings. Hence, the physical quark mass should be fixed using the mass parameter which gives either the correct kinematic

behaviour (M_2), or, in the case of quantities dependent on the $\vec{\sigma} \cdot \vec{B}$ term, the correct hyperfine splitting (M_3).

In the original proposal, Kronfeld et al. suggested using an action similar to the general Wilson action but with distinct hopping parameters for the spatial and temporal components [9]. Thus, by tuning the two κ values, the problem of $M_1 \neq M_2$ for $M_1 \gg 1$ can be removed; if the hyperfine mass is to be tuned simultaneously an additional term must be added to the action. For both this and the general Wilson action, the predictive power of the theory is reduced through the need to fix the physical quark mass with more than one mass parameter.

This approach parallels that of NRQCD [40, 41, 42]; the NRQCD action is discretised in the form of equation (3.7), although M_1 is ignored and normally omitted. Relativistic corrections, such as the hyperfine term, are added systematically to give the desired degree of accuracy. The coefficients of these higher order terms must be tuned in order to match the effective theory to full QCD, either by calculating the coefficients using perturbation theory or fixing to experiment. The former method allows a reduction in the predictive power of the theory to be avoided, while the speed and simplicity of the numerical calculations are a further attractive feature. However, NRQCD is only valid in the perturbative regime, and the power law divergences that arise in perturbation theory restricts $1 > M$. Thus, since present lattice spacings place the charm and bottom quark masses around $O(1)$, it remains advantageous to find an action which is behaved throughout the region of interest from $M \ll 1$ to $M \gg 1$.

This investigation is restricted to the general Wilson action of equation (1.15), and hence the three mass parameters in (3.7) are all functions of a single hopping parameter. Ignoring relativistic corrections, the static mass is the mass extracted from the exponential decay of the 2pt-correlation functions at zero momentum. In order to obtain the dynamical mass for each value of κ , equation (3.4) (where

M_1 and M_2 now represent meson mass parameters) must be matched to the finite-momentum behaviour of the heavy-light or heavy-heavy mesons. If the general Wilson action is suitable for non-relativistic QCD, the meson dispersion relation should have this continuum, albeit unconventional, form. In the following sections (3.4) will be referred to as the two-mass parameter non-relativistic (TMN) dispersion relation. The hyperfine mass is discussed in the next chapter.

If the general Wilson action is not valid for $M \gg 1$, the finite-momentum behaviour of the mesons will be best described by some lattice dispersion relation. Using equation (3.4) to parameterise the meson dispersion relation under these circumstances will result in estimates of the dynamical mass which are highly dependent on the value of the lattice spacing. However, apart from the likelihood of inconsistent estimates of M_2 from different values of momentum, it is difficult to discern any sensitivity to the value of the lattice spacing. The usual procedure of comparing estimates obtained at different β values and using the Wilson and clover actions, flounders since a comparison can only be made if the corresponding values of the static mass are matched. At each value of β , $M_2 \neq M_1$ around $1 \lesssim M_1$; this implies that, in physical units, different values of M_1 will correspond to the same value of M_2 ; hence, assuming the general Wilson action is valid in this limit, and M_2 corresponds to the physical mass, large discretisation errors are expected in M_1 . Thus, large discrepancies between the results for M_2 , for example, between the Wilson and clover actions are not necessarily an indication of large discretisation errors in M_2 .

A comparison with a lattice dispersion relation is necessary. The dispersion relation most relevant to pseudoscalar mesons is derived from the free scalar lattice (FSL) propagator and has the form,

$$4 \sinh^2\left(\frac{E(\vec{p})}{2}\right) = 4 \sinh^2\left(\frac{M}{2}\right) + 4 \sum_{i=1}^3 \sin^2 \frac{p_i}{2}. \quad (3.11)$$

Using this dispersion relation the normalisation of the states becomes $\sinh M$,

and not M ; this normalisation was originally used by Bernard et al. [43] for quark masses of $O(2)$, with the hope that in correctly treating the lattice dependence of the mass, assumed to be significant, other quantities, such as the decay constants, would be less sensitive to discretisation errors. The validity of the dispersion relation itself was not tested.

3.3 Computational Details

The results in the following sections are based on an analysis of 36 gauge configurations at $\beta = 6.0$ with a lattice size of $16^3 \times 48$, and 60 configurations at $\beta = 6.2$ using a lattice size of $24^3 \times 48$. Although the main results are for the clover action, results obtained using the Wilson action on the smaller lattice are presented for comparison. The simulation details are summarised in table 3.1.

The clover quark propagators at both β values were generated at three light quark masses close to the strange quark mass [31]. The κ values for $\beta = 6.0$ were chosen with the criteria that the resulting pseudoscalar masses in physical units should agree roughly with the corresponding masses at $\beta = 6.2$. In addition, heavy-propagators were generated for a range of quark masses in the charm quark region. The Wilson quark propagators were generated for a similar range of heavy-quark masses, and for one-light quark mass corresponding to a light-light pseudoscalar of 600 MeV. For the $\bar{q}Q$ meson channels at $\beta = 6.0$, the correlators were computed using the hopping parameter expansion [44], which provides the correlation function at any value of the heavy quark mass without explicitly calculating the heavy-quark propagators (subject to $\kappa_Q \geq \kappa_Q^{min}$, where $\kappa_Q^{min} \simeq 0.133$ for the clover action and 0.140 for the Wilson action).

The mass splittings between the ground state and excited states are much smaller

clover					
lattice	β	κ_q	κ_Q	smearing	no. cfgs
$16^3 \times 48$	6.0	0.1432, 0.1440	0.133, 0.129, 0.125	LS	36
		0.1445	0.121, 0.111, 0.092		
$24^3 \times 48$	6.2	0.14144, 0.14226	0.133, 0.129, 0.125	LS, SS	60
		0.14262	0.121		

Wilson, $\beta = 6.0, 16^3 \times 48$			
κ_q	κ_Q	smearing	no. cfgs
-	0.140, 0.135, 0.130 0.125	LL	36
0.1550	0.140, 0.135, 0.130 0.125, 0.113, 0.095	LS	16

Table 3.1: The data sets used in this analysis. κ_q and κ_Q are used to denote the values of the hopping parameter for the light and heavy quark respectively.

for mesons containing heavy quarks compared to those involving only light quarks. For this reason smearing becomes essential for heavy-quark propagators. At $\beta = 6.2$, the heavy-quark propagators were calculated using smeared sources, with both smeared and local sinks, and likewise for the $\bar{q}Q$ mesons at $\beta = 6.0$. The gauge-invariant Jacobi smearing technique, described in §(2.3), was used with $\{\kappa_S = 0.25, N = 75\}$ at $\beta = 6.2$ and $\{\kappa_S = 0.25, N = 50\}$ at $\beta = 6.0$, corresponding to smearing radii of ~ 5.2 and 4.2 respectively. These radii are larger in physical units than those used in the previous chapter, since the light-quark propagators used here are not smeared.

Only LL quark propagators were produced for the $\bar{Q}Q$ mesons at $\beta = 6.0$; the physical temporal length of the $16^3 \times 48$ lattice at $\beta = 6.0$ is a factor of $\frac{a^{-1}(\beta=6.2)}{a^{-1}(\beta=6.0)} = 2.7/2.0 \sim 1.4$ larger than that of the $24^3 \times 48$ lattice at $\beta = 6.2$, setting scales using m_ρ . This should compensate for the lack of smearing.

To allow a study of the meson dispersion relations, each correlator was computed at eleven values of momenta at $\beta = 6.2$, where

$$\begin{aligned} \left(\frac{2\pi}{L}\right)^{-1} \vec{p} = & (0, 0, 0), (1, 0, 0), (0, 1, 0), (0, 0, 1) \\ & (1, 1, 0), (1, 0, 1), (0, 1, 1), (1, 1, 1), \\ & (2, 0, 0), (0, 2, 0), (0, 0, 2) \end{aligned}$$

and $L = 24$, and the lowest eight values of these momenta at $\beta = 6.0$, where $L = 16$. To improve statistics the correlators are averaged over all equivalent momenta.

3.4 Fitting Ranges

An extensive and careful study was made of the fitting ranges for the $\bar{Q}Q$ and $\bar{q}Q$ mesons at both zero and finite momentum. The fitting ranges chosen for the

clover, $\beta = 6.2$						
$\frac{12}{\pi} \vec{p} $		0	1	$\sqrt{2}$	$\sqrt{3}$	2
$Q\bar{q}$	PS	11-23 (SS)	11-23 (SS)	11-23 (SS)	15-23 (LS)	15-22 (LS)
	V	13-23 (SS)	11-23 (SS)	11-23 (SS)	15-23 (LS)	15-22 (LS)
$Q\bar{Q}$	PS	15-22 (LS)	15-22(LS)	15-22 (LS)	15-22 (LS)	15-22 (LS)
	V	15-22 (LS)	15-22(LS)	15-22 (LS)	15-22 (LS)	15-22 (LS)

clover, $\beta = 6.0$										
$\frac{8}{\pi} \vec{p} $	0			1		$\sqrt{2}$		$\sqrt{3}$		
κ_Q	0.092	0.111	0.120 0.125 0.129 0.133	0.092	all others	0.092	all others	0.092	all others	
PS	15-23	15-23	15-23	15-22	14-22	15-22	14-22	15-22	14-22	
V	15-23	14-23	12-23	14-22	14-22	14-22	14-22	14-22	14-22	

Wilson, $\beta = 6.0$							
$\frac{8}{\pi} \vec{p} $	0		1			$\sqrt{2}$	$\sqrt{3}$
κ_Q	0.135	0.130, 0.125	0.135	0.130	0.125	all	all
PS	14-18	14-18	14-18	14-18	14-18	13-18	13-18
V	14-18	13-18	12-18	13-18	14-18	14-18	-

Table 3.2: The fitting ranges chosen for the $\bar{Q}Q$ meson correlators generated with LL Wilson and clover quark propagators at $\beta = 6.0$, and both the $\bar{Q}Q$ and $\bar{q}Q$ meson correlators using LS and SS clover quark propagators at $\beta = 6.2$. For the clover data at $\beta = 6.2$, it was not found necessary to use different fitting ranges for different κ values.

$\bar{Q}Q$ mesons at both β values and for both actions are given in table 3.2. Where different smearing combinations present a choice of correlators, the data with a fitting range which best satisfies the fitting procedure of §(1.6.4) was chosen.

For the $\bar{q}Q$ mesons, at $\beta = 6.2$ the fitting ranges used are also detailed in table 3.2, while at $\beta = 6.0$ the fitting range $t = 12$ to 18 was used to fit to the LS correlators for all propagators. The limited statistics available for the $\bar{q}Q$ mesons constructed from the Wilson propagators at $\beta = 6.0$ dictates the omission of alternate timeslices within the fitting range when fitting to the correlator. From the discussion of correlated fits in §(1.6.2), correlators at six different κ values, fitted simultaneously over N timeslices, require roughly $6N$ configurations. Thus, with 16 configurations, only three or four timeslices can be used.

The oscillating phase introduced to extract the correlator at finite momentum (see equation (1.39)) leads to increased statistical noise for higher momenta, and for the Wilson data at $\beta = 6.0$ there is no signal in the vector channel at $\frac{2L}{\pi}|\vec{p}| = \sqrt{3}$.

3.5 Results

3.5.1 A Comparison with the Continuum Dispersion Relation

To begin with, a comparison is made with the usual continuum dispersion relation (denoted here as the standard continuum (SC) dispersion relation),

$$E^2(\vec{p}) - M_1^2 = |\vec{p}|^2 \quad (3.12)$$

where $M_1 = E(\vec{0})$. In order to obtain a clear indication of any deviations from SC dispersion relation as M_1 increases, the energy difference $E^2(\vec{p}) - M_1^2$ is computed, which trivially from (3.12) is predicted to be independent of M_1 . Figures 3.1 and 3.2 present the results for the $\bar{q}Q$ and $\bar{Q}Q$ pseudoscalar meson channels respectively. The results for the vector meson channel show no significant additional features, and are not presented.

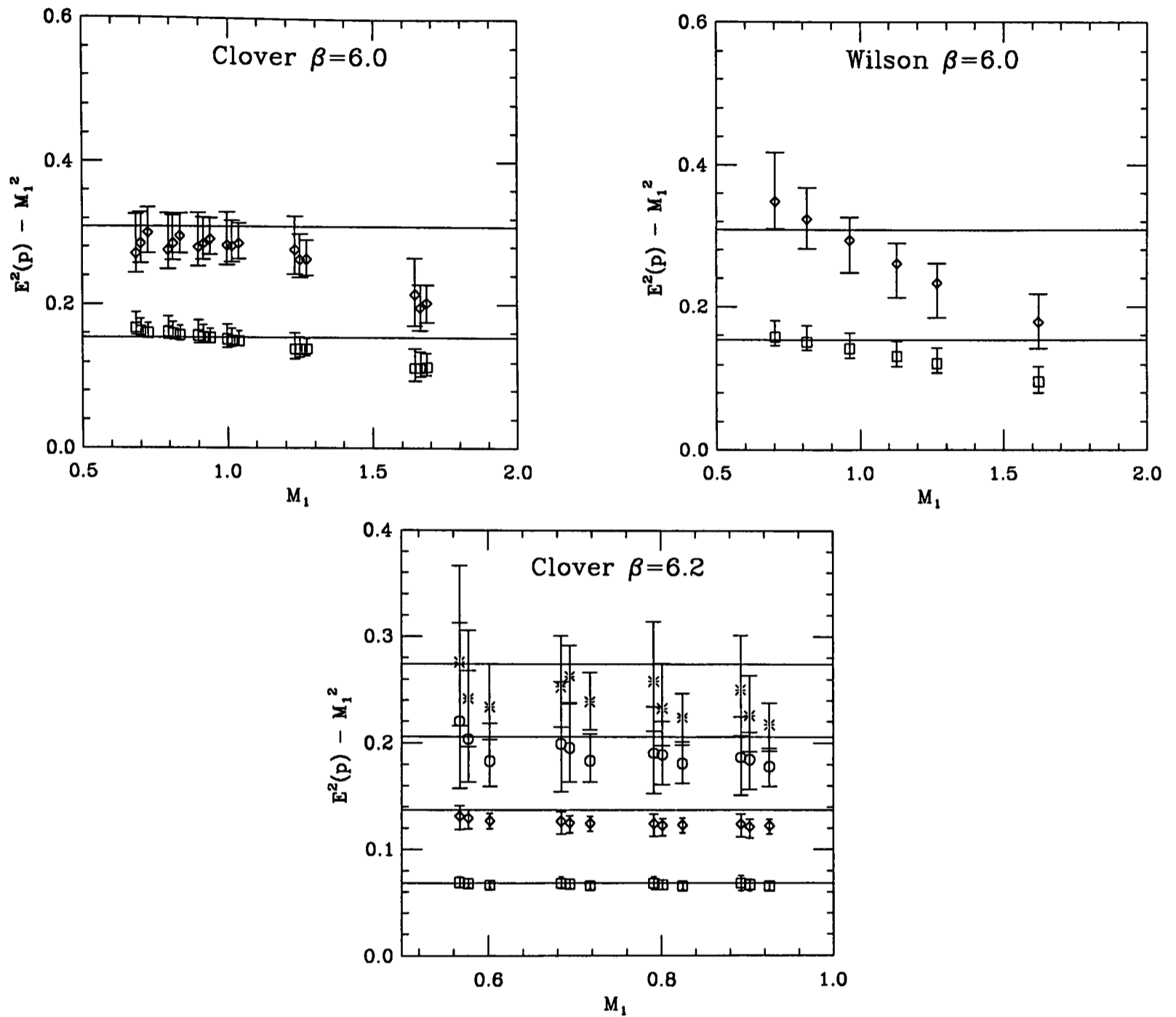


Figure 3.1: $E(\vec{p}^2) - M_1^2$ versus M_1 , for the $\bar{q}Q$ pseudoscalar meson using the clover action at $\beta = 6.2$ and 6.0 , and the Wilson action at $\beta = 6.0$. The results for all combinations of light and heavy-quark mass are shown. The bold lines, are the four(two) values of $|\vec{p}|^2$ at $\beta = 6.2(6.0)$.

Consider the $\bar{q}Q$ pseudoscalar meson channel initially; at $\beta = 6.2$, the static meson masses available for the clover action are below 1; the clover action is valid in this region, and SC behaviour is expected. The results shown in figure 3.1 confirm this, the behaviour of the clover data is consistent with equation (3.12) at all values of $|\vec{p}|$. There is a slight deviation in the results at $\frac{12}{\pi}|\vec{p}| = \sqrt{2}$ and 2, however, at less than 2σ , this is not significant. At $\beta = 6.0$, both the Wilson and clover data show a fair agreement with SC behaviour for static meson masses below $M_1 \sim 1$, but as M_1 increases, a significant disagreement emerges. In addition, the discrepancies between the values of $E^2(\vec{p}) - M_1^2$ and $|\vec{p}|^2$ are worse at larger values of momenta, and this trend suggests that $\partial E(\vec{p})/\partial p^2$ is over-estimated using equation (3.12), where $\partial E(\vec{p})/\partial p^2 = 1/2E(\vec{p})$. The highest momenta are omitted for both actions at this β value, as the statistical errors in $E^2(\vec{p}) - M_1^2$ are prohibitively large.

In figure 3.2 similar behaviour is seen in the $\bar{Q}Q$ pseudoscalar meson channel. For both actions and β values, as the static meson mass increases above 1 equation (3.12) clearly fails to account for the finite momentum behaviour; the discrepancy between the values of $E^2(\vec{p}) - M_1^2$ and $|\vec{p}|^2$ increases with the static meson mass. Note that the deviations from SC behaviour do not appear to depend on the heavy quark mass. For example, for the clover action at $\beta = 6.0$ and one unit of momentum, the value of the energy difference in the $\bar{Q}Q$ pseudoscalar channel is approximately half the value of $|\vec{p}|^2$ for $M_1 \sim 2$. In contrast, a $\bar{q}Q$ meson with the approximately the same static quark mass, i.e. a static meson mass of approximately 1, is consistent with SC behaviour.

3.5.2 Estimating the Dynamical Mass

In order to determine whether the deviations from the SC dispersion relation found for $M_1 > 1$ are due to the dispersion relation being of the TMN form (rather than the general Wilson action no longer being valid), an estimate must be obtained

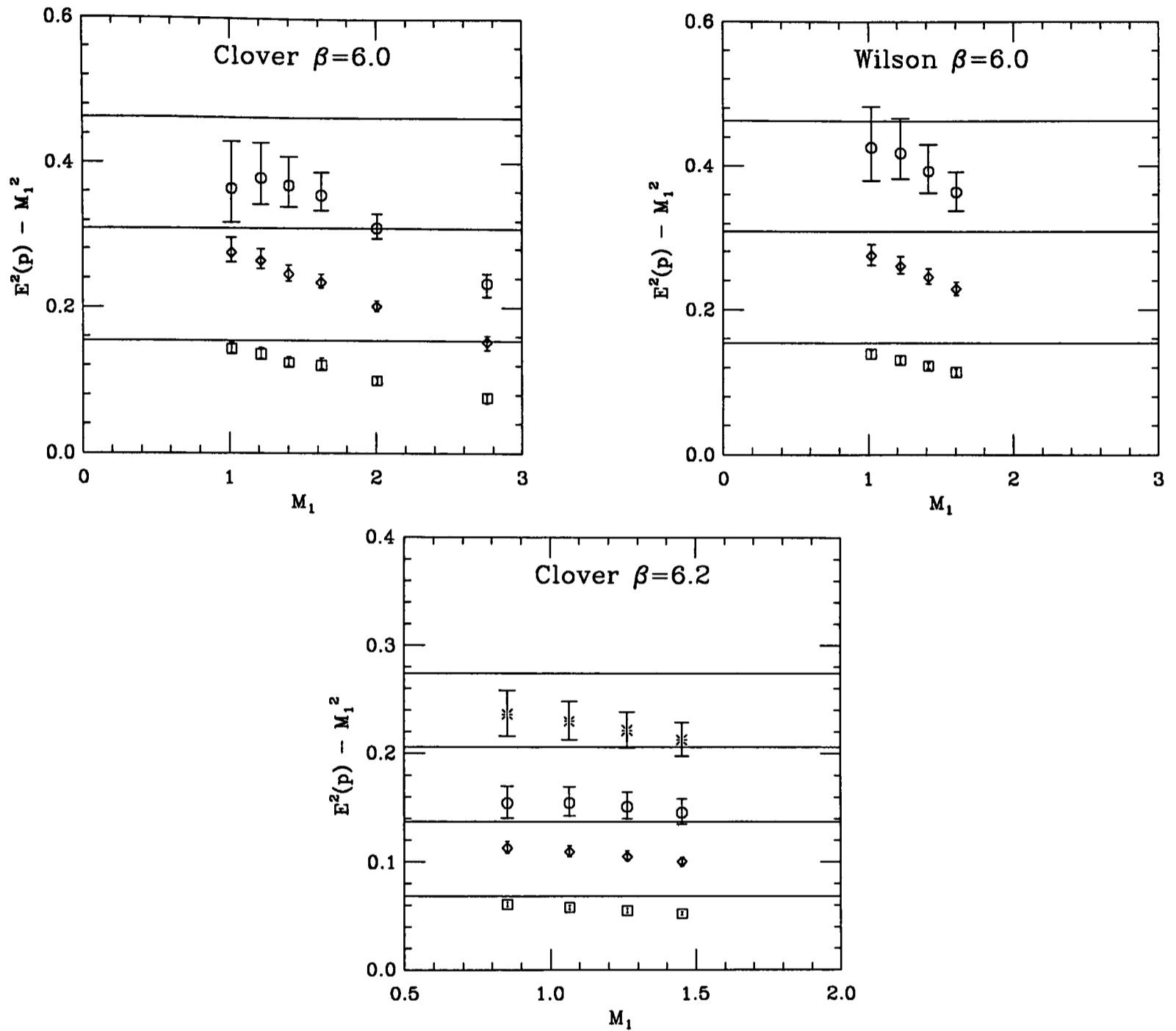


Figure 3.2: $E(\vec{p}) - M_1^2$ versus M_1 , for the $\bar{Q}Q$ pseudoscalar meson using the clover action at $\beta = 6.2$ and 6.0 , and the Wilson action at $\beta = 6.0$. Also shown, as bold lines, are the four(three) values of $|\vec{p}|^2$ at $\beta = 6.2(6.0)$.

for the dynamical mass.

For the $\bar{q}Q$ pseudoscalar meson masses under consideration, at one unit of momentum, $|\vec{p}|/M_1$ ranges between approximately 0.6 – 0.2 at $\beta = 6.0$, and 0.5 – 0.3 at $\beta = 6.2$. Hence, for the smallest heavy-quark masses available, where $M_1 < 1$, the finite momentum behaviour is likely to be relativistic. At the other end of the quark mass range, $|\vec{p}| \ll M_1$, and non-relativistic behaviour is probable. Similarly, for the $\bar{Q}Q$ pseudoscalar meson masses studied, $M_1 \lesssim 1$, $|\vec{p}|/M_1$ ranges between approximately 0.4 – 0.2 at $\beta = 6.0$, and 0.3 – 0.2 at $\beta = 6.2$, and non-relativistic behaviour is expected for all values of the heavy quark mass.

Thus, a definition of M_2 is needed which allows a smooth transition from $M_1 < 1$, where the behaviour is possibly relativistic and agreement was found with the SC dispersion relation, to $M_1 > 1$ where the dispersion behaviour is likely to be non-relativistic and possibly of the TMN form. Substituting equation (3.4) into the energy difference, $E(\vec{p})^2 - M_1^2$, and ignoring terms of $O(v^3)$, provides such a definition of the dynamical mass:

$$M_2 \equiv M_1 \frac{|\vec{p}|^2}{E(\vec{p})^2 - M_1^2}. \quad (3.13)$$

Using this definition, in conjunction with the data at one unit of momentum, the estimates for the ratio M_2/M_1 shown in figure 3.3 are obtained. For this value of the momentum, the restrictions on equation (3.4) of $\vec{p} \ll 1$ and $M_2 \gg |\vec{p}|$, are best satisfied.

Figure 3.3 shows that for $M_1 \lesssim 1$ the estimates of M_2/M_1 are consistent with 1, as expected in a region where the general Wilson action is certainly valid. However, for $M_1 > 1$, the dynamical mass is significantly larger than the static mass. The most surprising feature of the results is that in this region, the values of M_2/M_1 all roughly follow the same curve. Thus, the value of M_2 obtained from a $\bar{Q}Q$ meson with static meson mass M is not consistent with the dynamical mass obtained from a $\bar{q}Q$ meson of mass $M/2$. As noted in the previous section, the deviation

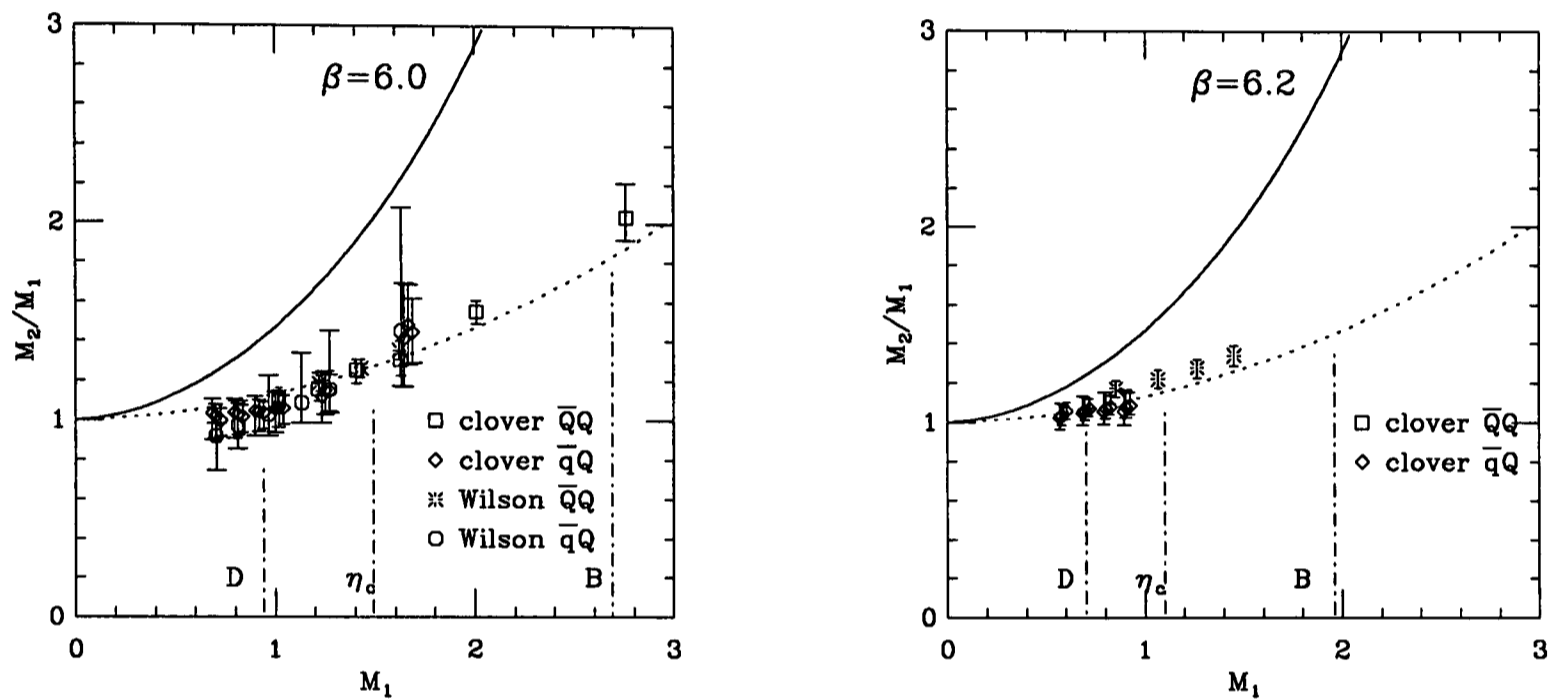


Figure 3.3: M_2/M_1 versus M_1 , for the $\bar{Q}Q$ and $\bar{q}Q$ pseudoscalar mesons. Also included is the predicted dependence of M_2 on M_1 for $\bar{Q}Q$ (dashed line) and $\bar{q}Q$ (bold line) mesons given in equation (3.10). The values of the static mass corresponding to the D , B and η_c mesons, shown in the figure, were obtained using the lattice spacing derived from m_ρ .

Wilson		clover	
M_1	M_2/M_1	M_1	M_2/M_1
1.02^{+3}_{-2}	1.12^{+5}_{-4}	1.02^{+2}_{-2}	1.10^{+4}_{-7}
1.22^{+3}_{-2}	1.19^{+4}_{-4}	1.22^{+2}_{-2}	1.16^{+4}_{-6}
1.43^{+2}_{-2}	1.26^{+4}_{-5}	1.41^{+3}_{-2}	1.25^{+5}_{-6}
1.62^{+2}_{-2}	1.35^{+5}_{-5}	1.63^{+2}_{-2}	1.30^{+5}_{-8}

Table 3.3: A comparison of the results for the ratio of the dynamical and static $\bar{Q}Q$ pseudoscalar meson masses from the Wilson and clover action at $\beta = 6.0$

from SC behaviour, and hence the value of the dynamical mass, is determined by the meson mass rather than the quark mass.

Equation (3.10) provides a prediction for the behaviour of M_2 with M_1 , where the dynamical mass is dependent on the quark mass. Figure 3.3 shows the results in $\bar{Q}Q$ meson channel are in fair agreement with this prediction; however, for the $\bar{q}Q$ mesons, where the agreement with a prediction for the dynamical mass dependent on the quark mass is possibly more expected, (3.10) is found to grossly overestimate the dynamical mass. In the absence of a measurement of M_2 , (3.10) has been used to estimate the magnitude of the dynamical mass for the $\bar{q}Q$ mesons [12, 35].

At $\beta = 6.0$, the static $\bar{Q}Q$ pseudoscalar meson masses from the Wilson and clover action are consistent to within 1σ , and this allows a comparison of the corresponding values of M_2/M_1 , detailed in table 3.3. The same level of consistency is found between the values of M_2/M_1 from the two actions, as expected from figure 3.3, even for the larger meson masses where $M_1 \gg 1$. However, from the discussion in §(3.2), this can only be taken as an indication that the dynamical and static

masses have a similar dependence on the lattice spacing.

Figure 3.3 also shows that at $\beta = 6.0$ the difference between fixing the meson mass on the lattice conventionally by using M_1 , and using the dynamical mass, M_2 , is small close to the D meson. However, extrapolating the $\bar{q}Q$ data along the general curve to the B meson mass, the two masses differ by approximately 40%. This will translate into significant discrepancies between the predictions for physical quantities, such as f_B , obtained using the dynamical and static masses to fix the physical meson mass. Studies of charmonium and bottomonium (for Υ , $M_1 \sim 5.0$ at $\beta = 6.0$), will also be affected. A similar picture is found at $\beta = 6.2$, although the static pseudoscalar meson masses are too small to estimate the magnitude of the dynamical mass for lattice masses of $O(2)$.

3.5.3 A Comparison with the Nonrelativistic Dispersion Relation

The estimates of the dynamical mass presented in the previous section can be used in conjunction with equation (3.4) to predict the dispersion behaviour in the pseudoscalar meson channel. Using the TMN relation, $|\vec{p}|^2$ is predicted to equal

$$[E^2(\vec{p}) - M_1^2] \times \frac{M_2}{M_1}, \quad (3.14)$$

if terms of $O(v^3)$ are neglected. Note that, (3.14) is consistent with the definition of M_2 , and enables a smooth transition from $M_1 > 1$ to $M_1 < 1$.

Figures 3.4 and 3.5 present the results for (3.14) at $\frac{L}{2\pi}|\vec{p}| > 1$, where M_1 is estimated at $\frac{L}{2\pi}|\vec{p}| = 1$. Consider the $\bar{q}Q$ mesons initially; at $\beta = 6.2$ there is reasonable agreement between the values of (3.14) and $|\vec{p}|^2$, at all momentum values and for all M_1 . Since $M_1 < 1$, and $M_1 \sim M_2$, this consistency is no more than that found using the SC dispersion relation. More significantly, at $\beta = 6.0$, the same level of

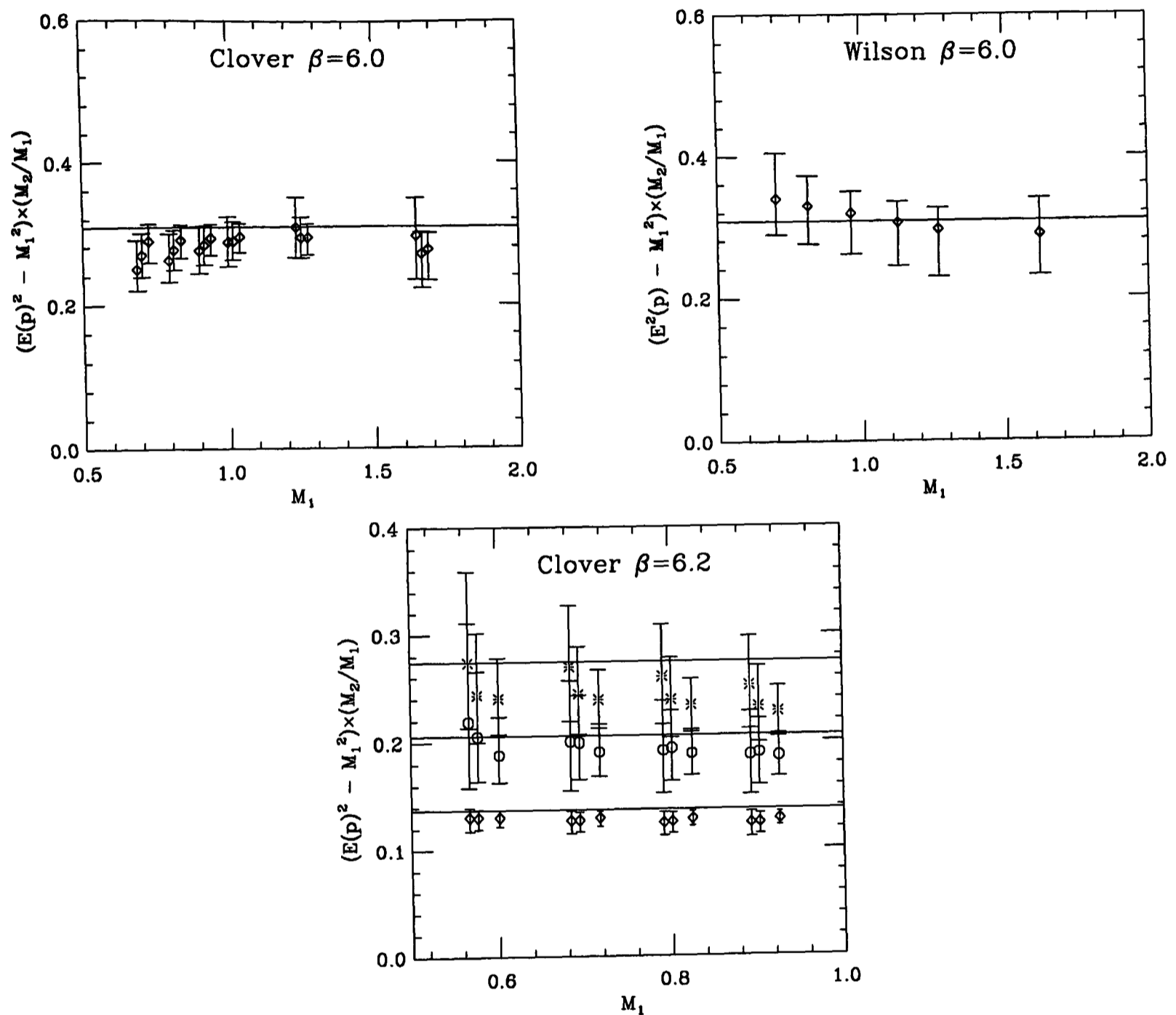


Figure 3.4: $(E(\vec{p})^2 - M_1^2) \times (M_2/M_1)$ versus M_1 , for the $\bar{q}Q$ pseudoscalar mesons. The results are shown for $\frac{12}{\pi}|\vec{p}| = \sqrt{2}, \sqrt{3}, 2$ at $\beta = 6.2$ and $\frac{8}{\pi}|\vec{p}| = \sqrt{2}$ at $\beta = 6.0$, where the value of $|\vec{p}|^2$ is shown as bold lines.

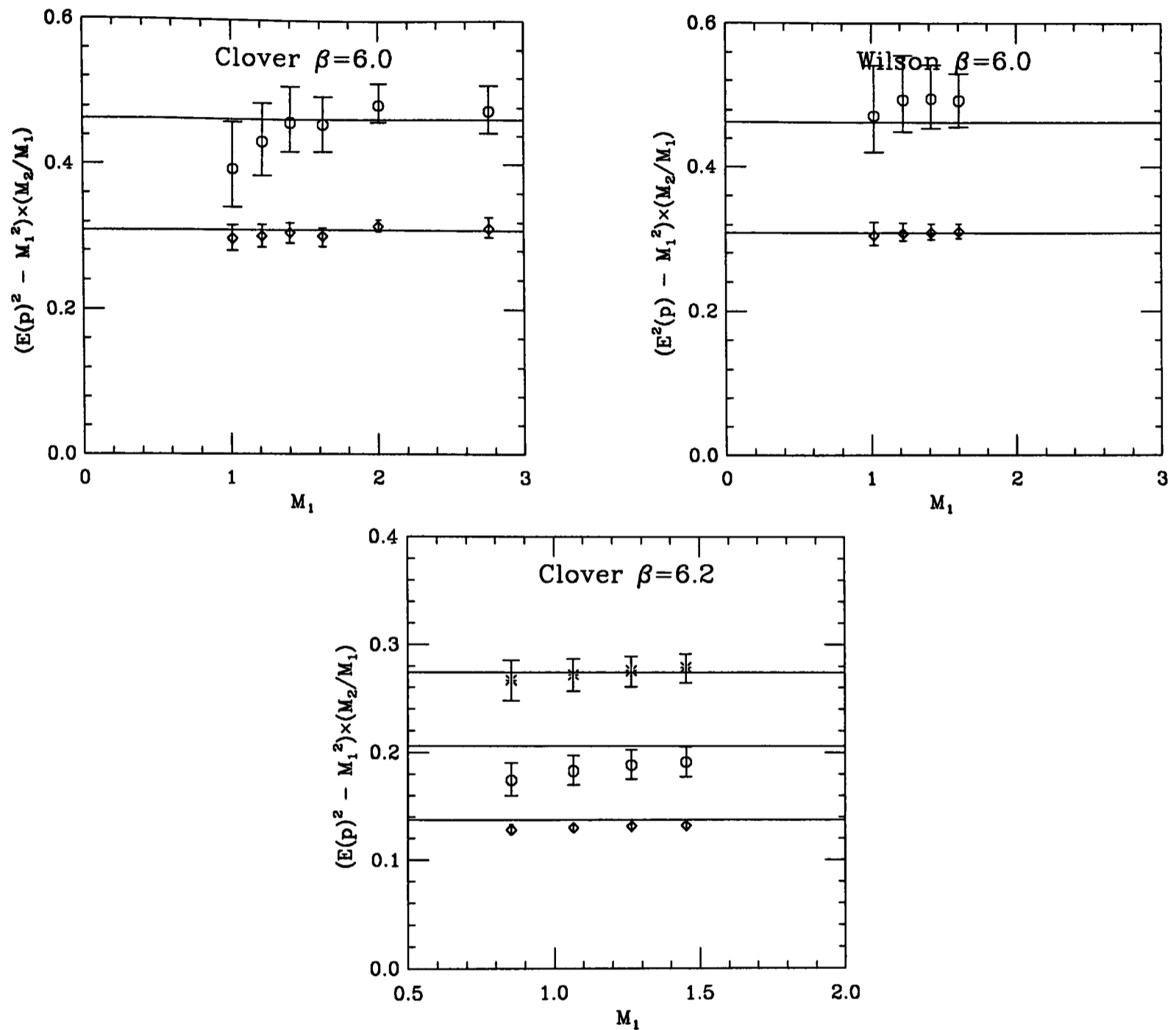


Figure 3.5: $(E(\vec{p})^2 - M_1^2) \times (M_2/M_1)$ versus M_1 , for the $\bar{Q}Q$ pseudoscalar mesons. The results are shown for $\frac{12}{\pi}|\vec{p}| = \sqrt{2}, \sqrt{3}, 2$ at $\beta = 6.2$ and $\frac{8}{\pi}|\vec{p}| = \sqrt{2}, \sqrt{3}$ at $\beta = 6.0$, where the value of $|\vec{p}|^2$ is shown as bold lines.

consistency is found in the results from both actions for $M_1 > 1$. From figure 3.3 $M_1 \neq M_2$, in this region of static quark masses, and the agreement between the values of (3.14) and $|\vec{p}|^2$ at $\frac{8}{\pi}|\vec{p}| = \sqrt{2}$ indicates that a consistent estimate of the dynamical mass would be obtained from the data at this value of momentum. This suggests that $\partial E(\vec{p})/\partial |\vec{p}|^2 \sim 1/2M_2$, and the TMN dispersion relation is a reasonable description of the finite-momentum behaviour.

This is more clearly seen in the results for the $\bar{Q}Q$ pseudoscalar mesons from the clover action at $\beta = 6.2$ and 6.0 , and the Wilson action at $\beta = 6.0$. In particular at $\beta = 6.0$, an impressive agreement is found between the values of (3.14) and $|\vec{p}|^2$, for M_1 as large as ~ 2.8 , at both values of momentum.

Although the accuracy of the predictions for the dispersion behaviour using the estimates of M_2 is the first evidence that the dispersion relation is of a continuum form, some lattice dispersion relation may perform equally well. In the spirit of the analysis thus far, the quantity

$$\sinh^2 \frac{E(\vec{p})}{2} - \sinh^2 \frac{M_1}{2} \quad (3.15)$$

is considered, which from equation (3.11) should equal $\sum_{i=1}^3 \sin^2 \frac{p_i}{2}$. Note that in the limit of $M_1 \ll 1$ and $|\vec{p}| \ll 1$, the FSL dispersion relation is equivalent to the SC dispersion relation.

The values of (3.15) extracted from the $\bar{q}Q$ pseudoscalar meson channel, presented in figure 3.6, show good agreement with the values of $\sum_{i=1}^3 \sin^2 \frac{p_i}{2}$ from all three data sets. At the higher values of momenta, slightly better agreement is found with the FSL dispersion relation than the SC dispersion relation, for static meson masses below 1 where the two dispersion relations are expected to be equivalent. Small discrepancies are seen in the clover data at $\beta = 6.0$ and one unit of momentum, but these are not statistically significant or dependent on the static meson mass.

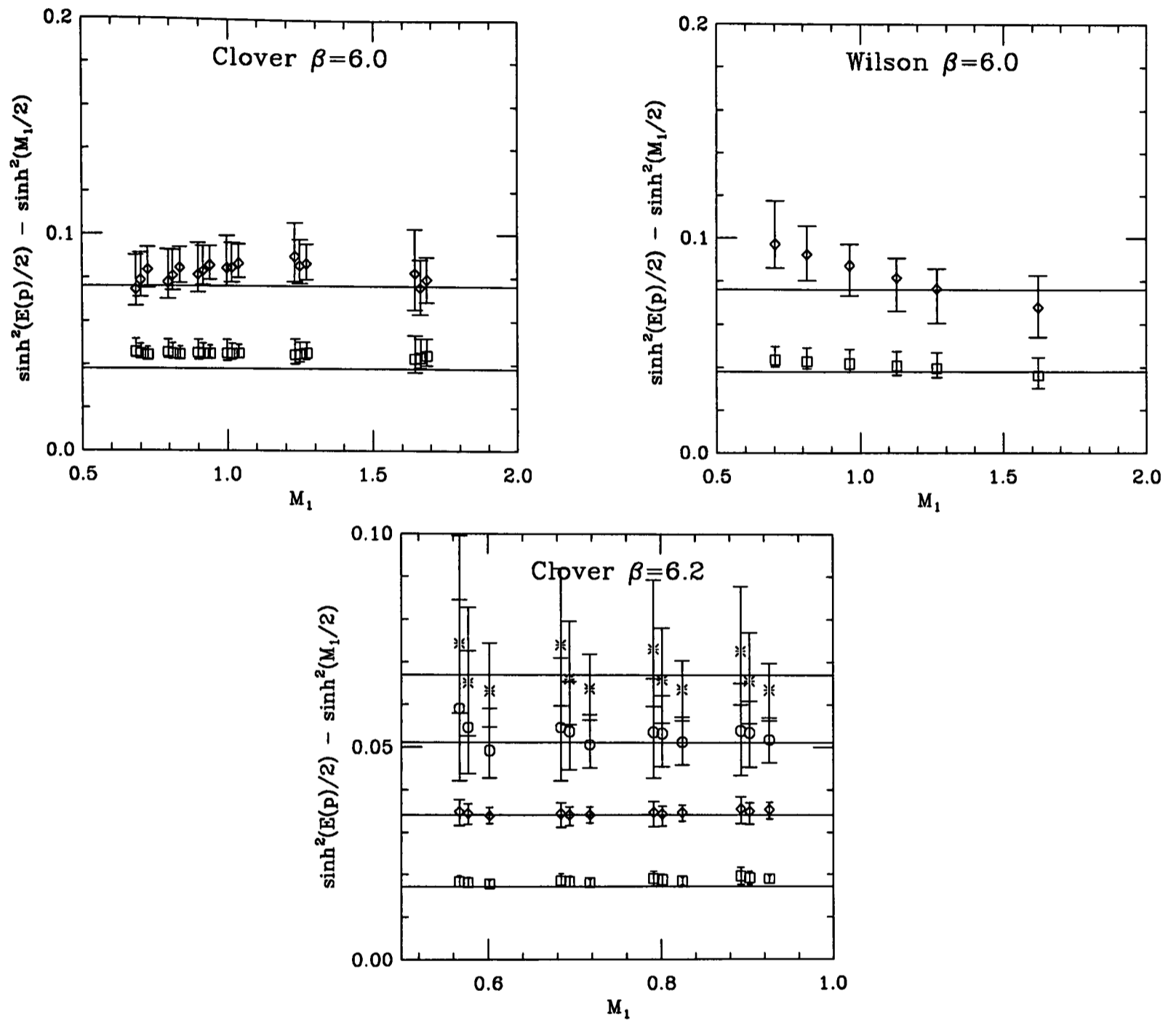


Figure 3.6: $\sinh^2(E(\vec{p}/2)) - \sinh^2(M_1/2)$ versus M_1 , for the $\bar{q}Q$ pseudoscalar mesons. The bold lines show the value of $\sum_{i=1}^3 \sin^2 \frac{p_i}{2}$ for the four(three) values of momenta at $\beta = 6.2(6.0)$.

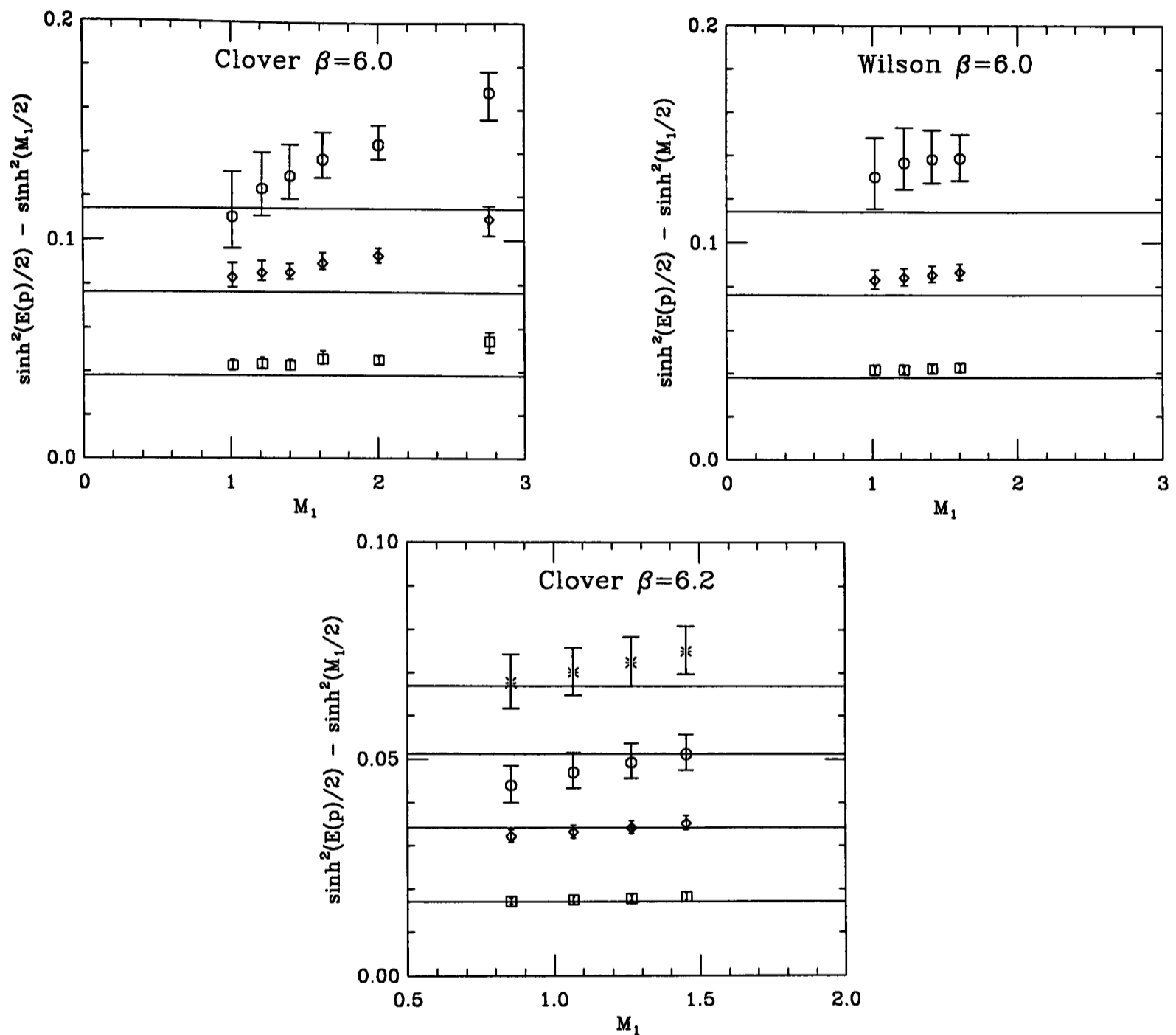


Figure 3.7: $\sinh^2(E(\vec{p}/2)) - \sinh^2(M_1/2)$ versus M_1 , for the $\bar{Q}Q$ pseudoscalar mesons. The bold lines show the value of $\sum_{i=1}^3 \sin^2 \frac{p_i}{2}$ for the four(three) values of momenta at $\beta = 6.2(6.0)$.

However, a serious inconsistency between the data and prediction is found in the results for the $\bar{Q}Q$ pseudoscalar meson, shown in figure 3.7. For the clover action at $\beta = 6.0$, the deviation from the behaviour of equation (3.11) reaches several σ . The deviations are larger for higher values of momentum, and this suggests $\partial E(\vec{p})/\partial|\vec{p}|^2$ is under estimated using the FLS dispersion relation, where $\partial E(\vec{p})/\partial|\vec{p}|^2 \sim 1/\sinh E(\vec{p})$. Equation (3.11) is not valid as a description of finite-momentum behaviour of the $\bar{Q}Q$ pseudoscalar meson channel in this region of static mass values. At $\beta = 6.2$ the FLS dispersion relation still provides a reasonable description of the finite-momentum data. However the values of (3.15) are not independent of M_1 , suggesting large deviations are likely for larger static masses, as found at $\beta = 6.0$.

3.6 Summary

To recap, the finite momentum behaviour of the pseudoscalar mesons with static meson masses below 1 is consistent with the SC dispersion relation. However, as the static meson mass increases above this threshold, the SC dispersion relation clearly provides an under-estimate of $\partial E(\vec{p})/\partial|\vec{p}|^2$. Furthermore, it is the static *meson* mass rather than the quark mass which determines the deviation from SC behaviour. These deviations were quantified through the calculation of the dynamical meson mass. A comparison with a prediction for the dynamical meson mass, where this mass *is* dependent on the quark mass, showed it to be the mesons containing a single heavy quark which are in disagreement with this prediction; the deviations from SC behaviour were found to be smaller than predicted by equation (3.10);

The estimates of the dynamical meson mass obtained at one unit of momentum provided successful predictions for the dispersion behaviour of both the $\bar{Q}Q$ and

$\bar{q}Q$ mesons at higher values of momentum, and even for $M_1 \gg 1$. This strongly suggests that $\partial E(\vec{p})/\partial|\vec{p}|^2 = 1/(2M_2)$ and the dispersion relation in the meson channels is of a TMN form. In comparison, the FSL dispersion relation was found to reproduce the $\bar{q}Q$ meson dispersion behaviour for the range of static meson masses available; however, this agreement does not appear to be fundamental, since equation (3.12) was found to seriously under-estimate $\partial E(\vec{p})/\partial|\vec{p}|^2$ for the $\bar{Q}Q$ mesons.

Only the TMN dispersion relation, of the three dispersion relations considered here, provides the desired description of the finite-momentum behaviour of both the $\bar{Q}Q$ and $\bar{q}Q$ mesons for values of M_1 from $M_1 \ll 1$ to $M_1 \gg 1$, although, as noted in §(3.5.2), the possibility remains for significant discretisation errors in the estimates of the dynamical meson mass. The next step towards a validation of the use of the general Wilson action for $M_1 > 1$, is an investigation of whether the dynamical mass is the correct mass parameter with which to fix the physical quark mass; this is discussed in the next section. An independent measurement of the dynamical mass, is also necessary to provide a check on the results of this section, and quantities suitable for such measurements are indicated in the following sections.

3.7 Determination of the Quark Masses

In order to extract predictions for physical quantities from lattice calculations, the value of the hopping parameter must be found which corresponds to the experimentally observed mass for each quark flavour. In the light quark sector it is generally assumed that the $SU(3)$ flavour symmetry is only broken by the strange quark mass, i.e. $m_u = m_d = 0$. κ_d , the value of κ corresponding to zero quark mass, can be obtained by extrapolating the mass of the pseudoscalar meson

containing $\bar{Q}Q$ quarks according to the PCAC relation,

$$m_{PS}^2 \propto m_q, \quad (3.16)$$

where from equation (1.12)

$$m_{PS}^2 = b_{PS} \left(\frac{1}{\kappa} - \frac{1}{\kappa_d} \right). \quad (3.17)$$

For finite quark mass, it is necessary to obtain the lattice scale by fixing a dimensionful quantity, usually m_ρ , to its experimental value. With this, and an assumption for the functional form for the dependence of hadron masses on the component quark masses based on (3.16), κ_s can be obtained by tuning combinations of hadron masses to their experimental values.

A detailed analysis of the chiral extrapolation and extraction of κ_s for the clover action at $\beta = 6.2$ is contained in references [31] and [45]. In this analysis, equation (3.17) was extended to include $\bar{q}Q$ mesons, where the chiral extrapolation becomes a planar fit in two κ values. Thus, for example, if only one κ value is extrapolated to the chiral limit, m_K^2/m_ρ^2 can be used to obtain κ_s . Using this quantity,

$$\kappa_d = 0.14315 \begin{matrix} + 2 \\ - 2 \end{matrix} \quad \kappa_s = 0.1419 \begin{matrix} + 1 \\ - 1 \end{matrix}. \quad (3.18)$$

Similarly for the clover data at $\beta = 6.0$,

$$\kappa_d = 0.14556 \begin{matrix} + 6 \\ - 6 \end{matrix} \quad \kappa_s = 0.1437 \begin{matrix} + 4 \\ - 5 \end{matrix}. \quad (3.19)$$

In the heavy-quark sector equation (3.17) no longer applies; however, theoretical predictions for the functional dependence of physical quantities on the heavy-quark mass are usually available. Furthermore, it is this dependence which is normally desired. If a theoretical prediction does not exist then any function of the heavy-quark mass, which reproduces the data, may be used providing only an interpolation is necessary. Thus, the value of a physical quantity at, for example,

the charm quark mass is found by interpolating or extrapolating in the meson or quark mass; the lattice scale is used to obtain the quark mass corresponding to charm.

When extracting predictions using the general Wilson action for $M_1 > 1$, where the dynamical, hyperfine and static masses are not equal, it is necessary in the first instance to identify the mass parameter relevant to each physical quantity. Predictions are then extracted following the procedure described in the previous paragraph. If the correct identification has been made and the general Wilson action is valid for $M_1 > 1$, the predictions for each quantity dependent on a particular mass parameter should be consistent with experiment. A comparison of the functional dependence of the quantity on the mass parameter with theoretical prediction provides a further test. However, in practice, the presence of systematic errors in the estimates of physical quantities from, for example, quenching and the finite lattice spacing, means that even if the general Wilson action is valid and the correct mass parameters have been used, the predictions for all physical quantities are unlikely to be consistent with experiment.

In the following sections the dependence of the pseudoscalar and vector decay constants on the dynamical and static masses is compared. The vector decay constant is calculated in the $\bar{Q}Q$ meson channel. Experimental measurements have been made of f_ψ and a determination of the correct mass parameter with which to set the physical quark mass can be attempted. The pseudoscalar decay constant is computed for the $\bar{q}Q$ mesons, and only preliminary experimental measurements have been made of this quantity even for the D meson. Hence, it is difficult to determine whether or not the dynamical mass is the correct mass parameter to use, and only an analysis of the uncertainty in the predictions due to the uncertainty in the mass scale is attempted. However, a rough ¹ comparison of the predictions extracted at $\beta = 6.2$ and 6.0 from the Wilson and clover actions can be made. An

¹A detailed analysis of the errors in the estimates in lattice spacing is not presented here

indication of a reduction in the discretisation errors in the estimates of f_D and f_B using the dynamical mass (through a reduction in the dependence on the value of the lattice spacing) is a positive sign for the dynamical mass being the correct mass parameter with which to fix the physical quark mass.

3.8 Renormalisation Constants: Z_A and Z_V

Before the decay constants calculated on the lattice can be compared with the experimental values, they must be multiplied by the appropriate renormalisation constants. For the clover action with rotated operators these have been calculated at one-loop order in perturbation theory:

$$Z_V^C = 1 - 0.10g^2 \quad (3.20)$$

$$Z_A^C = 1 - 0.02g^2 \quad (3.21)$$

Using the boosted coupling, $g^2 = 6/(\beta u_0^4)$, mentioned in §(1.2.3), with the definition of the average link $u_0 = (8\kappa_d)^{-1}$, $Z_A^C \simeq 0.97(0.96)$ and $Z_V^C \simeq 0.83(0.82)$ at $\beta = 6.2(6.0)$ are obtained. It should be noted that recent non-perturbative determinations of Z_A , at $\beta = 6.0$, suggest the non-perturbative value could be larger by about 15% [46], and thus a considerable uncertainty exists in the value of this renormalisation constant. In the same study, Z_V was found to be consistent with the perturbative result.

For the Wilson action, with the conventional quark field normalisation, $\sqrt{2\kappa}$,

$$Z_V^W = 1 - 0.17g^2 \quad (3.22)$$

$$Z_A^W = 1 - 0.13g^2 \quad (3.23)$$

to be compared with [9],

$$Z_V^W = 1 - (0.17 - 0.11)g^2 \quad (3.24)$$

$$Z_A^W = 1 - (0.13 - 0.11)g^2 \quad (3.25)$$

	$\beta = 6.0$		$\beta = 6.2$
	clover	Wilson	clover
\sqrt{K}	2.02 ⁺³ ₋₃		2.73 ⁺⁵ ₋₅
m_ρ	2.0 ⁺² ₋₂	2.2 ⁺¹ ₋₁	2.7 ⁺¹ ₋₁
f_π	2.1 ⁺² ₋₁	-	3.4 ⁺² ₋₁
1P-1S	2.2 ⁺⁴ ₋₃	-	2.8 ⁺¹ ₋₁

Table 3.4: The estimates of a^{-1} extracted from various quantities for the clover action at $\beta = 6.2$ and 6.0 and the Wilson action at $\beta = 6.0$.

for the heavy-quark normalisation, $\sqrt{1 - 6\tilde{\kappa}}$. Thus, using the $\sqrt{2\kappa}$ prescription at $\beta = 6.0$,

$$Z_V^W = 0.57, \quad Z_A^W = 0.67 \quad (3.26)$$

compared to

$$Z_V^W = 0.84, \quad Z_A^W = 0.95 \quad (3.27)$$

using $\sqrt{1 - 6\tilde{\kappa}}$.

3.9 Setting the Physical Scale

In order to convert a lattice quantity into physical units it is necessary to know the value of the lattice scale. This can be obtained by relating a dimensionful quantity to its physical value. It is desirable to calculate the lattice scale from as many quantities as possible, since consistency between the estimates of a^{-1} is proof that scaling has been achieved. Table 3.4 gives the estimates of a^{-1} obtained from the most commonly-used quantities, for the clover action at $\beta = 6.2$ and 6.0, and the Wilson action at $\beta = 6.0$. Details of the extraction of a^{-1} from the string

tension (\sqrt{K}), m_ρ and f_π at $\beta = 6.2$, are contained in references [47] and [31] respectively, while the results from the $1P - 1S$ splitting at both β values are preliminary [48].

With the exception of f_π at $\beta = 6.2$, the consistency between the various estimates of a^{-1} is encouraging. There is a large uncertainty in the lattice spacing from f_π due to the need to use the renormalisation constant Z_A . The perturbative values of Z_A detailed in §(3.8) were used to obtain the values given in the table; however, as noted in the previous section, Z_A may be significantly larger than the perturbative estimates, which would lead to a reduced estimate of a^{-1} . Furthermore, in reference [47], the ratio f_K/f_π (which does not require Z_A) was found to be in good agreement with experiment.

The predictions for physical quantities are presented in this thesis as part of an exploratory study of the correct mass parameter to use to fix the quark mass; only a rough comparison of the predictions at different β values and with experiment is necessary. Thus, the uncertainties in the predictions introduced by the statistical and systematic errors in the lattice spacing are not considered, and the lattice spacing taken to be

$$a^{-1} = 2.0 \text{ GeV} \quad \beta = 6.0, \quad (3.28)$$

$$a^{-1} = 2.7 \text{ GeV} \quad \beta = 6.2. \quad (3.29)$$

3.10 Decay Constants From Zero- and Finite-Momentum Propagators

3.10.1 Pseudoscalar Decay Constant

The decay constant, f_{PS} , of the pseudoscalar meson is defined as

$$f_{PS}p_\mu = \langle 0|A_\mu|PS\rangle, \quad (3.30)$$

where A_μ represents the axial-vector current. In this study, f_{PS} was found by computing the ratio

$$\frac{C_{A_\mu P}^{LS}(t)}{C_{PP}^{SS}(t)} \equiv \frac{\sum_{\vec{x}} \langle A_L^\mu(\vec{x}, t) P_S^\dagger(0) \rangle}{\sum_{\vec{x}} \langle P_S(\vec{x}, t) P_S^\dagger(0) \rangle} \sim \frac{f_{PS}p^\mu}{Z_A \langle 0|P_S|PS\rangle} \tanh E(\vec{p})(L_t/2 - t), \quad (3.31)$$

where P_S represents a smeared pseudoscalar operator. Following the reasoning of §(3.2), for $M_1 \gg 1$, the dynamical meson mass corresponds to the physical pseudoscalar meson mass appearing in the l.h.s. of equation (3.30) at zero-momentum, and must be distinguished from the static meson mass appearing in the hyperbolic function in (3.31). This implies that at finite momentum, the fourth component of equation (3.30) behaves as,

$$f_{PS}E^{phys}(\vec{p}) = f_{PS}(M_{PS2} + \frac{|\vec{p}|^2}{2M_{PS2}} + \dots) \quad (3.32)$$

for $M_{PS2} \gg |\vec{p}|$, where M_{PS2} represents the dynamical pseudoscalar meson mass and $E^{phys}(\vec{p})$ is the fourth component of p_μ in (3.30). Note that an estimate of f_{PS} can be obtained without any assumptions about the mass parameter using the spatial components of the ratio (3.31), and likewise for the combination $f_{PS}E^{phys}(\vec{p})$. Thus, the dispersion behaviour in equation (3.32), and hence the assumption $M_{PS}^{phys} = M_{PS2}$, can be verified.

In the heavy-quark limit, the quantity $f_{PS}\sqrt{M_{PS}^{phys}}$ scales like

$$f_{PS}\sqrt{M_{PS}^{phys}} = \text{const.} \times [\alpha_a(M_{PS}^{phys})]^{-2/\beta_0}, \quad M_{PS}^{phys} \rightarrow \infty \quad (3.33)$$

Since $f_{PS}M_{PS}^{phys}$, rather than (3.33), is extracted from $C_{A_\mu P}^{SS}(t)/C_{PP}^{LS}(t)$ at zero-momentum, possible deviations from this scaling law are studied by computing the quantity

$$\Phi(M) \equiv (\alpha_s(M)/\alpha_s(M_B))^{2/\beta_0} Z_A^{-1} \frac{f_{PS}M_{PS}^{phys}}{\sqrt{M}} \quad (3.34)$$

for $M = M_{PS1}$ (which assumes implicitly that $M_{PS}^{phys} = M_{PS1}$), and $M = M_{PS2}$ (which assumes that $M_{PS}^{phys} = M_{PS2}$). If the correct mass parameter is not determined, by comparing $\Phi(M_{PS1})$ and $\Phi(M_{PS2})$ the resulting uncertainty in any such deviations can be found. The strong coupling, $\alpha_s(M)$, is approximated using

$$\alpha_s(M) = \frac{2\pi}{\beta_0 \log(M/\Lambda_{QCD})} \quad (3.35)$$

where $\beta_0 = 11 - \frac{2}{3}n_f$, with $n_f = 0$ in the quenched approximation, and $\Lambda_{QCD} = 200$ MeV. It should be noted that $\Phi(M)$ is fairly insensitive to different choices of Λ_{QCD} (e.g. using $\Lambda_{QCD} = 250$ MeV) or for the anomalous dimension (e.g., taking $n_f = 4$).

The decay constant can be extracted in different ways, however, (3.31) was found to give the most precise determination. At $\beta = 6.2$ for the clover action, the ratio of correlators was fitted in the range $t = 15$ to 22 for all combinations of light and heavy-quark masses, at all but the highest value of momentum. The values of $E(\vec{p})$ and $\langle 0|P_S|PS\rangle$ extracted from the SS pseudoscalar correlators, using the fitting ranges detailed in table (3.2), were then used to obtain the decay constant. At $\beta = 6.0$, the fitting range $t = 12$ to 18 was chosen for the ratio obtained using the clover action, while $t = 11$ to 17 , omitting alternate timeslices, was used for the Wilson data; the SS pseudoscalar correlators were fitted between $t = 12$ and 18 for both actions. Only results at zero momentum were obtained for both actions, as the statistical errors in the fourth component of the ratio was found to be prohibitively large at finite values of momentum. Unfortunately, no signal was found for $C_{A_i P}^{LS}(t)$ at $\beta = 6.2$, while at $\beta = 6.0$ the relevant correlators were not available.

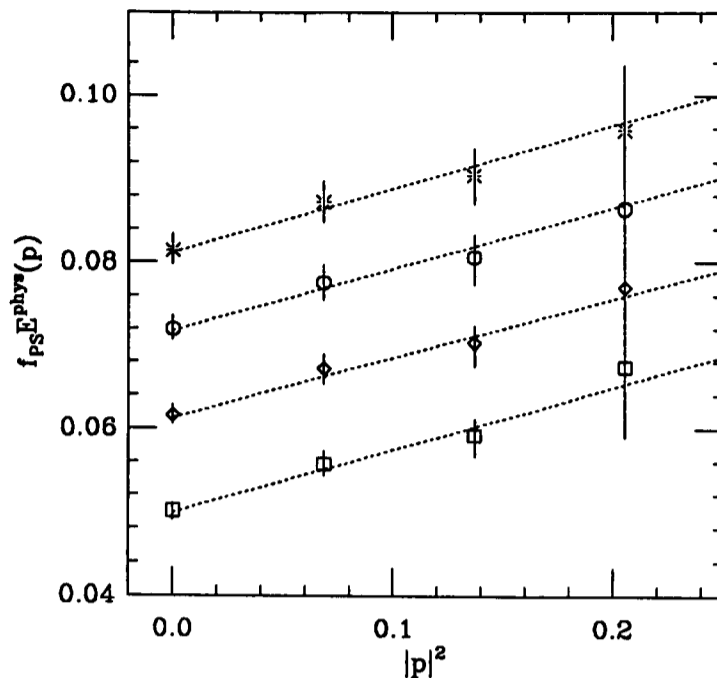


Figure 3.8: $f_{PS} E^{phys}(\vec{p})$ as a function of $|\vec{p}|^2$, from the clover action at $\beta = 6.2$ with $\kappa_q = 0.14144$ and $\kappa_Q = 0.121$ (bursts), 0.125 (circles), 0.129 (diamonds) and 0.133 (squares). The dashed lines represent linear fits to the data for each value of the heavy-quark mass.

3.10.2 Results for the Pseudoscalar Decay Constant

The results for $f_{PS} E^{phys}(\vec{p})$ from the clover action for one value of the light quark mass at $\beta = 6.2$ are presented in figure 3.8, plotted against $|\vec{p}|^2$. A linear dependence on $|\vec{p}|^2$ is apparent and fits were performed to the data at each value of the heavy-quark mass, using

$$f_{PS} E^{phys}(\vec{p}) = a_1 + a_2 |\vec{p}|^2, \quad (3.36)$$

The fit parameters obtained are given in table 3.5. In the absence of an independent measurement of f_{PS} from the spatial components of (3.31) it is not possible to test whether the dispersion behaviour is equivalent to the SC behaviour of a pseudoscalar meson of mass M_{PS2} . However, for the dynamical and static pseudoscalar meson masses corresponding to these values of the heavy-quark mass (also detailed in the table), $M_{PS1} \sim M_{PS2}$, and the dispersion behaviour can be expected to be of the form in equation (3.32) even if this is not true at heavier quark

κ_Q	0.133	0.129	0.125	0.121
a_1	0.050^{+1}_{-1}	0.060^{+1}_{-1}	0.072^{+2}_{-1}	0.081^{+2}_{-2}
a_2	0.08^{+1}_{-1}	0.07^{+1}_{-1}	0.07^{+2}_{-1}	0.08^{+2}_{-2}
χ^2	1.1/2	1.3/2	1.4/2	1.4/2
$\sqrt{a_1/2a_2}$	0.58^{+4}_{-4}	0.66^{+7}_{-5}	0.70^{+8}_{-6}	0.73^{+9}_{-7}
M_{PS1}	0.601^{+3}_{-1}	0.717^{+3}_{-1}	0.824^{+4}_{-1}	0.926^{+4}_{-1}
M_{PS2}	0.62^{+2}_{-3}	0.75^{+3}_{-3}	0.86^{+5}_{-4}	0.97^{+6}_{-4}

Table 3.5: The fit parameters obtained from a linear fit to $f_{PS}E^{phys}(\vec{p})$ using equation 3.36, for the clover action at $\beta = 6.2$ with $\kappa_q = 0.14144$.

masses when $M_{PS1} \ll M_{PS2}$. From (3.36) and (3.32),

$$\sqrt{a_1/2a_2} \sim M_{PS2} \sim M_{PS1}. \quad (3.37)$$

The results detailed in table 3.5 are in rough agreement with this.

In figure 3.9 (i), the values of $\Phi(M_{PS1})$ obtained using the clover action at $\beta = 6.2$ are shown as a function of $1/M_{PS1}$. At each value of the light quark mass, $\Phi(M_{PS1})$ increases as the heavy-quark mass increases, and it is interesting to note that this increase is more rapid for larger values of the light quark mass. For the chirally extrapolated data, it was possible to perform a linear fit using a fit function of the form:

$$\Phi(M) = b_1 \left(1 - \frac{b_2}{M} \right) \quad (3.38)$$

The fit parameters obtained are detailed in table 3.6. Using the extrapolation to the limit of infinite heavy-quark mass, the non-scaling corrections at the D and B meson masses are found to be of order 30% and 10% respectively. If the logarithmic dependence in equation (3.33) is ignored, the slope of $f_{PS}M_{PS}^{phys}/\sqrt{M_{PS1}}$

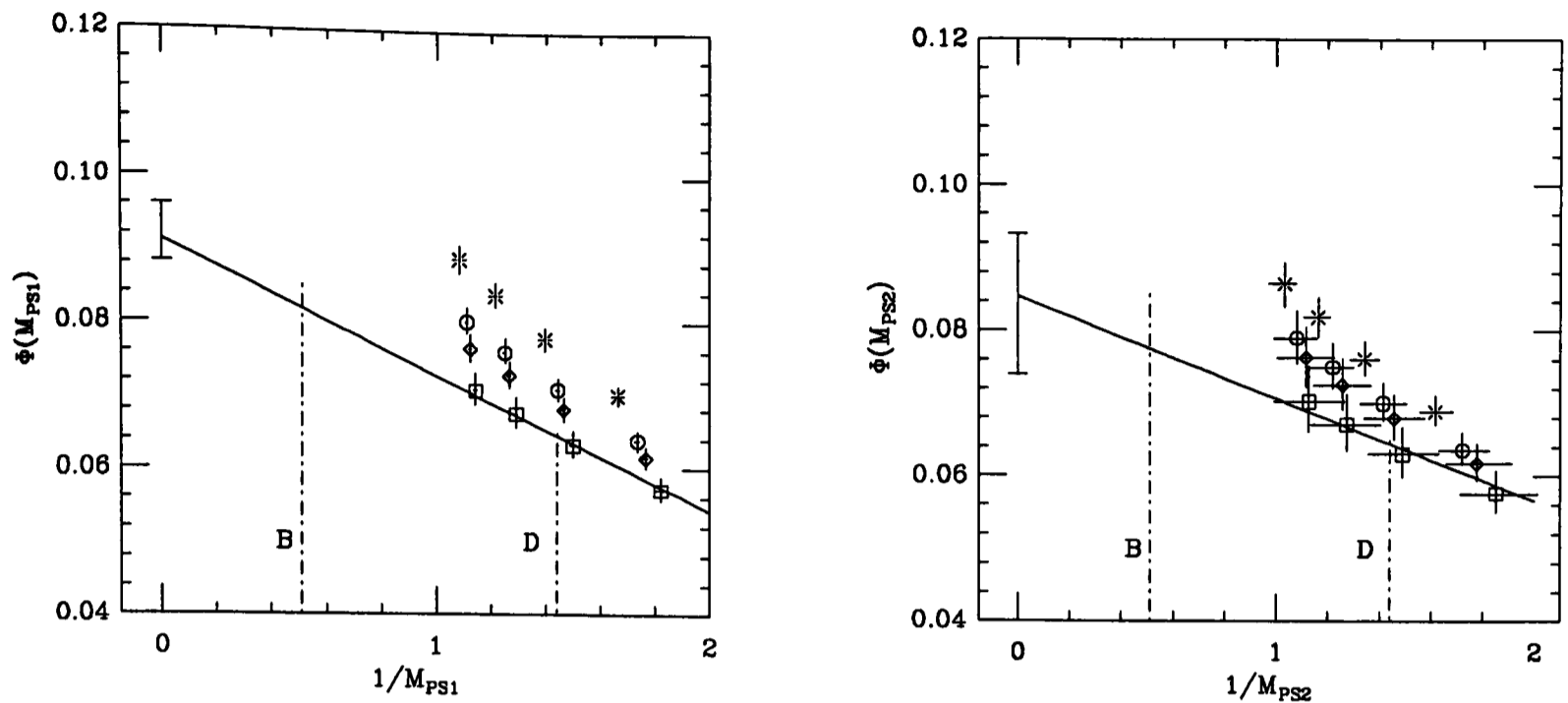


Figure 3.9: $\Phi(M)$ as a function of $1/M$, where (i) $M = M_{PS1}$ and (ii) $M = M_{PS2}$, for the clover action at $\beta = 6.2$. Linear fits to the chirally-extrapolated points (squares) are represented by the solid lines. Also shown are the statistical errors of the extrapolation to the infinite mass limit.

clover $\beta = 6.2$			
	b_1	b_2	χ^2
M_{PS1}	$0.091 \begin{smallmatrix} + 5 \\ - 3 \end{smallmatrix}$	$0.20 \begin{smallmatrix} + 1 \\ - 2 \end{smallmatrix}$	1.3/2
M_{PS2}	$0.085 \begin{smallmatrix} + 9 \\ - 11 \end{smallmatrix}$	$0.17 \begin{smallmatrix} + 4 \\ - 3 \end{smallmatrix}$	1.4/2

Table 3.6: The values of the fit parameters of the linear fits to the behaviour of $\Phi(M)$, where M is either the dynamical or static pseudoscalar meson mass, for the clover data at $\beta = 6.2$.

with $1/M_{PS1}$ becomes more pronounced but a linear function is still successfully fitted to the data.

For comparison, figure 3.9 (ii) presents the results for $\Phi(M_{PS2})$, plotted against $1/M_{PS2}$. As noted previously, for the range of heavy-quark masses available,

clover $\beta = 6.2$ $\kappa_q = \kappa_d = 0.1419$				
	c_1	c_2	c_3	χ^2
M_{PS1}	$0.13 \begin{smallmatrix} + 1 \\ - 1 \end{smallmatrix}$	$0.38 \begin{smallmatrix} + 3 \\ - 3 \end{smallmatrix}$	$0.11 \begin{smallmatrix} + 2 \\ - 3 \end{smallmatrix}$	0.2/1
M_{PS2}	$0.13 \begin{smallmatrix} + 2 \\ - 2 \end{smallmatrix}$	$0.43 \begin{smallmatrix} + 17 \\ - 9 \end{smallmatrix}$	$0.17 \begin{smallmatrix} + 7 \\ - 12 \end{smallmatrix}$	0.0/1

Table 3.7: The values of the fit parameters of the quadratic fits to the behaviour of $\Phi(M)$, where M is either the dynamical or static pseudoscalar meson mass, for the clover data at $\beta = 6.2$ and $\kappa_q = \kappa_s$.

$M_{PS1} \sim M_{PS2}$, and there is no qualitative difference between results from the static and dynamical masses. This is reflected in the $\sim 25\%$ and $\sim 10\%$ non-scaling corrections found for f_D and f_B respectively, by performing a linear fit on the data points. The fit parameters obtained are also given in table 3.6.

As seen in the figures, a prediction for f_D can be obtained by interpolating between existing data point, using the fit parameters in table 3.6, while an extrapolation is necessary to reach f_B . In order to extract estimates for f_{D_s} and f_{B_s} , the same procedure must be applied to data which has been interpolated to $\kappa_q = \kappa_s$. At this value of the light quark mass, it was found that a successful fit could not be performed to data points without the inclusion of a quadratic term in the fitting function, which becomes

$$\Phi(M) = c_1 \left(1 - \frac{c_2}{M} + \frac{c_3}{M^2} \right) \quad (3.39)$$

Not surprisingly, the fit parameters obtained, given in table 3.7, show the quadratic term is significant for both $M = M_{PS1}$ and M_{PS2} .

The resulting estimates for the decay constants are presented in table 3.8, where the perturbative estimates given in §(3.8) are used for Z_A . There are scant experimental measurements with which to compare. Currently, only an upper bound

clover $\beta = 6.2$						
	f_D	f_B	f_{D_s}	f_{B_s}	f_{D_s}/f_D	f_{B_s}/f_B
M_{PS1}	186^{+6}_{-5}	150^{+7}_{-4}	212^{+5}_{-5}	194^{+7}_{-6}	1.14^{+2}_{-3}	1.29^{+5}_{-5}
M_{PS2}	186^{+15}_{-16}	142^{+13}_{-16}	207^{+12}_{-11}	190^{+15}_{-21}	1.11^{+6}_{-4}	1.34^{+13}_{-13}

Table 3.8: The estimates of the decay constants of the D , B , D_s and B_s mesons obtained from the clover data at $\beta = 6.2$ using the dynamical and static pseudoscalar meson masses.

on f_D of 290 MeV exists. However, the first measurement of f_{D_s} has been made by the WA75 collaboration [49], who found

$$f_{D_s} = 232 \pm 45 \pm 20 \pm 48 \text{ GeV}. \quad (3.40)$$

Considering the large uncertainty in this estimate, little can be read into the consistency between this and the values of f_{D_s} in table 3.8.

The ratios f_{D_s}/f_D and f_{B_s}/f_B can be determined to a greater degree of accuracy, and since they are independent of the values of the lattice spacing and Z_A , some of the systematic errors are expected to cancel. Table 3.8 shows the ratios obtained using the dynamical and static masses are consistent.

At $\beta = 6.0$, the range of quark masses available probe a region much closer to the b quark mass, and the difference between using the dynamical and static masses is more striking. Non-linear behaviour with $1/M_{PS1}$ is clearly seen in the results for $\Phi(M_{PS1})$ from the clover action, plotted in figure 3.10 (i). In contrast, if the dynamical mass is used instead linear behaviour is apparent. Quadratic and linear fits were performed to $\Phi(M_{PS1})$ and $\Phi(M_{PS2})$ respectively, yielding the fit parameters detailed in table 3.9. Although the statistical errors in $\Phi(M)$ and M are larger for $M = M_{PS2}$,

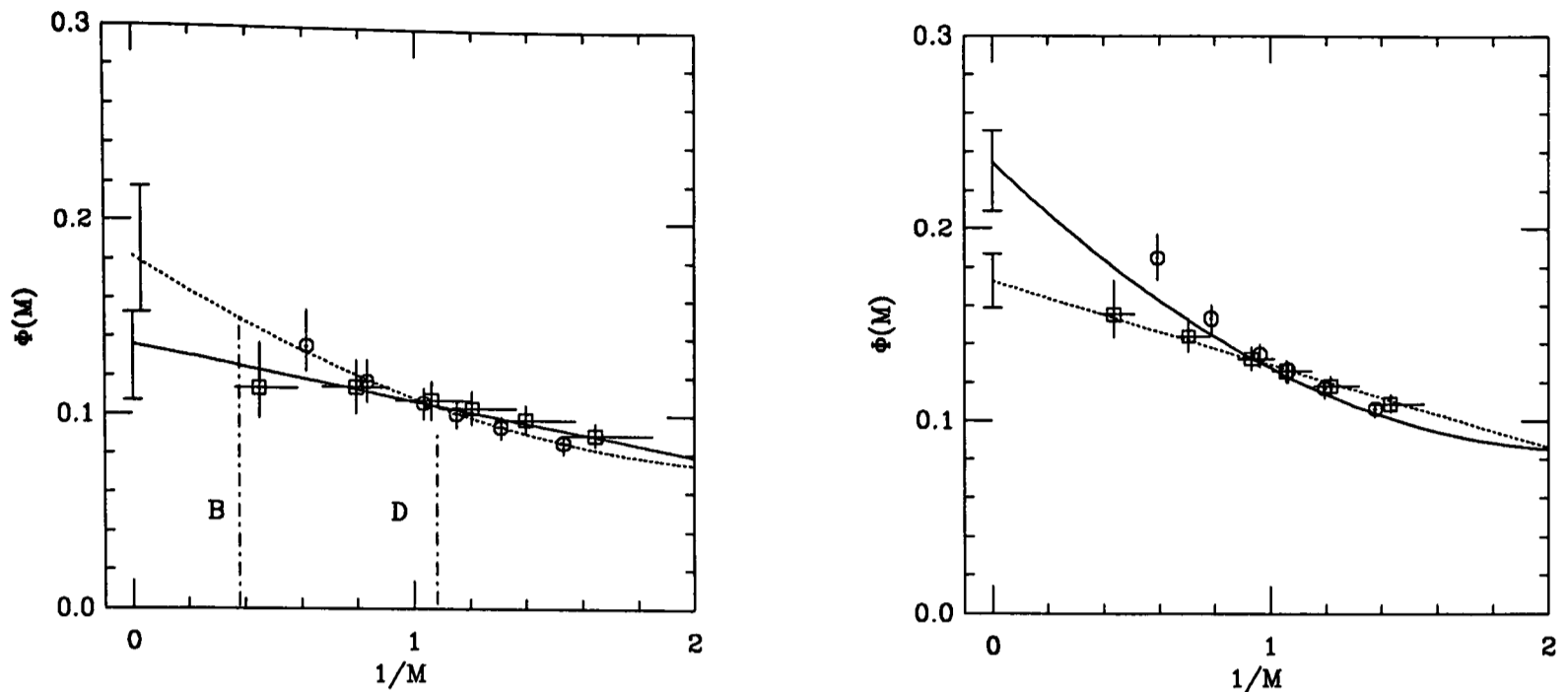


Figure 3.10: $\Phi(M)$ as a function of $1/M$, where the circles denote $M = M_{PS1}$ and the squares $M = M_{PS2}$, from the clover action at $\beta = 6.0$. In (i) the results for the chirally-extrapolated data are presented, while (ii) shows the results for $\kappa_q = 0.1432$. Linear and quadratic fits to the data are represented by the solid and dashed curves, respectively. Also shown are the intercepts at $1/M = 0$.

clover $\beta = 6.0$ $\kappa_q = \kappa_d$				
	c_1	c_2	c_3	χ^2
M_{PS1}	$0.18 + 4$ $- 3$	$0.51 + 12$ $- 13$	$0.21 + 10$ $- 10$	1./3
M_{PS2}	$0.14 + 2$ $- 3$	$0.21 + 10$ $- 4$	-	1./4
clover $\beta = 6.0$ $\kappa_q = 0.1432$				
M_{PS1}	$0.23 + 2$ $- 3$	$0.59 + 6$ $- 5$	$0.27 + 4$ $- 5$	6.8/3
M_{PS2}	$0.17 + 1$ $- 1$	$0.25 + 4$ $- 3$	-	1.4/4

Table 3.9: The fit parameters of the linear and quadratic fits to $\Phi(M)$, where M is either the dynamical or static mass, for the Wilson and clover data at $\beta = 6.0$.

The reduction in the dependence of $\Phi(M)$ on M compared to using the static mass, compensates for the larger statistical errors and leads to a determination of $\Phi(M = \infty)$ of comparable accuracy. Furthermore, the extrapolated value is 2σ below that for $M = M_{PS1}$. The non-scaling corrections are of order 20% and 10% for f_D and f_B respectively, using $M = M_{PS1}$, compared to 40% and 20% for $M = M_{PS2}$. It should be noted that for the lightest values of the heavy-quark mass, the dynamical pseudoscalar meson mass is slightly less than the corresponding static mass; however, the effect is not significant, at less than 1σ in the statistical errors.

In addition, it is significant that at finite values of the light quark mass, where the dynamical masses are more accurately determined and the quadratic behaviour with $1/M_{PS1}$ is more marked, there is also only a linear dependence of $\Phi(M_{PS2})$ on $1/M_{PS2}$. This is illustrated in figure 3.10 (ii), which shows the values of $\Phi(M)$ obtained for the largest value of the light quark mass. The fit parameters resulting from a quadratic fit to $\Phi(M_{PS1})$ and a linear fit to $\Phi(M_{PS2})$ are given in table 3.9.

Following the same procedure as for the data at $\beta = 6.2$, the values for the decay constants of the D , D_s , B and B_s mesons given in table 3.10 are obtained. Encouragement can be found in a comparison of these results with those at $\beta = 6.2$. For the D meson, where the static and dynamical masses are approximately equal, the results for f_D and f_{D_s} differ by less than 1σ between the two β values. More significantly, this level of consistency is also found between the estimates of f_B and f_{B_s} , extracted using the dynamical mass at $\beta = 6.0$, and those obtained at $\beta = 6.2$.

The results for f_{B_s}/f_B , in table 3.10, show this ratio to be less dependent on the mass parameter used than are the individual decay constants; consistency is seen between the values obtained using the dynamical and static masses, and the results at $\beta = 6.2$.

clover $\beta = 6.0$						
	f_D	f_B	f_{D_s}	f_{B_s}	f_{D_s}/f_D	f_{B_s}/f_B
M_{PS1}	200^{+10}_{-10}	180^{+30}_{-20}	230^{+10}_{-20}	220^{+30}_{-20}	1.16^{+5}_{-5}	1.20^{+10}_{-10}
M_{PS2}	200^{+20}_{-30}	150^{+20}_{-30}	230^{+20}_{-20}	180^{+20}_{-20}	1.10^{+10}_{-10}	1.20^{+20}_{-10}

Table 3.10: The estimates of the decay constants of the D , B , D_s and D_s mesons obtained from the clover data at $\beta = 6.0$ using the static and dynamical pseudoscalar meson masses.

For the Wilson action, $\Phi(M_{PS1})$ was computed using both the conventional normalisation for the quark fields, $\sqrt{2\kappa}$, and the mean-field heavy-quark normalisation, $\sqrt{1-6\tilde{\kappa}}$, mentioned in §(1.2.3); the definition $u_0 = (8\kappa_d)^{-1}$ is used here. Figure 3.11 shows a comparison of these results with those from the clover action at $\kappa_q = 0.1440$; this value of the hopping parameter corresponds to a $\bar{Q}Q$ pseudoscalar meson static mass roughly equal to that of the Wilson action at $\kappa_q = 0.1550$.

Using the conventional normalisation, there is a clear discrepancy between the results from the two actions for pseudoscalar meson masses above $M_{PS1}^{-1} \sim 1$. This difference is dramatically reduced if $\sqrt{1-6\tilde{\kappa}}$ is used; as noted in reference [50], it is presumably effects at $O(m_Q a)$ which account for the discrepancy between the results from the two actions using $\sqrt{2\kappa}$. The reduction in this discrepancy using the mean-field heavy-quark normalisation supports the suggestion of Bernard et al. [12], that these effects are largely absorbed by this normalisation. If the dynamical mass is used in conjunction with this normalisation, figure 3.12 shows a similar absence of non-linear behaviour in $\Phi(M_{PS2})$ to that found in the clover data.

Bernard et al. also investigated the effects of the dynamical mass, using mean field

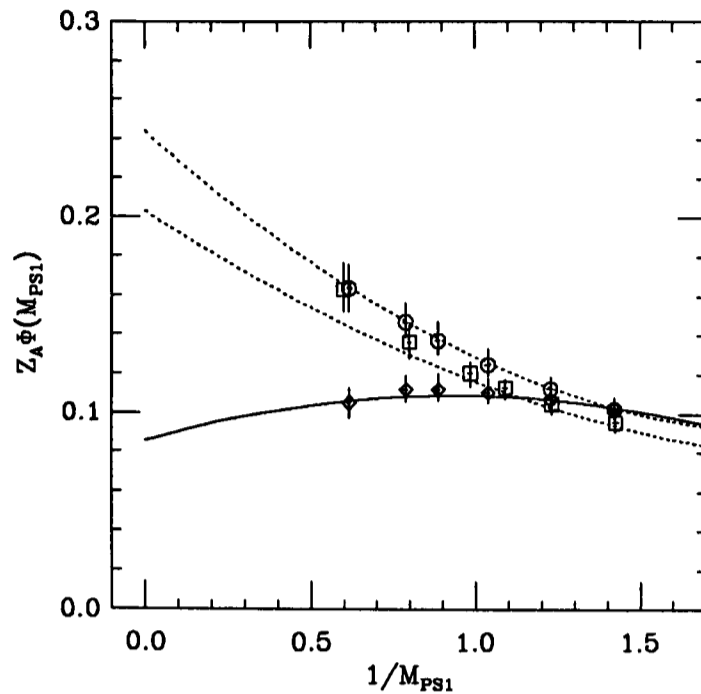


Figure 3.11: $Z_A \Phi(M)$ versus $1/M_{PS1}$, at $\beta = 6.0$, for the Wilson action using the normalisation, $\sqrt{1 - 6\tilde{\kappa}}$ (circles), and the clover action (squares). Quadratic fits to the data points are represented as dashed lines. Also shown, are the results obtained for the Wilson action using the conventional normalisation (diamonds), $\sqrt{2\kappa}$. The solid curve is to guide the eye.

Wilson $\beta = 6.0$ $\kappa_q = 0.1550$				
	c_1	c_2	c_3	χ^2
M_{PS1}	$0.26 \begin{smallmatrix} + 3 \\ - 3 \end{smallmatrix}$	$0.63 \begin{smallmatrix} + 13 \\ - 8 \end{smallmatrix}$	$0.31 \begin{smallmatrix} + 7 \\ - 13 \end{smallmatrix}$	0.1/3
M_{PS2}	$0.15 \begin{smallmatrix} + 2 \\ - 2 \end{smallmatrix}$	$0.18 \begin{smallmatrix} + 8 \\ - 6 \end{smallmatrix}$	-	1.3/4

Table 3.11: The values of the fit parameters of the linear and quadratic fits to the behaviour of $\Phi(M)$, where M is either the dynamical or static mass, for the Wilson data at $\beta = 6.0$.

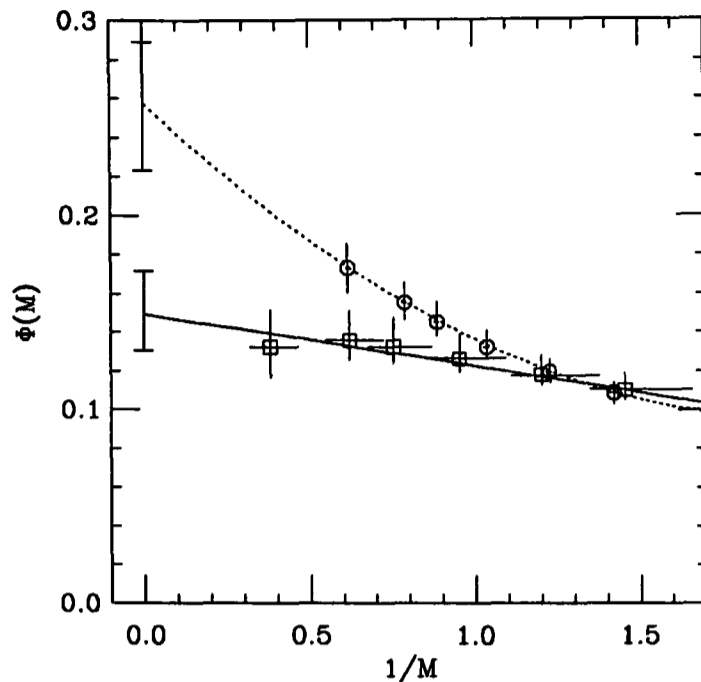


Figure 3.12: $\Phi(M)$ versus $1/M$, at $\beta = 6.0$, for the Wilson action using the normalisation, $\sqrt{1 - 6\tilde{\kappa}}$, and $M = M_{PS1}$ (circles) and $M = M_{PS2}$ (squares). Quadratic and linear fits to the data points are represented as dashed and solid lines respectively and the intercepts in the infinite mass limit are indicated. The fit parameters obtained are detailed in table 3.11.

heavy-quark normalisation, on the scaling behaviour of $f_{PS}\sqrt{M}$ for the Wilson action at $\beta = 6.3$. These authors found the difference in f_D and f_B using M_{PS2} to be less than 4%, compared to the $> 5\%$ and $> 40\%$ ² changes, respectively, seen here. There are several differences in method, however. Firstly, the dynamical mass was estimated by using equation (3.10) to calculate the mass shift from M_{PS1} to M_{PS2} , and as noted in §(3.5.2), this is likely to lead to an overestimate of the mass shift. Secondly, the mass factor arising from the matrix element was assumed to be the static mass, and the effects of the dynamical mass were only included in the dependence on $1/M$. Thus, for a given physical mass fixed using M_{PS2} , the value of f_{PS} is lower than that obtained from M_{PS1} , but not to the extent found if M_{PS}^{phys} is taken to be the dynamical mass. Considering the possible overestimate of M_{PS2} , the small change found in the estimates of f_B is surprising.

²Since the scaling violations decrease with the light quark mass those found at $\kappa_q = 0.155$ represent upper bounds on the scaling violations at zero light quark mass

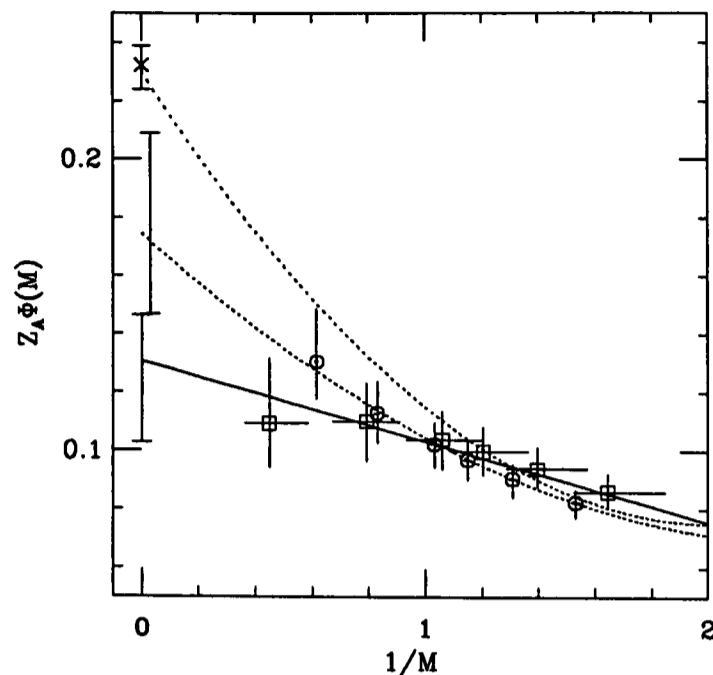


Figure 3.13: $Z_A \Phi(M)$ at $\beta = 6.0$, from the static theory (cross), and the simulation with propagating quarks with the clover action for $M = M_{PS1}$ (circles) and M_{PS2} (squares). Quadratic and linear fits to the data points are represented as dashed and solid lines respectively and the intercepts in the infinite mass limit are indicated.

However, fits to the data points were constrained by the inclusion of the results obtained both in the static limit, and at lighter masses where $M_{PS1} \sim M_{PS2}$.

Figure 3.13 compares the value of $Z_A \Phi(M)$ obtained in the static limit for the clover action at $\beta = 6.0$ on 36 configurations, with the results from propagating quarks, previously presented in figure 3.10 (i). Details of the calculation of the static theory result are contained in reference [50]. The extrapolation of the data derived using $M = M_{PS1}$, lies about 2σ below the static result; however, a fit can be successfully performed which includes the static point and yields $\chi^2 = 1.1$. This is not possible using $M = M_{PS2}$, where the discrepancy between the static theory result and the result using propagating quarks is $\sim 5\sigma$.

3.10.3 Summary of Pseudoscalar Decay Constant Results

To summarise: for the correlators available a determination of whether or not the dynamical meson mass should be used to fix the physical quark mass was not possible. At $\beta = 6.2$, for the range of heavy-quark masses available, $M_{PS1} \sim M_{PS2}$, and hence the uncertainty in the mass scale does not translate into significant uncertainties in the predictions for f_D , f_{D_s} , f_B and f_{B_s} . Large negative $O(M_{PS}^{-1})$ corrections to the scaling law $f_{PS}\sqrt{M_{PS}} \sim \text{constant}$ were found in the chirally extrapolated data, of order 30% and 10% at the D and B meson masses respectively. Interpolating the light quark mass to the strange quark mass, positive corrections at $O(M_{PS}^{-2})$ were found to be significant.

At $\beta = 6.0$, where for the larger heavy-quark masses available, $M_{PS1} > 1$ and $M_{PS1} < M_{PS2}$, striking differences were found in the dependence of $\Phi(M)$ on the dynamical and static meson masses. Significant non-linear behaviour with M_{PS1}^{-1} was found in $\Phi(M_{PS1})$ for the $\bar{q}Q$ pseudoscalar mesons with zero *and* finite light-quark mass; the non-scaling corrections are of order 40% and 20% at the D and B meson masses respectively. In contrast, $\Phi(M_{PS2})$ was found to be less dependent on $1/M_{PS2}$; only corrections to the scaling law at $O(M_{PS2}^{-1})$ are significant at *all* values of the light-quark mass, and are of order 20% at the D meson mass and 10% at the B meson mass. The weaker dependence of the pseudoscalar decay constant on the dynamical mass provides greater confidence in the extrapolations to the B and infinite meson mass limit; the latter is 2σ below that obtained using the static meson mass and $\Phi(M_{PS1})$.

Since the dynamical and static meson masses are approximately equal around the D meson mass, the predictions for f_D and f_{D_s} do not depend significantly on the meson mass parameter used, and are also consistent with those obtained at $\beta = 6.2$. However, the values obtained for f_B and f_{B_s} using the dynamical meson mass lie $\sim 2\sigma$ below the corresponding values derived using the static meson mass;

the closer agreement between the predictions for these decay constants extracted using M_{PS_2} at $\beta = 6.2$ and $\beta = 6.0$ is a hint that the dynamical mass may be the correct mass parameter with which to fix the physical quark mass. However, the correct mass parameter with which to fix the physical quark mass. However, the different dependence of $\Phi(M_{PS_2})$ on $1/M_{PS_2}$ found at the two β values for finite light-quark mass, suggests there may be significant discretisation errors in the estimates of the dynamical meson mass. Furthermore, it is worrying that the results for $\Phi(M_{PS_2})$ at $\beta = 6.0$ are not consistent with the results of the static theory, although any comparison of the two approaches is difficult because of the uncertainties in the renormalisation constants (different for the static and propagating theories); the possibility also exists for significant discretisation errors in the pseudoscalar decay constant.

3.10.4 Vector Decay Constant

The decay constant for the vector meson, f_V , is defined as

$$\frac{M_V^2}{f_V} \varepsilon_\mu^r(\vec{p}) = \langle 0 | V_\mu | V, r \rangle, \quad (3.41)$$

where V_μ represents the vector operator and $\varepsilon_\mu^r(\vec{p})$ represents the polarisation vector. In this analysis, where LL propagators are available f_V is determined through the vector correlator, $C_{VV}^{LL}(t)$:

$$\begin{aligned} C_{VV}^{LL}(t) &\equiv \sum_{\mu=1}^3 \sum_{\vec{x}} \langle V_\mu^L(\vec{x}) V_\mu^{L\dagger}(0) \rangle \\ &\sim -\xi(\vec{p}) \left(\frac{M_V^2}{Z_V f_V} \right)^2 \frac{1}{2E(\vec{p})} e^{-E(\vec{p})T/2} \cosh E(\vec{p})(T/2 - t) \end{aligned} \quad (3.42)$$

$\xi(\vec{p})$ arises from the sum over polarisations and components:

$$\xi(\vec{p}) = \sum_{\mu=1}^n \sum_{r=1}^3 \varepsilon_\mu^r(\vec{p}) \varepsilon_\mu^r(\vec{p}) \quad (3.43)$$

$$= \sum_{\mu=1}^n g_{\mu\mu} - \frac{p_\mu^2}{M_V^2} \quad (3.44)$$

In this case only the spatial components are averaged over; $n = 3$ and

$$\xi(\vec{p}) = 3 - \frac{|\vec{p}|^2}{M_V^2} \quad (3.45)$$

Ideally, the fourth component of the vector correlators would also be included in the average; in this case, $\xi(\vec{p}) = 3$ independent of momentum. Unfortunately these correlator were not available. Alternatively, where smeared propagators are available, the vector decay constant is extracted from the ratio

$$\begin{aligned} \frac{C_{VV}^{LS}(t)}{C_{VV}^{SS}(t)} &\equiv \frac{\sum_{\mu=1}^4 \sum_{\vec{x}} \langle V_{\mu}^L(\vec{x}) V_{\mu}^{S\dagger}(0) \rangle}{\sum_{\mu=1}^4 \sum_{\vec{x}} \langle V_{\mu}^S(\vec{x}) V_{\mu}^{S\dagger}(0) \rangle} \\ &\sim -\frac{1}{A_{Vs}} \frac{M_V^2}{Z_V f_V} \end{aligned} \quad (3.46)$$

where A_{Vs} is defined through,

$$\epsilon_{\mu}^r(\vec{p}) A_{Vs} = \langle 0 | V_{\mu}^S(0) | V, r \rangle \quad (3.47)$$

and appears in the amplitudes of $C_{VV}^{LS}(t)$ and $C_{VV}^{SS}(t)$. For example,

$$C_{VV}^{SS}(t) \sim -3 \frac{A_{Vs}^2}{2E(\vec{p})} e^{-E(\vec{p})T/2} \cosh E(\vec{p})(T/2 - t). \quad (3.48)$$

The vector decay constant in the charmonium system, f_{ψ} , has been measured:

$$M_V^2 / f_{\psi} = 1.19 \pm 4 \text{ GeV}^2 \quad (3.49)$$

$$1/f_{\psi} = 0.124 \pm 5 \quad (3.50)$$

In this analysis, $M_{V1} > 1$ and hence $M_{V1} < M_{V2}$ around the mass of J/ψ , where M_{V1} and M_{V2} denote the static and dynamical vector meson masses respectively. Thus, a comparison of (3.50) with the prediction of f_{ψ} obtained using the dynamical mass, provides a test of whether $M_{V2} = M_V$, where M_V appearing in (3.42) and (3.48) is identified as the physical vector meson mass. However, note that $M_V^2 / (Z_V f_V)$ can be extracted from $C_{VV}^{LS}(t) / C_{VV}^{SS}(t)$ and $C_{VV}^{LL}(t)$ without any assumption about the mass parameter. Thus, it is the more natural quantity to calculate. In addition, since the results for M_{PS2} , not M_{V2} , have been presented

previously, a prediction for $M_V^2/(Z_V f_V)$ at the charm quark mass will be obtained by matching the pseudoscalar mass parameter to the mass of η_c .

As mentioned in §(3.7) any disagreement found between prediction and experiment may be due to systematic errors, possibly from quenching or the finite lattice spacing, in the estimate of the decay constant, rather than use of the wrong mass parameter. In quarkonia, it is possible to obtain an estimate of the effect of quenching on the predictions for f_ψ using potential models. Consider the leptonic decay amplitude, $V_{\bar{Q}Q} \equiv M_V^2/f_V$; this is related to the leptonic width, Γ , where

$$\Gamma = \frac{4\pi\alpha_s^2(m_Q)V_{\bar{Q}Q}^2}{3M_V^3} \quad (3.51)$$

Comparing this with the van Royen-Weisskopf formula [51] for Γ :

$$\Gamma = \frac{16\pi\alpha_s^2(m_Q)e_Q^2}{M_V^2}|\psi(0)|^2, \quad (3.52)$$

where e_Q and m_Q are the charge and mass of the heavy quark, and the wavefunction has been normalised for coloured quarks, $V_{\bar{Q}Q}$ is simply the wavefunction at the origin. An estimate of the effect of quenching on $|\psi(0)|$ has been obtained by A. El-khadra [52] using the Richardson potential [53]; details of this calculation and the potential model approach are given in §(4.1.3). The absence of sea quarks was estimated to reduce $|\psi(0)|$, and hence $V_{\bar{c}c}$, by 14%. Thus, a lattice calculation of V_ψ should be compared to $V_{\bar{c}c}^{quench} \approx 1.0 \text{ GeV}^2$ rather than (3.49). It is encouraging that the effect of quenching, from this preliminary calculation at least, appears to be small.

The hyperfine splitting is also related to the wavefunction at the origin (see §(4.1.2)). This suggests that both $V_{\bar{Q}Q}$ and the hyperfine splitting are determined by the same mass parameter. Thus, if for $V_{\bar{Q}Q}$ the dynamical mass proves the correct mass parameter to use to fix the physical quark mass, it is also likely to be a good approximation of the hyperfine mass parameter.

It is worth noting that using equation (3.45) with estimates of $\xi(\vec{p})$ extracted

from $C_{VV}^{LL}(t)$ or $C_{VV}^{SS}(t)$ (if only the spatial components of the vector correlator are averaged) it is possible to test whether or not $M_{V_2} = M_V$ more directly. In practice, however, $|\vec{p}|^2/M_V^2 \ll 1$ for $M_{V_1} > 1$, and the momentum dependence of $\xi(\vec{p})$ cannot be determined accurately enough to obtain estimates of M_V^3 .

For the clover action at $\beta = 6.2$, the ratio $C_{VV}^{LS}(t)/C_{VV}^{SS}(t)$ is fitted to a constant in the fitting range $t = 15$ to 22 at $\frac{12}{\pi}|\vec{p}| = 0, 1$ and $\sqrt{2}$; the statistical errors in the ratio are prohibitively large at higher momenta. A_{Vs} is needed in order to extract $M_V^2/(Z_V f_V)$, and this is obtained by fitting to $C_{VV}^{SS}(t)$ in the time interval $t = 11$ to 23 . At $\beta = 6.0$, only LL propagators are available, and $M_V^2/(Z_V f_V)$ was extracted from the amplitude of C_{VV}^{LL} for both the Wilson and clover action at $\frac{8}{\pi}|\vec{p}| = 0, 1$ and $\sqrt{2}$, using the fitting ranges detailed in §(3.4). $\langle V_4^S(\vec{x})V_4^{S\dagger}(0) \rangle$ was not available for either action at this β value, and $\xi(\vec{p}) \approx 3$ was assumed. This assumption was checked using the data at $\beta = 6.2$, by calculating the ratio of the amplitudes obtained from fitting to $C_{VV}^{SS}(t)$ with, and without, including the fourth component of the vector correlator. The ratio was found to be consistent with 1 for all values of the heavy quark mass, indicating $|\vec{p}|^2/M_V^2 \ll 1$. Since a similar range of the heavy quark masses is available at $\beta = 6.0$, it seems reasonable to use $\xi(\vec{p}) = 3$.

3.10.5 Results for the Vector Decay Constant

The values of $M_V^2/(Z_V f_V)$ obtained from the clover action at $\beta = 6.2$ and 6.0 , and the Wilson action at $\beta = 6.0$ are presented in table 3.12. Agreement is expected between the values obtained at different values of momentum; table 3.12 shows that, to within 2σ , this is the case. However there is a slight increase in $M_V^2/(Z_V f_V)$ with momentum at $\beta = 6.0$ for both actions and a slight decrease at $\beta = 6.2$. At $\beta = 6.0$, where $M_V^2/(Z_V f_V)$ is extracted from the amplitude of $C_{VV}^{LL}(t)$,

³This is likely since $|\vec{p}|^2/M_{V_1} \ll 1$ for $M_{V_1} > 1$

this trend is consistent with a residual contribution from excited states to the vector correlators at finite momentum in the fitting regions chosen, thus leading to an over-estimate of the amplitude. At $\beta = 6.2$, it is likely that there is a residual contribution from excited states to the estimate of A_{Vs} , since from equation (3.46) an over-estimate of A_{Vs} leads to a smaller value for $M_V^2/(Z_V f_V)$. Alternatively, the fitting range chosen for the ratio $C_{VV}^{LS}(t)/C_{VV}^{SS}(t)$ may not correspond to the asymptotic region at finite momentum.

Figure 3.14 shows the results for $V_{\bar{Q}Q}$ from the clover action at $\beta = 6.2$ and zero-momentum, plotted against both the static and dynamical pseudoscalar meson masses (the perturbative values of Z_V given in §(3.8) are used throughout). Since the estimated effect of quenching is fairly small, statistical errors of order 5% in the value of $V_{\bar{Q}Q}$ at $M_{PS1} \sim a\eta_c$ are large enough to provide agreement with both the experimental value and $V_{\bar{c}c}^{quench}$; although from figure 3.14 the results are consistent with a prediction for $V_{\bar{c}c}$ which lies closer to the former. However, using M_{PS2} , the values of $V_{\bar{Q}Q}$ are consistent with a value of $V_{\bar{c}c}$ 2σ below $V_{\bar{c}c}^{quench}$ at $M_{PS2} \sim a\eta_c$

The situation is reversed at $\beta = 6.0$. Figures 3.15 (i) and (ii) present the results for $V_{\bar{Q}Q}$ obtained at zero-momentum, plotted against M_{PS1} and M_{PS2} respectively. Figure 3.15 (i) shows that using the static pseudoscalar meson mass to fix the physical mass, leads to a prediction for $V_{\bar{c}c}$ that is significantly larger than the experimental value. In contrast, using M_{PS2} the results are consistent with (3.50) (and within 2σ of $V_{\bar{c}c}^{quench}$) at $M_{PS2} = a\eta_c$.

For the Wilson action at $\beta = 6.0$ the values of $V_{\bar{Q}Q}$ obtained are dependent on normalisation of the quark-fields. Figure 3.15 (i) also presents a comparison of the results obtained using the conventional normalisation, $\sqrt{2\kappa}$, and the mean-field heavy-quark normalisation, $\sqrt{1 - 6\tilde{\kappa}}$ with M_{PS1} . As the heavy-quark mass increases there is a clear divergence between the the results of the clover action

clover $\beta = 6.2$				
$\frac{12}{\pi}\vec{p}$	0.133	0.129	0.125	0.121
0	0.135^{+4}_{-6}	0.183^{+5}_{-8}	0.234^{+6}_{-10}	0.289^{+7}_{-13}
1	0.134^{+4}_{-6}	0.181^{+6}_{-9}	0.232^{+8}_{-12}	0.287^{+9}_{-15}
$\sqrt{2}$	0.130^{+8}_{-10}	0.179^{+10}_{-13}	0.230^{+12}_{-16}	0.285^{+13}_{-19}

Wilson $\beta = 6.0$				
$\frac{8}{\pi}\vec{p}$	0.140	0.135	0.13	0.125
0	0.221^{+5}_{-4}	0.258^{+5}_{-5}	0.292^{+6}_{-7}	0.325^{+6}_{-9}
1	0.230^{+8}_{-6}	0.264^{+8}_{-7}	0.298^{+8}_{-9}	0.329^{+8}_{-10}
$\sqrt{2}$	0.244^{+15}_{-10}	0.275^{+11}_{-10}	0.306^{+10}_{-10}	0.335^{+10}_{-12}

clover $\beta = 6.0$						
$\frac{8}{\pi}\vec{p}$	0.133	0.129	0.125	0.121	0.111	0.092
0	0.251^{+7}_{-5}	0.322^{+7}_{-6}	0.403^{+8}_{-8}	0.517^{+8}_{-13}	0.764^{+11}_{-18}	1.62^{+4}_{-3}
1	0.264^{+11}_{-6}	0.335^{+10}_{-8}	0.415^{+10}_{-11}	0.529^{+10}_{-14}	0.777^{+16}_{-20}	1.65^{+4}_{-4}
$\sqrt{2}$	0.277^{+22}_{-11}	0.346^{+16}_{-10}	0.425^{+14}_{-12}	0.538^{+15}_{-15}	0.791^{+21}_{-21}	1.69^{+4}_{-4}

Table 3.12: The values obtained for $m_V^2/(Z_V f_V)$ at 0, 1 and $\sqrt{2}$ units of momenta, from the clover action at $\beta = 6.0$ and 6.2, and the Wilson action at $\beta = 6.0$.

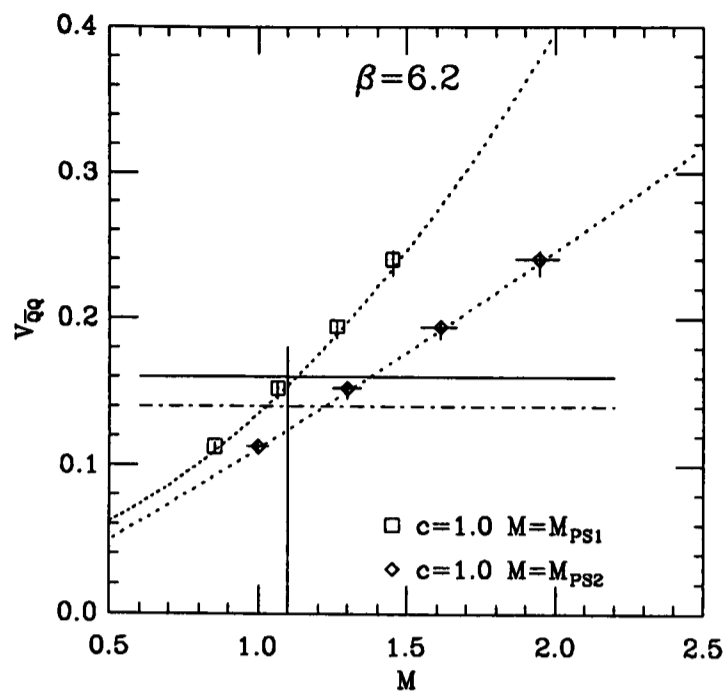
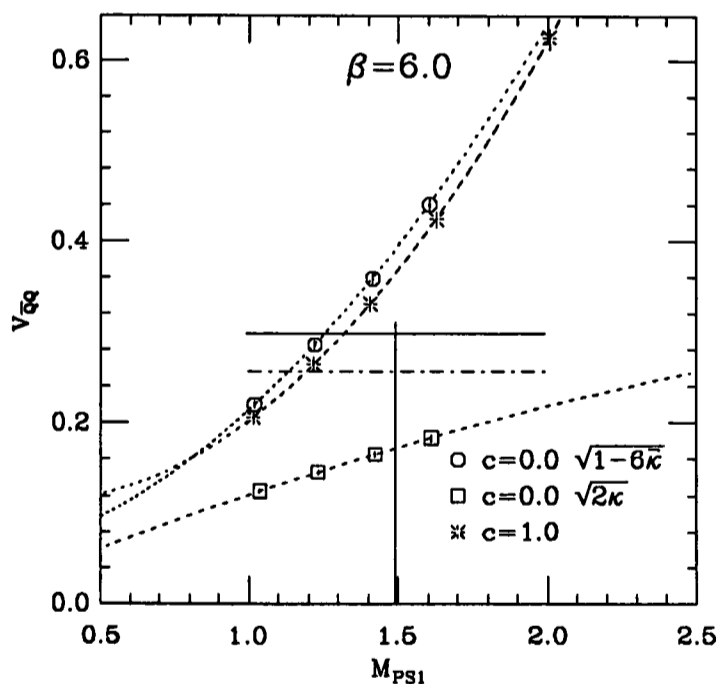
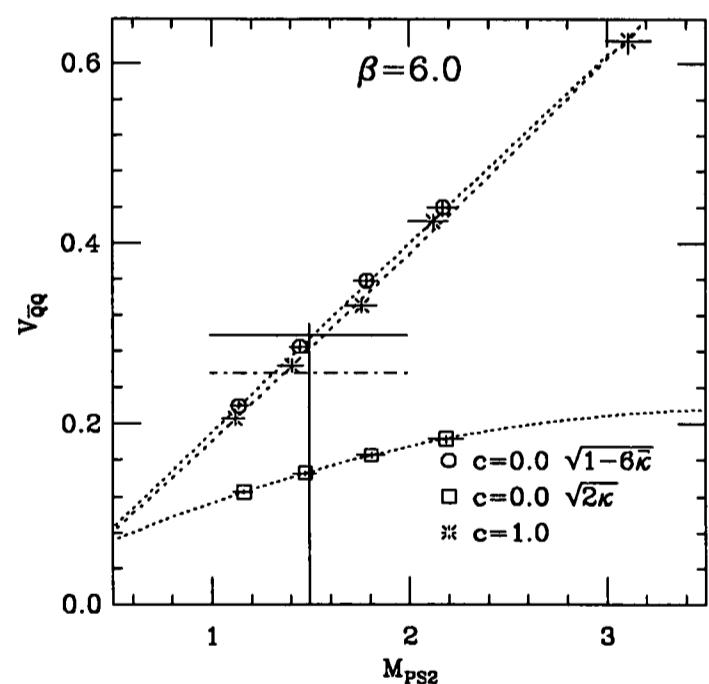


Figure 3.14: $V_{\bar{Q}Q}$ versus the pseudoscalar meson mass from the clover at $\beta = 6.2$. The solid vertical and horizontal lines represent the experimental values for m_{η_c} and $V_{\bar{c}c}$, respectively, while the dashed horizontal line indicates the estimate of $V_{\bar{c}c}^{quench}$ obtained by [52]. The dotted curves are to guide the eye.



(i)



(ii)

Figure 3.15: $V_{\bar{Q}Q}$ versus (i) M_{PS1} (ii) M_{PS2} from the clover and Wilson action at $\beta = 6.0$. The solid vertical and horizontal lines represent the experimental values for m_{η_c} and $V_{\bar{c}c}$, respectively, while the dashed horizontal line indicates the estimate of $V_{\bar{c}c}^{quench}$ obtained by [52]. The dotted curves are to guide the eye.

and Wilson action using $\sqrt{2\kappa}$. Using the mean-field heavy-quark normalisation, however, consistency to within 2σ is found between the results of the two actions; this adds further support to the suggestion, noted in §(3.10.2), that large $O(m_Q a)$ effects are possibly being absorbed through using this normalisation. Figure 3.15 (ii) shows consistency is also found between the clover and Wilson results using the dynamical pseudoscalar meson mass and the mean-field heavy-quark normalisation.

It is disappointing that the results at $\beta = 6.2$ do not provide clear confirmation that the dynamical mass corresponds to the physical mass, as suggested by the data at $\beta = 6.0$, and there does not seem to be a significant difference between using the dynamical or static mass. The difference between the results at the two β values may be due to significant discretisation errors in either V_{QQ} or M_{PS1} and M_{PS2} . However, the dependence on the lattice spacing is expected to be less at $\beta = 6.2$, suggesting, if the dynamical mass is the correct mass parameter, that the effect of quenching is significant. The agreement with experiment using the dynamical mass at $\beta = 6.0$ and the static mass at $\beta = 6.2$ may be misleading. The results from the Wilson action suggest that reducing the discretisation errors increases the V_{QQ} , while the effect of quenching and using the dynamical mass decreases it. Thus, it is difficult to predict how reducing the systematic errors further will alter the results.

3.11 Conclusions

The results presented in this chapter have shown some encouraging signs that the Wilson action is valid for meson masses above 1, provided that it is reinterpreted as an effective action. The clearest indication of this was found in the finite-momentum behaviour of the $\bar{Q}Q$ and $\bar{q}Q$ pseudoscalar mesons for $M_{PS1} \gg 1$,

where significant deviations from SC dispersion behaviour was seen in this range of meson masses. Assuming a TMN form for the dispersion relation, and obtaining an estimate of M_{PS_2} from the data at the lowest value of momentum, dispersion behaviour at higher momenta was accurately predicted, even for masses of $O(3)$.

In comparison, the FSL dispersion relation, which would be expected to perform better than a dispersion relation with a continuum form if the discretisation errors are significant, was found to adequately describe the finite-momentum behaviour of the $\bar{q}Q$ pseudoscalar mesons, but markedly over-estimated $\partial E(\vec{p})/\partial|\vec{p}|^2$ for the $\bar{Q}Q$ mesons. This differentiation of the $\bar{q}Q$ and $\bar{Q}Q$ meson cases is indicative of the deviations from SC behaviour being dependent on the meson mass. Thus, the dynamical mass is determined by the meson mass not the quark mass. From the discussion of §(3.2), large discretisations errors are expected in the static meson mass as it increases above 1, and it is assumed to be the dynamical mass which corresponds to the physical meson mass.

For the $\bar{q}Q$ mesons, use of this assumption was found to have a significant effect on the violations of the scaling law $f_{PS}\sqrt{M_{PS}^{phys}} \sim \text{constant}$ found in the results from the clover action at $\beta = 6.0$, but not $\beta = 6.2$. Around the charm quark mass, the static pseudoscalar meson mass was found to be approximately equal to the dynamical meson mass for the $\bar{q}Q$ mesons at both $\beta = 6.0$ and $\beta = 6.2$. Thus, at $\beta = 6.2$, where the heavy-quark masses available are restricted to this region, no significant differences were found between the results obtained using the two mass parameters.

At $\beta = 6.0$, where $M_{PS_1} \gg 1$ and corrections to the scaling law to order $1/M^2$ were found to be significant using the static meson mass, only $O(1/M)$ corrections were significant using M_{PS_2} . That $O(1/M^2)$ corrections are not found, rather than simply reduced in magnitude, seems significant, and even more so considering this was the case at all values of the light quark mass. This weaker dependence on the

dynamical meson mass provides greater confidence in the extrapolations to the B and infinite meson mass limit.

However, no test of the assumption $M_{PS2} = M_{PS}^{phys}$ was possible, and hence there is no firm evidence in favour of using the dynamical mass over the static mass to fix the physical quark mass for the pseudoscalar decay constant. In addition, the large $O(1/M^2)$ corrections to the scaling law found at light-quark masses close to the strange-quark at $\beta = 6.2$ suggest that there are significant discretisation errors in the estimates of M_{PS2} . Heavy-quark masses closer to those available at $\beta = 6.0$ are needed in order to clarify this, and also to confirm the linear behaviour of $\Phi(M)$ with $1/M$ found in the chirally-extrapolated data. Similarly, increased statistics are needed at $\beta = 6.0$ in order to test the significance of the reduction in the scaling violations found using the dynamical mass.

For the $\bar{Q}Q$ mesons, the difference between the dynamical and static meson masses around the charm quark mass is approximately 25% at both β values. Thus, with an experimental measurement of the vector decay constant, f_ψ , a clear test was expected of whether or not the dynamical mass is the correct parameter to use to fix the physical mass. At $\beta = 6.0$, the dynamical mass was found to provide results for V_{QQ} consistent with both the quenched corrected and experimental values, compared to a significant discrepancy found using M_{PS1} .

However, at $\beta = 6.2$ the difference in the results using the two mass parameters was of the same order of magnitude as the estimated effect of quenching. It is difficult to discern whether the agreement with the experimental value of $V_{\bar{c}c}$ found using the static mass is significant or if the effect of quenching is of the order estimated using a potential model analysis. Certainly, it is disappointing that for a quantity where the statistical errors are small, and $M_{PS1} \neq M_{PS2}$ a decisive indication of the correct mass parameter was not found. A similar analysis using a mean-field improved value of the clover coefficient at $\beta = 6.0$, where lattice

artifacts are expected to be more significant, may provide a clearer understanding of discretisation errors. However, it may only be in the region of the bottom quark, where $M_{PS1} \ll M_{PS2}$, that the effects of a different mass parameter can be seen above the systematic errors. Conversely, there is no evidence to rule out the dynamical mass being the correct mass parameter with which to set the physical mass; given the suggestion that V_{QQ} and the hyperfine splitting are determined by the same mass parameter, an analysis of the hyperfine splitting using the dynamical mass may prove more fruitful.

Chapter 4

Mass Splittings in Heavy-Quark Systems

In a continuation of the analysis of quarkonia and mesons containing a single heavy quark, this chapter explores the dependence of the mass splittings on the heavy quark mass and $SU(3)$ light flavour symmetry breaking. The theoretical predictions for these splittings from chiral HQET and potential model calculations are outlined in §(4.1.1) and §(4.1.2) respectively. The success of the potential models as a description of quarkonia, allows a quantitative estimate of the effect of quenching on the hyperfine splitting, which is possibly a source of large systematic error; this is discussed in §(4.1.3).

The splittings computed from the data sets detailed in the previous chapter are presented in §(4.3) and §(4.4) for the $\bar{Q}Q$ and $\bar{q}Q$ mesons respectively. For each splitting, the results from the clover and Wilson action are compared in order to quantify the magnitude of discretisation errors. In addition, the dependence of the splittings on both the dynamical and static quark mass is found, with the view of determining the correct mass parameter with which to fix the heavy quark mass.

4.1 Theoretical Predictions

4.1.1 Heavy-Light Mesons: Chiral Heavy Quark Effective Theory

The theoretical approach to a meson containing a single heavy-quark embodied in HQET treats the contributions from the light degrees of freedom as being nonperturbative. No insight is offered into the dependence of the properties of $\bar{q}Q$ mesons on the light quark mass. However, the reduced dependence of $f\sqrt{m}$ on m_Q in the chiral limit, seen in the results of §(3.10.2), suggests the effect of the light valence quark on the corrections to scaling behaviour is far from negligible. To enable a perturbative study of the dependence on the light quark mass in the chiral regime, a union of chiral perturbation theory and HQET in the form of chiral HQET [54, 55, 56] has been developed. The latter introduces terms into the lagrangian representing the interaction of $\bar{q}Q$ mesons with low momentum pions.

Initial calculations using chiral HQET have centered on the dependence of the $\bar{q}Q$ meson mass on the heavy-quark mass (m_Q) and the light degrees of freedom (q). To order $O(1/m_Q)$ this meson mass has the form,

$$m(Ql) = m_Q + \epsilon(Ql) + \frac{\Delta(Ql)}{m_Q} \langle \mathbf{S}_Q \cdot \mathbf{S}_l \rangle + O\left(\frac{1}{m_Q^2}\right), \quad (4.1)$$

where both the static binding energy, $\epsilon(Ql)$, and the hyperfine coefficient $\Delta(Ql)$ depend on the light degrees of freedom and are of order Λ_{QCD} . In the chiral limit $\epsilon(Ql)$, and $\Delta(Ql)$ become constant; equation (4.1) is then of the form predicted by Aglietti [57]. If both the $SU(3)_V$ light flavour and heavy-quark symmetries are broken, $\Delta(Ql)$ and $\epsilon(Ql)$ have expansions in powers of $1/m_Q$ and m_q beginning at order 1 and m_q respectively.

A prediction for the splitting between a pseudoscalar ($\langle \mathbf{S}_Q \cdot \mathbf{S}_l \rangle = -\frac{3}{4}$) and a vector ($\langle \mathbf{S}_Q \cdot \mathbf{S}_l \rangle = \frac{1}{4}$) meson follows immediately from equation (4.1):

$$m_V(Q\bar{q}) - m_{PS}(Q\bar{q}) = \frac{\Delta(Q\bar{q})}{m_Q} + O\left(\frac{1}{m_Q^2}\right) \quad (4.2)$$

Note the term $\epsilon(Ql)$ is independent of the heavy spin and flavour as a result of heavy-quark symmetry, and so is cancelled in the hyperfine splitting. However it can be studied using the spin-average of the meson masses:

$$\frac{1}{4}[m_{PS}(Q\bar{q}) + 3m_V(Q\bar{q})] = m_Q + \epsilon(Q\bar{q}) + O\left(\frac{1}{m_Q^2}\right). \quad (4.3)$$

In the chiral limit, equation (4.3) provides an improved approximation for m_Q over using the individual meson masses. Therefore m_Q is approximated here as:

$$\bar{m}_Q \equiv \lim_{m_q \rightarrow 0} \frac{1}{4}[m_{PS}(Q\bar{q}) + 3m_V(Q\bar{q})] \quad (4.4)$$

The hyperfine splitting then becomes,

$$m_V(Q\bar{q}) - m_{PS}(Q\bar{q}) \approx \frac{\Delta(Ql)}{\bar{m}_Q}, \quad (4.5)$$

and hence in the chiral limit, when $\Delta(Ql)$ becomes constant, the splitting is inversely proportional to the heavy-quark mass.

Using Chiral HQET, the form of $\epsilon(Ql)$ and $\Delta(Ql)$ can be calculated explicitly, and therefore the $SU(3)_V$ mass splittings can be determined. Assuming that isospin symmetry remains exact, $m_u = m_d = 0$, but the flavour symmetry is broken by the strange quark mass, the difference in the hyperfine splitting between $\bar{q}Q$ mesons containing a d and those containing an s quark is predicted to be [58]:

$$\begin{aligned} \Delta_{s-d}(m_V - m_{PS}) &\equiv [m_V(Q\bar{s}) - m_{PS}(Q\bar{s})] - [m_V(Q\bar{d}) - m_{PS}(Q\bar{d})] \quad (4.6) \\ &= -\frac{g^2 \Delta_0}{m_Q} \frac{M_K^2}{16\pi^2 f^2} \ln\left(\frac{M_K^2}{\Lambda_\chi^2}\right) \\ &\quad - \frac{g^2 \Delta_0}{2m_Q} \frac{M_\eta^2}{16\pi^2 f^2} \ln\left(\frac{M_\eta^2}{\Lambda_\chi^2}\right) + \frac{2\Delta_1}{m_Q} m_s, \quad (4.7) \end{aligned}$$

where Δ_0 and Δ_1 are the coefficients corresponding to the zeroth and first terms in the expansion of $\Delta(Ql)$ in m_q , at zeroth order in $1/m_Q$. The axial vector coupling

g is constrained by the radiative and pion decay widths of the vector mesons, $g^2 \lesssim 0.5$. Λ_χ is the chiral symmetry breaking scale; estimated at $4\pi f_\pi \sim 1$ GeV [59], the chiral logarithms in equation (4.7) have a value of ~ 28 MeV. This should be considered in the context of the experimental values for the hyperfine splittings:

$$D_s^{*+} - D_s^+ = 141.5 \pm 1.9 \text{ MeV [32]} \quad (4.8)$$

$$D^{*+} - D^+ = 140.64 \pm 0.08 \pm 0.06 \text{ MeV [60]} \quad (4.9)$$

$$B_s^* - B_s = 47.0 \pm 2.6 \text{ MeV [61]} \quad (4.10)$$

$$B^* - B = 46.2 \pm 0.3 \pm 0.8 \text{ MeV [62]} \\ \text{or } 45.4 \pm 1.0 \text{ MeV [61]} \quad (4.11)$$

The observed $s - d$ hyperfine splitting of order 1 MeV motivates Jenkins [58] to choose the counterterm $\frac{2\Delta_1}{m_Q}m_s$ to be ~ -27 MeV. Equation (4.7) indicates the leading order nonscaling contributions from light-flavour symmetry-breaking are all terms of $O(1/m_Q)$. This implies,

$$\frac{(B_d^* - B_d)}{(D_d^* - D_d)} \approx \frac{\Delta_{s-d}(B^* - B)}{\Delta_{s-d}(D^* - D)} \approx \frac{m_c}{m_b}. \quad (4.12)$$

The ratio of (4.9) and (4.11) support this relation, assuming $m_c \approx 1.5$ and $m_b \approx 5.0$ GeV.

Applying chiral HQET to the spin-average of the meson masses,

$$\Delta_{s-d} \left[\frac{1}{4}(m_{PS} + 3m_V) \right] \equiv \frac{1}{4}[m_{PS}(Q\bar{s}) + 3m_V(Q\bar{s})] - \frac{1}{4}[m_{PS}(Q\bar{d}) + 3m_V(Q\bar{d})] \\ = 2\epsilon_1 m_s - g^2 \left(1 + \frac{4}{3\sqrt{3}} \right) \frac{M_K^3}{16\pi f^2} \\ - 2\epsilon_1 m_s \left(\frac{1}{2} + \frac{9}{2}g^2 \right) \frac{M_K^2}{16\pi^2 f^2} \ln \left(\frac{M_K^2}{\Lambda_\chi^2} \right) \\ - \frac{4}{3}\epsilon_1 m_s \frac{M_\eta^2}{16\pi^2 f^2} \ln \left(\frac{M_\eta^2}{\Lambda_\chi^2} \right) + 4\epsilon_2 m_s^2 + 4\epsilon_2' m_s^2. \quad (4.14)$$

The static binding energy coefficient ϵ_1 is directly analogous to Δ_1 (in equation (4.7)). ϵ_2 and ϵ_2' are coefficients of the quadratic terms in the expansion in

powers of m_q and also of order 1 in the expansion in powers of $1/m_Q$. Since the light flavour symmetry breaking in the hyperfine splitting is only of order a few percent the predictions for the spin-averaged splittings can be compared to the experimental values for $m_{PS}(Q\bar{s}) - m_{PS}(Q\bar{d})$:

$$D_s^+ - D^+ = 99.5 \pm 0.6 \text{ MeV [32]} \quad (4.15)$$

$$B_s - B = 82.5 \pm 2.5 \text{ MeV,} \\ 121 \pm 9 \text{ MeV [61]} \quad (4.16)$$

$$\text{or } 96 \pm 6 \text{ MeV [63].} \quad (4.17)$$

There is a large uncertainty in the experimental value of the $s - d$ splitting for the B meson; however, these results suggest the dependence of the splitting on m_Q may be up to 10 – 20%. In contrast, equation (4.14) shows $\Delta_{s-d}[\frac{1}{4}(m_{PS} + 3m_V)]$ is independent of m_Q to leading order.

When considering a lattice calculation of these mass splittings using the general Wilson action, care must be taken when identifying the quark mass appearing in each equation if $m_Q a \sim 1$. The results of the previous chapter suggest that the heavy quark mass associated with the hyperfine term $\Delta(Ql)/m_Q$ in equation (4.1), and consequently (4.5), (4.7) and (4.14), should be distinguished from the heavy-quark mass defined in equation (4.4); the latter corresponding to the static heavy-quark mass. Thus an independent measurement of the hyperfine quark mass, m_{Q3} , is necessary before the dependence of the mass splittings on the heavy-quark mass can be determined. Unfortunately it is not possible to define m_{Q3} other than through these mass splittings, and therefore it must be approximated using either the static or dynamical mass.

For the dynamical mass, support for this approximation is found in the tree level result for the hyperfine mass, discussed in §(3.2). Equation (3.10) shows that the tree level value for the coefficient of the clover term, used in this simulation, is such that the dynamical mass equals the hyperfine mass. Using the mean field theory

approach, discussed in §(1.2.3), higher order corrections are estimated to change c to 1.5(1.4) at $\beta = 6.0(6.2)$. In the same analysis the mean field value of c is required for $m_{Q_3} = m_{Q_2}$. However in equation (3.8) the hyperfine and dynamical quark masses are equal, and independent of c , in the limit of very heavy-quark masses.

Alternatively the uncertainty in the value of m_{Q_3} can be removed if it is fixed to reproduce the experimental value of the hyperfine splitting. Such a procedure is more relevant to NRQCD where the hyperfine term appears explicitly in the action. The mass parameter is fixed to a given physical quark mass, using the lattice scale. By tuning the coefficient of the hyperfine term, distinct from the mass parameter, the $\bar{q}Q$ hyperfine splitting is matched to experiment. The value of the coefficient obtained can then be used to predict the splitting for the degenerate meson with the same heavy quark. As suggested by Thacker et al. [42], this is relevant in the $\bar{b}b$ system where a measurement of the hyperfine splitting would allow a prediction of the η_b mass.

The discussion in the following section will show that there is no clear theoretical prediction for the dependence of the hyperfine splitting on m_Q in the $\bar{Q}Q$ system. Since the non-relativistic approach used here assumes a continuum form for the dependence of lattice energy states on the heavy-quark mass, fixing m_{Q_3} using the non-degenerate mesons will not allow a prediction in the corresponding degenerate case. Furthermore it is undesirable to fix the heavy-quark mass using a quantity where the affect of quenching is unaccounted for and may be large.

The dynamical heavy-quark mass (\bar{m}_{Q_2}) can be defined in an identical way to \bar{m}_Q in equation (4.4), using the dynamical vector and pseudoscalar meson masses. For the comparison of the $s - d$ pseudoscalar and spin-averaged meson splittings only the static quark mass need be considered; the dependence on m_Q is introduced through the static binding energy $\epsilon(Ql)$.

4.1.2 Heavy-Heavy Mesons: Potential Models

The non-relativistic description of heavy-quark mesons using potential models has long been established as successful (for a review see [64]). The quark-antiquark bound states are modelled in a similar way to positronium, using the Schrödinger equation with a spherical potential; relativistic corrections are then added as perturbations. The largest correction for S -state mesons is the chromomagnetic hyperfine interaction. To this order the dependence of the meson mass $m(\bar{Q}_1 Q_2)$ on the constituent heavy-quark masses, m_{Q_1} and m_{Q_2} , can be summarised as

$$m(\bar{Q}_1 Q_2) = m_{Q_1} + m_{Q_2} + \frac{\xi(m_{Q_1}, m_{Q_2}) \langle \mathbf{S}_{Q_1} \cdot \mathbf{S}_{Q_2} \rangle}{m_{Q_1} m_{Q_2}} \quad (4.18)$$

where the hyperfine constant, ξ , can be expressed in terms of the wavefunction at the origin:

$$\xi = \frac{32\pi}{9} \alpha_s(m) |\psi(0)|^2. \quad (4.19)$$

Note that ξ is zero for non-zero orbital angular momentum, since the wavefunction vanishes at the origin. The dependence of ξ on the heavy-quark masses becomes explicit when $|\psi(0)|^2$ is related to the potential $V(r)$:

$$|\psi(0)|^2 = \frac{1}{2\pi} \frac{m_{Q_1} m_{Q_2}}{(m_{Q_1} + m_{Q_2})} \left\langle \frac{\partial V(r)}{\partial r} \right\rangle \quad (4.20)$$

This is a fundamental property of solutions to Schrödinger's equation for spherically symmetric potentials. Combining (4.19) and (4.20), the S -wave mass splittings in quarkonia become,

$$m_V(\bar{Q}Q) - m_{PS}(\bar{Q}Q) = \frac{8}{9} \frac{\alpha_s(m_Q)}{m_Q} \langle V'(r) \rangle \quad (4.21)$$

$$(m_V(\bar{Q}Q))^2 - (m_{PS}(\bar{Q}Q))^2 = \frac{32}{9} \alpha_s(m_Q) \langle V'(r) \rangle \quad (4.22)$$

In equation (4.22) terms of order $1/m_Q^2$ have been neglected.

In order to uncover further heavy-quark dependence in these splittings it is instructive to consider a specific potential for $\langle V'(r) \rangle$. A commonly used form for

$V(r)$ is the funnel potential,

$$V(r) = -\frac{4}{3} \frac{\alpha_s(m_Q)}{r} + br + V_0 \quad (4.23)$$

where the strong coupling, $\alpha_s(m_Q)$, can be approximated using equation (3.35). When the quark is light, the linear term in the funnel potential is more influential than the Coulomb term, and $\langle V'(r) \rangle$ can be approximated by a constant. Hence the difference of the squared meson masses depends on the quark mass only through the slowly varying strong coupling (the hyperfine splitting has an additional $1/m_Q$ dependence). The experimental values of $m_V^2 - m_{PS}^2$, for the light degenerate, and non-degenerate mesons

$$m_\rho^2 - m_\pi^2 = 0.57 \text{ GeV}^2 \quad (4.24)$$

$$m_{K^*} - m_K = 0.55 \text{ GeV}^2 \quad (4.25)$$

shows the splitting to be roughly constant, supporting this analysis. However, it cannot be assumed that a potential model is still valid in this region of quark mass, since it is unlikely the behaviour of the valence quarks is non-relativistic.

At the other extreme, where the quark mass is very large, the linear term in the potential can be discarded. From the pure Coulomb term remaining,

$$\langle V'(r) \rangle \sim \alpha_s^3(m_Q) m_Q^2, \quad (4.26)$$

and thus the hyperfine splitting becomes,

$$m_V(\bar{Q}Q) - m_{PS}(\bar{Q}Q) \sim \alpha_s^4(m_Q) m_Q \sim m_Q \ln^{-4}(m_Q/\Lambda_{QCD}) \quad (4.27)$$

The $m_V^2 - m_{PS}^2$ splitting has the same form with an additional factor of m_Q . This prediction is valid over the c to b quark mass range of interest, but (4.27) is clearly an overestimate in the limit of infinite quark mass. The gradient of the potential, and hence the wavefunction at the origin, becomes singular and the spin dependent term in equation (4.18) can no longer be viewed as a relativistic perturbation. Other potential models can be constructed which weaken the Coulomb singularity

and produce different behaviour for the hyperfine splitting [65]. This serves to illustrate how speculative the theoretical predictions are for the dependence of the mass splittings on the heavy-quark mass. Little experimental data exists to provide any guidance. The mass splittings for the charmonium system are,

$$m_{J/\psi} - m_{\eta_c} = 0.117 \text{ GeV} \quad (4.28)$$

$$m_{J/\psi}^2 - m_{\eta_c}^2 = 0.72 \text{ GeV}^2 \quad (4.29)$$

It remains to calculate the splitting nonperturbatively to find the dependence of $\langle V'(r) \rangle$ on the quark mass. A definition is required for m_Q ; this can be obtained analogously to equation (4.4):

$$m_Q \approx \bar{m}_Q \equiv \frac{1}{8} [m_{PS}(\bar{Q}Q) + 3m_V(\bar{Q}Q)]. \quad (4.30)$$

For the charmonium and bottomonium systems, the lattice quark masses are of order a^{-1} . In this regime it is particularly important to distinguish between the different mass scales present, and therefore a comparison of the dynamical and static quark masses, as crude estimates of m_{Q3} , will be made. In addition, the leptonic width, m_V^2/f_V , will be used to fix the charm quark mass. As mentioned in §(3.10.4), the leptonic width is related to the value of the wavefunction at the origin, and this suggests it is also determined by m_{Q3} .

It is worth noting that the hyperfine splitting obtained on the lattice must always be positive for degenerate mesons. This follows from the observation of §(1.5) that the $\bar{q}q$ pseudoscalar correlator is the absolute value of the quark propagator squared (see equation (1.37)). Hence an operator constructed from any other combination of gamma matrices will result in a correlator of smaller magnitude. Consider the asymptotic form of any 2pt-correlator in Euclidean space, $C(t) \sim e^{-mt}$. In order for the pseudoscalar correlator to be larger in magnitude, the slope, and hence the mass, of the vector correlator must always be greater than the pseudoscalar mass.

4.1.3 The Effect of Quenching on the Hyperfine Splitting

The effect of the quenched approximation on the hyperfine splitting can be understood qualitatively for charmonium. The energy level spectrum can be described reasonable well by a potential model of the form (4.23), and therefore only the effect of the sea quarks on the potential itself must be considered. If the physical scale for the lattice calculation is set at an energy scale corresponding to intermediate separations of the quark and antiquark, and hence the quenched and unquenched potentials are matched in this region. At smaller separations, where the linear term in equation (4.23) can be neglected, the potentials will differ. The strong coupling appearing in the funnel potential varies less rapidly with distance in the quenched approximation and hence the quenched potential must be less steep at small distances. If this remains true out to separations where the potentials are matched, the quenched potential must lie above the unquenched one at short distances. Thus the strong coupling is weaker at short distances, in the absence of sea quarks. From equation (4.22) this will translate into a smaller value for the hyperfine splitting. The amplitude of the wavefunction at the origin is also a quantity dependent on short distance effects. Equation (4.20) and (4.26) show that a smaller strong coupling will decrease the hyperfine splitting further through $|\psi(0)|$.

A quantitative estimate of this effect has been obtained by El-Khadra [52]. The Richardson potential was used,

$$V(q^2) = \frac{4\pi}{\beta_0^{(n_f)}} \frac{1}{q^2 \ln(1 + q^2/\Lambda_{QCD}^2)}, \quad (4.31)$$

which has the same form as the funnel potential in configuration space. Fitting the Richardson potential to the experimental charmonium system, with $n_f = 3$ and $n_f = 0$, the difference in the amplitude of wavefunction at the origin was found to be:

$$\frac{|\psi^{(0)}(0)|}{|\psi^{(3)}(0)|} = 0.86 \quad (4.32)$$

The effect of quenching on $\alpha_s(m_Q)$ was also estimated [66]:

$$\frac{\alpha_s^{(0)}(m_c)}{\alpha_s^{(3)}(m_c)} = 0.81 \begin{matrix} + 6 \\ - 6 \end{matrix} \quad (4.33)$$

This is in agreement with the naive value of 9/11, derived from equation (3.35). The overall reduction in the hyperfine splitting is approximately $\sim 40\%$. The “quenched corrected” estimate for the hyperfine splitting in charmonium is then:

$$(m_{J/\psi} - m_{\eta_c})^{\text{quenched}} \approx 70 \text{ MeV} \quad (4.34)$$

Since the Richardson potential has only been tested in the $n_f = 3$ case, this result can only be viewed as preliminary. Furthermore, a similar analysis of other models may show the correction to be very model dependent. Nevertheless (4.34) does indicate the possible order of magnitude of the quenched correction.

The effect of using the quenched approximation can also be estimated for the leptonic width. As noted in §(3.10.4), $V_{\bar{c}c}$ is simply the wavefunction at the origin, and therefore is less sensitive to the effect of sea quarks on the potential compared to the hyperfine splitting. Using (4.32), $V_{\bar{c}c}$ is reduced by approximately 14%, from 1.19 GeV² [32] to $V_{\bar{c}c}^{\text{quench}} = 1.02 \text{ GeV}^2$.

4.2 Computational Details and Fitting Procedure

The results for this chapter were obtained using the zero momentum correlators detailed in §(3.3). For the Wilson action, additional meson correlators exist at $\beta = 6.2$ on 18 configurations at one value of the hopping parameter, $\kappa_Q = 0.135$, corresponding to a pseudoscalar static mass roughly equal to η_c . The hyperfine splitting was obtained from the ratio of the vector and pseudoscalar correlators, using a fitting function of the form,

$$\frac{\sum_{\mathbf{x},i} \langle V_i(\mathbf{x}, t) V_i^\dagger(0) \rangle}{\sum_{\mathbf{x}} \langle P(\mathbf{x}, t) P^\dagger(0) \rangle} \sim R e^{-(m_V - m_{PS})t}, \quad t < L_t/2. \quad (4.35)$$

degenerate		
Clover		
β	κ_Q	fitting range
6.2	0.133, 0.129, 0.125	16-22 (SL)
	0.121	16-21 (SL)
6.0	all	12-21 (SL)
Wilson		
6.2	0.135	14-20 (LL)
6.0	all	10-16 (LL)

non-degenerate			
Clover			
β	κ_q	κ_Q	fitting range
6.2	all combinations		11-17 (SS)
6.0	0.1432	0.092, 0.111	16-20 (SL)
		others	12-21 (SL)
	0.1440, 0.1445	0.092, 0.111	16-20 (SL)
		others	12-20 (SL)
Wilson			
6.0	0.1550	all	10-16 (SL)

Table 4.1: The fitting ranges for hyperfine splitting from the ratio of propagators, where the smearing used is shown in brackets.

The fitting ranges chosen, using the standard fitting procedure of §(1.6.4), are shown in table 4.1 along with the smearing combination used for the heavy-quark propagator. For the Wilson action at $\beta = 6.0$, the fit to the ratio of non-degenerate correlators omits alternate timeslices within the fitting range; the limited number of configurations available presented an identical problem to that found when fitting to the individual correlators, as discussed in §(3.3). All the fits were performed taking the correlations between different timeslices into account and the errors were obtained using the bootstrap method outlined in §(1.6.3). For a comparison of the dependence of the hyperfine splitting on the static and dynamical quark mass, the dynamical meson masses presented in chapter 3 are used in conjunction with equation (4.4). This comparison is not possible for the Wilson action at $\beta = 6.2$ since there are no finite momentum correlators with which to estimate \bar{m}_{Q2} .

4.3 Results for the Hyperfine Splitting in Heavy-Heavy Mesons

The results for $m_V^2 - m_{PS}^2$ at $\beta = 6.0$ and 6.2 are presented in figure 4.1. Also shown are the values of the splittings obtained for degenerate mesons at three different light quark masses for the clover action at $\beta = 6.2$ and 6.0, and the Wilson action at 6.2; there is one light quark mass available at $\beta = 6.0$ for the Wilson action.

From the discussion in §(4.1.2) $m_V^2 - m_{PS}^2$ is expected to be roughly constant in the light quark sector. As the quark mass increases, (4.25) and (4.29) show the splitting should also increase. In figure 4.1, the splitting at the lightest quark mass from the clover action at both β values, is consistent with the experimental value for $\rho^2 - \pi^2$. As the quark mass increases, the splitting shows little variation at

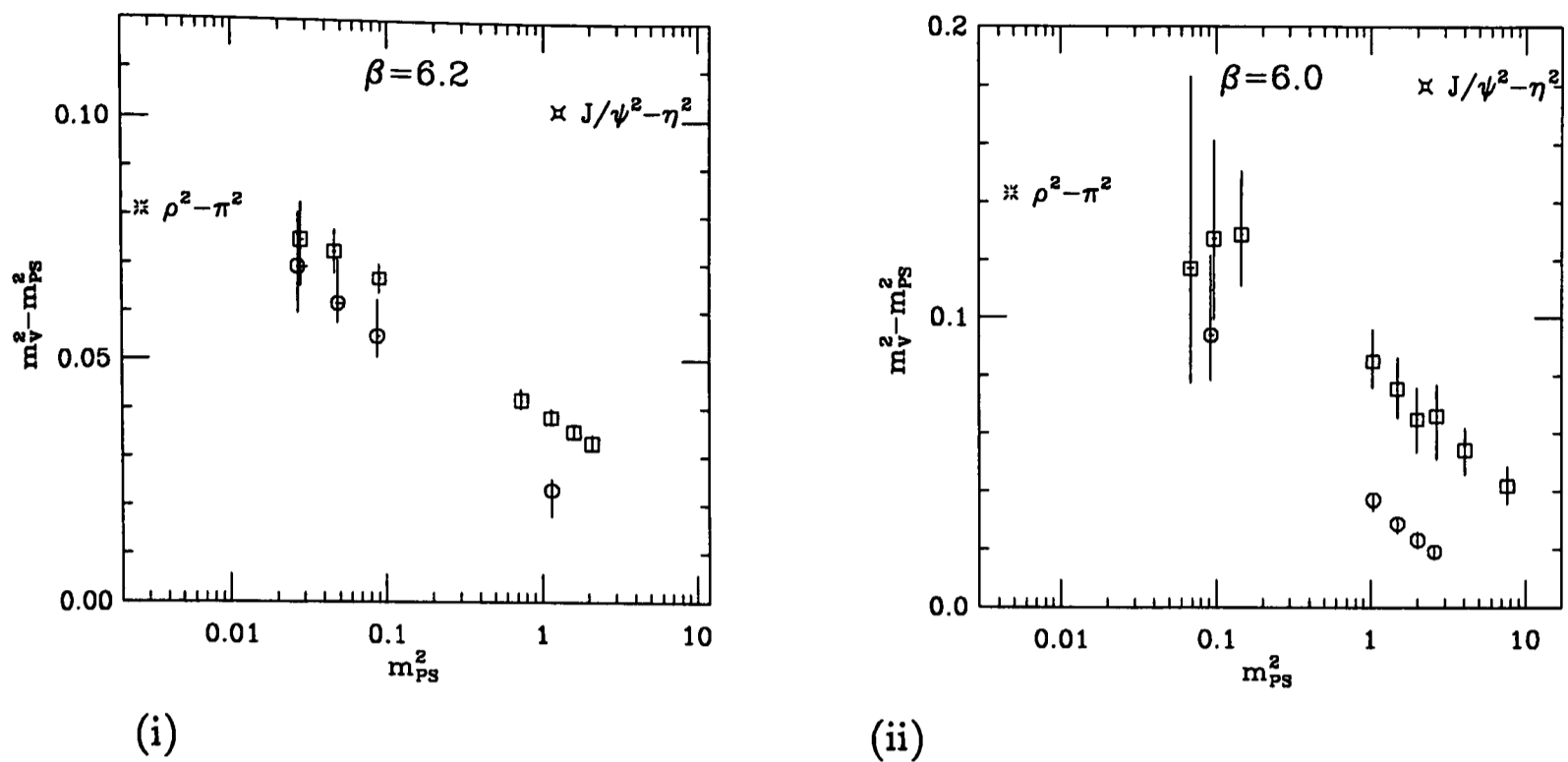


Figure 4.1: $m_V^2 - m_{PS}^2$ versus m_{PS}^2 , in lattice units, for the Wilson (circles) and clover (squares) actions, at (i) $\beta = 6.2$ and (ii) 6.0. Also shown are the experimental results for charmonium and $\rho^2 - \pi^2$.

$\beta = 6.0$, while for $\beta = 6.2$, where the statistical errors are smaller, a slow decrease is seen. This trend continues into the heavy-quark sector where $m_V^2 - m_{PS}^2$ falls significantly, contrary to the experimental results. However as the meson mass increases the difference between the Wilson and Clover results becomes more significant at both values of β .

The values obtained for the hyperfine splitting are shown in figures 4.2 (i) and (ii), plotted against the inverse of the static and dynamical quark masses respectively. The lattice scale from m_ρ was used to convert the results into physical units. A fit to the functional form,

$$m_V - m_{PS} = a_1 + \frac{a_2}{\bar{m}_Q} + \frac{a_3}{\bar{m}_Q^2}, \quad (4.36)$$

was performed to each data set, taking the correlations between different quark masses into account; the values of the fit parameters obtained are detailed in table 4.2.

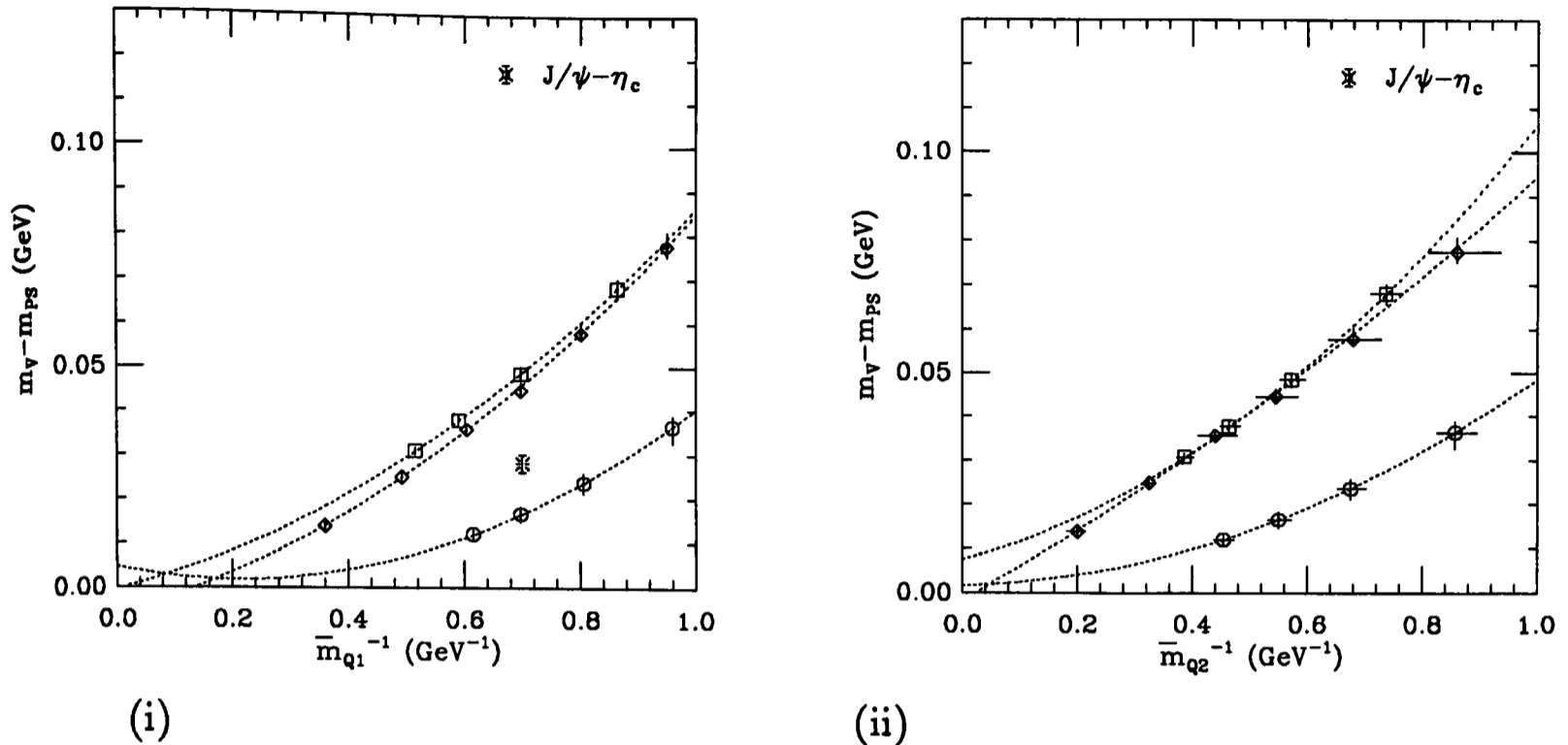


Figure 4.2: $m_V - m_{PS}$ versus (i) $1/\bar{m}_{Q1}$ (ii) $1/\bar{m}_{Q2}$, in physical units, for the Wilson action at $\beta = 6.0$ (circles) and $\beta = 6.2$ (bursts), and for the clover action at $\beta = 6.0$ (diamonds) and $\beta = 6.2$ (squares). The broken and solid lines show a quadratic and linear fit to the data, respectively. The experimental value for $m_{J/\psi} - m_{\eta_c}$ is also included (fancy square)

\vec{a}	Wilson, $\beta = 6.0$		Clover, $\beta = 6.0$		Clover, $\beta = 6.2$	
	\bar{m}_{Q1}	\bar{m}_{Q2}	\bar{m}_{Q1}	\bar{m}_{Q2}	\bar{m}_{Q1}	\bar{m}_{Q2}
a_1	$0.00 + 1$ - 2	$0.00 + 1$ - 1	$-0.006 + 5$ - 7	$-0.001 + 5$ - 5	$-0.000 + 5$ - 4	$0.007 + 2$ - 4
a_2	$-0.03 + 6$ - 4	$0.00 + 4$ - 3	$0.034 + 23$ - 18	$0.075 + 24$ - 24	$0.032 + 17$ - 13	$0.04 + 2$ - 1
a_3	$0.13 + 5$ - 8	$0.09 + 4$ - 6	$0.11 + 3$ - 4	$0.043 + 44$ - 55	$0.11 + 2$ - 3	$0.13 + 3$ - 4
χ^2	.1/1	0.01/1	3.3/3	2./3	0.3/1	1.1/1

Table 4.2: The parameters obtained from fitting to the hyperfine splitting using the static and dynamical quark masses.

Figure 4.2 (i) shows the hyperfine splitting is very sensitive to the presence of the spin dependent improvement term. Using the clover action instead of the Wilson action, results in a marked increase in the splitting and a reduction in the dependence on the lattice spacing. m_{Q_1} is also likely to be sensitive to discretisation errors. However, the Wilson and clover data can only be compared if the corresponding values of \bar{m}_{Q_1} are matched, and in the absence of a theoretical prediction for the dependence of the splitting on the heavy-quark mass it is difficult to untangle the discretisation errors arising from \bar{m}_{Q_1} , from those present in the splitting. Nevertheless, for the purposes of a comparison with m_{Q_2} , the results of §(3.5.2) suggest both masses have a similar dependence on a .

Another important feature of the figure is the nonlinear dependence of the splitting on the heavy-quark mass, for both the Wilson and clover data. A successful fit to the data points could not be obtained without the inclusion of the quadratic term in (4.36). The extrapolations of the fits, at both β values, are consistent with positive values of the hyperfine splitting for all \bar{m}_{Q_1} , and the intercepts of the fits are consistent, within $\sim 1\sigma$, with the splitting vanishing in the limit of infinite quark mass. A slight increase is seen in the splitting from the Wilson data as \bar{m}_{Q_1} increases, however this is not statistically significant.

If, instead, the hyperfine splitting is plotted against \bar{m}_{Q_2} , figure 4.2 (ii) shows that similar behaviour is found. The dynamical quark mass corresponding to each κ value is greater than the static quark mass. Thus, since the splitting increases with decreasing heavy quark mass, using \bar{m}_{Q_2} produces a larger estimate for the hyperfine splitting compared to \bar{m}_{Q_1} at a given physical mass. Over the range of quark mass values used, there is less dependence on the lattice spacing in the clover data compared to that seen in figure 4.2 (i). However, the errors in \bar{m}_Q are larger, and the extrapolations of the fits to both lighter and heavier quark masses suggest the agreement is not significant. The differing sensitivity to the value of a found using \bar{m}_{Q_1} and \bar{m}_{Q_2} illustrates how lattice artifacts can be over

or underestimated if the wrong mass scale is used.

At $\beta = 6.0$ the data obtained using the clover action can be fitted to a straight line; the intercept is still within 1σ of the origin. If the dynamical quark mass is a close approximation to the hyperfine quark mass in the region of very large m_Q , the difference in the functional dependence at $\beta = 6.2$ and 6.0 for the clover data would suggest either m_{Q2} or m_{Q3} is sensitive to the value of the lattice spacing. However in the absence of a firm theoretical prediction for the behaviour of the hyperfine splitting as the heavy-quark mass diverges, it is impossible to determine which, between m_{Q1} and m_{Q2} , is a better approximation to m_{Q3} . Conversely, there is no firm indication from the data of the functional dependence of the splitting on m_Q .

Predictions for the hyperfine splitting in charmonium and bottomonium can be extracted from the data. Experimental estimates of m_c and m_b are needed, but since the quark mass is not a well defined quantity, only very approximate values are available. Using the definition of the heavy-quark mass in equation (4.4) with the experimental meson masses, $m_c \sim 1.5$ GeV and $m_b \sim 4.7$ GeV. These values are within the mass ranges predicted using potential model calculations, where $m_c = 1.3 - 1.7$ GeV and $m_b = 4.7 - 5.3$ GeV [32].

From figures 4.2(i) and (ii), m_c lies between existing data points and $m_{J/\psi} - m_{\eta_c}$ can be obtained by interpolation using the fit parameters detailed in table 4.2, while an extrapolation is needed to reach $m_Q = m_b$. Table 4.3 shows the results for $\bar{c}c$ and $\bar{b}b$, using the clover action at $\beta = 6.0$ and 6.2 . The uncertainty in the value of m_Q creates a systematic error in the splitting. Using the bounds for m_c and m_b from the potential model calculations, leads to a $\sim 20\%$ and $\sim 10\%$ variation in the hyperfine splitting for charmonium and bottomonium respectively.

The values obtained for $m_{J/\psi} - m_{\eta_c}$ using the dynamical mass are significantly

	charmonium		bottomonium	
	$\beta = 6.0$	$\beta = 6.2$	$\beta = 6.0$	$\beta = 6.2$
m_{Q1}	40^{+2}_{-1}	44^{+1}_{-1}	9^{+2}_{-2}	-
m_{Q2}	56^{+4}_{-6}	57^{+3}_{-3}	15^{+1}_{-1}	18^{+1}_{-1}
expt	117^{+2}_{-2}		-	

Table 4.3: The predicted values of the hyperfine splitting in charmonium and bottomonium, in MeV, obtained using the dynamical and static quark masses for clover action at $\beta = 6.0$ and 6.2

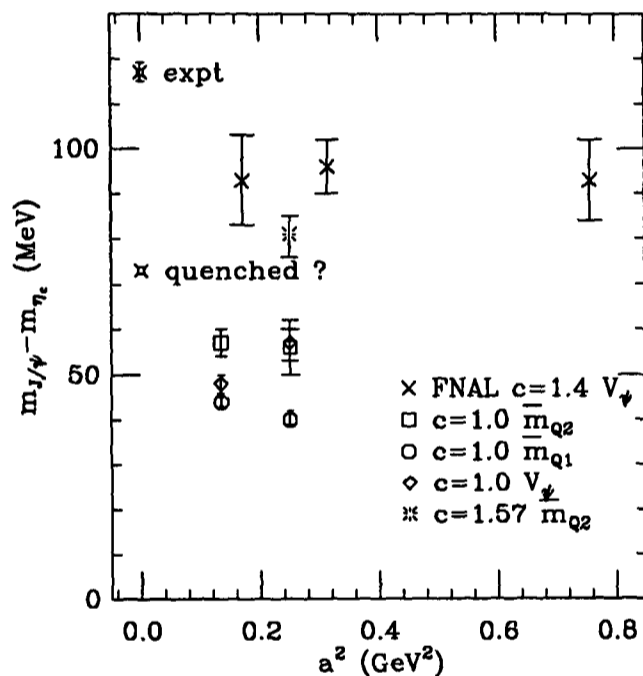


Figure 4.3: $m_{J/\psi} - m_{\eta_c}$ versus a^2 in physical units. Also shown is the value of the hyperfine splitting obtained if the leptonic width is used to set the charm quark mass.

larger compared to the static mass results, but all lie well below the experimental result. Quenching may account for a large part of this discrepancy; this effect is likely to be even more significant in bottomonium, since heavier quark masses are more sensitive to changes in the potential at short distances.

Figure 4.3 shows the variation of the hyperfine splitting with a^2 for charmonium, where a lattice scale of 2(2.7) GeV is used at $\beta = 6.0(6.2)$. Also included are the results derived using $V_{\bar{c}c}^{quench}$ to set the charm quark mass. At $\beta = 6.0$, using the leptonic width yields a splitting which is consistent with the value obtained using \bar{m}_{Q_2} . This is a reflection of the agreement found between the prediction for $V_{\bar{c}c}$ obtained by setting m_c using m_{Q_2} , and $V_{\bar{c}c}^{quench}$, discussed in §(3.10.4). The splittings from both quantities are ~ 15 MeV lower than the predicted quenched corrected value of the hyperfine splitting.

Also shown in figure 4.3 is a *preliminary* result for the hyperfine splitting obtained using $c = 1.57$ at $\beta = 6.0$ on the $16^3 \times 48$ lattice with 36 configurations [48]. This value of the clover coefficient corresponds to the mean-field estimate of c at $\beta = 6.0$, if $u_0 = (8\kappa_d)^{-1}$ is taken as the definition of the mean link. Using $c = 1.57$ may be a slight overestimate of the effect of the higher order corrections, since the plaquette definition of u_0 yields $c = 1.5$. However, results obtained using the latter value, at a quark mass slightly less than charm, show no indication of a significant change in the splitting. An equivalent calculation at a much smaller or larger value of β is needed to test for a reduction in the sensitivity to the value of the lattice spacing using a mean-field value of c compared to $c = 1.0$.

The charm quark mass was fixed using the dynamical mass. Figure 4.3 shows the resulting splitting is approximately 25 MeV larger than that for $c = 1$, and closer to the quenched corrected value. Using $V_{\bar{c}c}$ to fix m_c produces a consistent result, however Z_V has yet to be determined, and this leads to a 15% uncertainty in the splitting. The hyperfine splitting is also in closer agreement, with the results of the Fermilab group [52] for $c = 1.4$. These authors used $V_{\bar{c}c}^{quench}$ to set the charm quark mass, and determined the lattice spacing from the $1P - 1S$ splitting.

At $\beta = 6.2$, the $\sim 3\sigma$ discrepancy between the splittings obtained by setting the charm quark mass using the dynamical mass and leptonic width is expected from

the results of §(3.10.4). Considering the sensitivity of the hyperfine splitting to the value of the clover coefficient, the small dependence on a seen in the splitting obtained using \bar{m}_{Q_2} is unlikely to be fundamental.

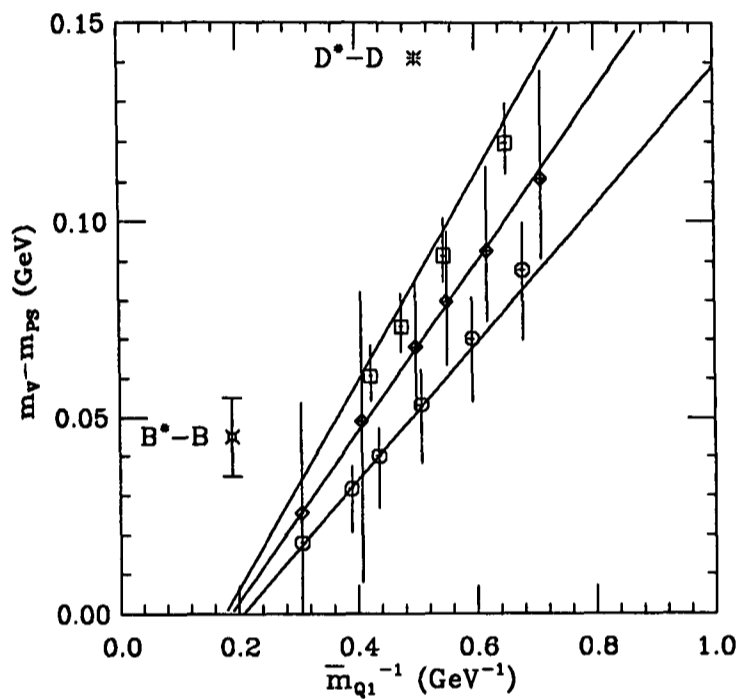
4.4 Results for Heavy-Light Mesons

4.4.1 The Hyperfine Splitting

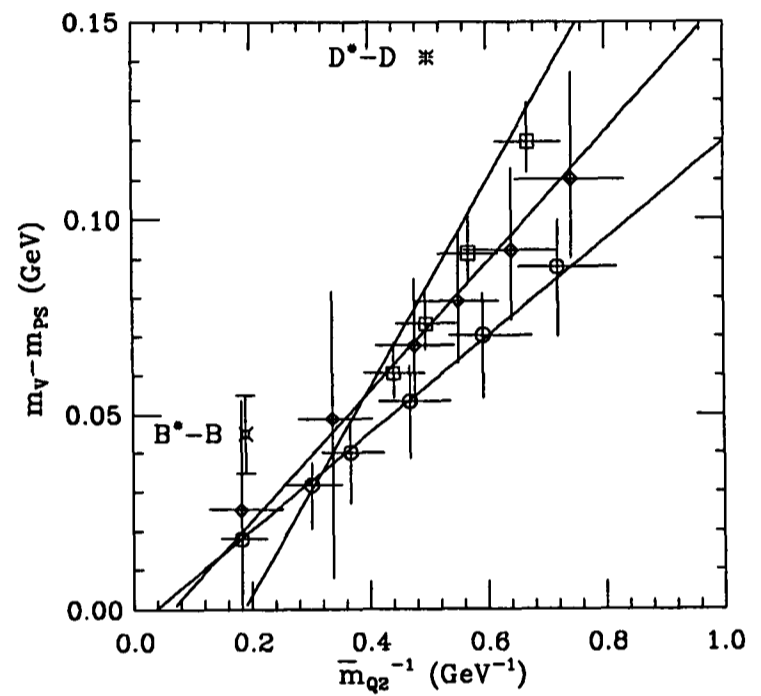
The values of the hyperfine splitting obtained from a chiral extrapolation of the light quark mass, for the clover action at $\beta = 6.0$ and 6.2 , are shown in figures 4.4 (i) and (ii), plotted against the inverse of \bar{m}_{Q_1} and \bar{m}_{Q_2} respectively; \bar{m}_{Q_i} corresponds to the spin-average of the chirally extrapolated meson masses. The results for the Wilson action are also shown for a single value of the light quark mass close to strange. Note that, as the light quark mass of the mesons used in equation (4.4) increases, \bar{m}_Q becomes a less reliable estimate of m_Q . Using the range of light quark masses available for the clover data at $\beta = 6.0$, the decrease in \bar{m}_{Q_1} and \bar{m}_{Q_2} is of order 3% and 10% respectively, as m_q is reduced from $\sim m_s$ to zero. This decrease is of the same order of magnitude as the statistical errors, 5% and 10% for \bar{m}_{Q_1} and \bar{m}_{Q_2} respectively, in the Wilson data.

A noticeable feature in the clover data at $\beta = 6.0$ is the larger statistical errors for the two heaviest values of \bar{m}_Q . A decrease in the errors in the splitting is expected as the quark mass increases, however the fitting range used begins at timeslice 16, compared to 12 for the smaller values of \bar{m}_Q .

Linear behaviour with $1/\bar{m}_Q$ is apparent in both figures and correlated fits to the data were performed using the functional form of equation (4.36), with $a_3 = 0$; the parameters obtained are given in table 4.4.



(i)



(ii)

Figure 4.4: $m_V - m_{PS}$ versus (i) $1/\bar{m}_{Q1}$ (ii) $1/\bar{m}_{Q2}$, in physical units, for the clover action at $\beta = 6.0$ (diamonds) and $\beta = 6.2$ (squares) and the Wilson action at $\beta = 6.0$ (circles). The solid lines show a linear fit to the data. Also included are the experimental values for the $D^* - D$ (burst) and $B^* - B$ (fancy square) splittings.

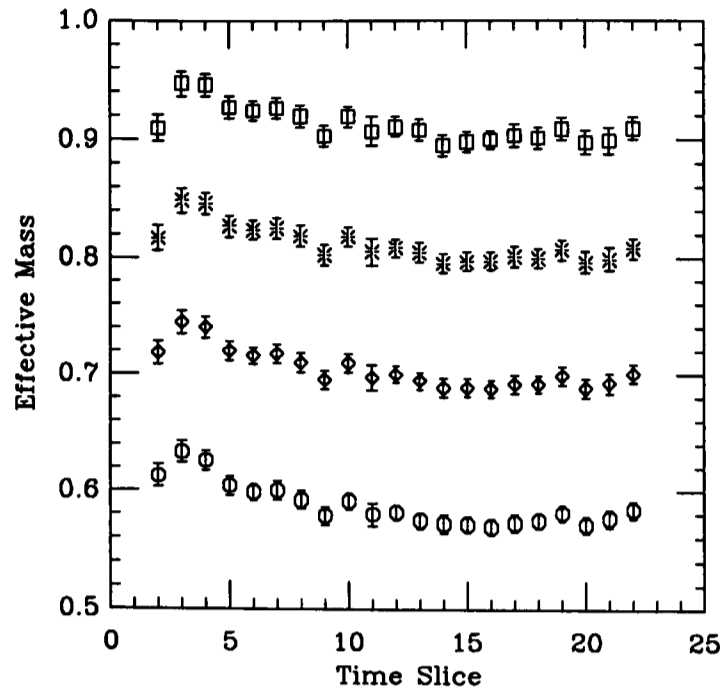


Figure 4.5: The effective masses derived from the SS correlators in the pseudoscalar channel, for the clover action at $\beta = 6.2$ with $\kappa_q = 0.14226$ and $\kappa_Q = 0.133$ (circles), 0.129 (diamonds), 0.125 (bursts) and 0.121 (squares).

The correlated fit obtained for the clover data at $\beta = 6.2$ warrants some discussion. Figure 4.4 shows the correlated fit lies above all the data points. This is due to the presence of large correlations between the data points, and hence an almost singular correlation matrix; in these circumstances a correlated fit becomes extremely sensitive to any deviation in the data from the behaviour specified by the model function. These deviations can become amplified and the fit can lie several σ from the data points [67]. However, a bad fit is still reliably indicated by a large value for the χ^2 . Hence, since the χ^2 is reasonable, the effect is not statistically significant for this data. Likewise, although performing a quadratic fit produces a curve which is, to the eye, in closer agreement with the data, the quadratic term is also not statistically significant.

High correlations between data points corresponding to different values of the heavy quark mass is not unexpected. The heavy quark propagator has little sensitivity to the fluctuations in the gauge fields, reflected in the small statistical errors in the correlators constructed from heavy quark propagators. This is il-

illustrated in figure 4.5, which shows the effective masses extracted from the SS correlators in the non-degenerate pseudoscalar channel at $\beta = 6.2$ using the clover action. The variation of the effective mass with timeslice is identical for the four values of the heavy quark mass. If the same fitting range is used to extract a quantity from a function of the correlators, for all κ_Q , the correlations between data values obtained is increased. In this case the increase in the correlations is to a point where the correlation matrix is close to singular. For the clover data at $\beta = 6.0$, where different fitting ranges are used for different values of κ_Q , the correlated fit is well behaved.

Clover, $\beta = 6.2$, $\kappa_d = 0.14313$			
	a_1	a_2	χ^2
\bar{m}_{Q1}	$-0.047 \begin{smallmatrix} + 7 \\ - 8 \end{smallmatrix}$	$0.26 \begin{smallmatrix} + 2 \\ - 3 \end{smallmatrix}$	3./2
\bar{m}_{Q2}	$-0.05 \begin{smallmatrix} + 3 \\ - 2 \end{smallmatrix}$	$0.27 \begin{smallmatrix} + 3 \\ - 6 \end{smallmatrix}$	6./2
Clover, $\beta = 6.0$, $\kappa_d = 0.14513$			
\bar{m}_{Q1}	$-0.04 \begin{smallmatrix} + 3 \\ - 4 \end{smallmatrix}$	$0.21 \begin{smallmatrix} + 9 \\ - 6 \end{smallmatrix}$	0.1/4
\bar{m}_{Q2}	$-0.01 \begin{smallmatrix} + 3 \\ - 3 \end{smallmatrix}$	$0.17 \begin{smallmatrix} + 6 \\ - 6 \end{smallmatrix}$.6/4
Wilson, $\beta = 6.0$, $\kappa_l = 0.1550$			
\bar{m}_{Q1}	$-0.04 \begin{smallmatrix} + 1 \\ - 1 \end{smallmatrix}$	$0.18 \begin{smallmatrix} + 3 \\ - 4 \end{smallmatrix}$	2./4
\bar{m}_{Q2}	$-0.00 \begin{smallmatrix} + 1 \\ - 1 \end{smallmatrix}$	$0.12 \begin{smallmatrix} + 1 \\ - 4 \end{smallmatrix}$	0.5/4

Table 4.4: The parameters obtained from fitting to the hyperfine splitting using the dynamical and static quark masses.

Equation (4.5) predicts a linear dependence for the hyperfine splitting on $1/m_Q$. However the splitting is also expected to vanish as the heavy-quark mass diverges. At $\beta = 6.0$ this feature is seen in the results for both actions if \bar{m}_{Q2} is used.

Although the statistical errors are large, this suggests the dynamical quark mass is a good approximation to the hyperfine quark mass. The behaviour of the clover data at $\beta = 6.2$ is effectively unchanged by the use of the dynamical mass; over the range of heavy-quark masses used $\bar{m}_{Q1} \sim \bar{m}_{Q2}$. The intercept lies more than 2σ below the origin. However, since there are just four data points and a large range of quark mass over which to extrapolate, an increase of only approximately 1σ is needed in the dynamical mass estimates in order to obtain an intercept consistent with the origin. Alternatively, the discrepancy between the behaviour at the different β values may be significant, suggesting either \bar{m}_{Q2} or \bar{m}_{Q3} is sensitive to the lattice spacing.

Using both the dynamical and static quark masses, the discrepancies between the results of the clover action at the two β values, and similarly the Wilson and clover action at $\beta = 6.0$ suggests the discretisation errors in the hyperfine splitting maybe significant. A similar analysis at $\beta = 6.2$ for the Wilson action is needed to check whether the dependence on the lattice spacing is reduced at this value of β .

Substituting the experimental values of the D and B meson masses into equation (4.4), the c and b quark masses are approximately 2.0 and 5.3 GeV respectively. These estimates are rather large compared to the values used in the previous section and the results of the potential model calculations. The correlated fit to the clover data at $\beta = 6.2$, served to provide the functional dependence of the splitting on the heavy-quark mass, but is unsuitable for interpolation or extrapolation to a particular \bar{m}_Q . Instead, $\kappa_Q = 0.129$ is chosen to correspond to the charm quark mass, since $\bar{m}_{Q1} = 1.9$ for this value of the hopping parameter. In order to facilitate a comparison between the clover data at both β values, this value of the heavy-quark mass will also be used for the $\beta = 6.0$ data; $\bar{m}_Q \sim 5.3$ will be used for the bottom quark mass.

	$\beta = 6.0$		$\beta = 6.2$	expt
	\bar{m}_{Q1}	\bar{m}_{Q2}	\bar{m}_{Q1}	
$D^* - D$	76^{+18}_{-14}	78^{+17}_{-17}	91^{+1}_{-1}	140.6^{+1+1}_{-1-1}
$B^* - B$	-	20^{+23}_{-21}	-	45^{+1}_{-1}
$D_s^* - D_s$	73^{+9}_{-10}	77^{+10}_{-11}	85^{+6}_{-5}	142^{+2}_{-2}
$B_s^* - B_s$	-	20^{+12}_{-12}	-	47^{+3}_{-3}

Table 4.5: Predictions for the hyperfine splitting in the D , D_s , B and B_s mesons systems, in MeV, obtained using both the dynamical and static heavy-quark masses with the clover action.

Table 4.5 shows the predicted values of the hyperfine splitting for the D and B mesons, where the scale obtained from m_ρ has been used to convert into physical units; the results for D_s and B_s are also included in the table. The smaller statistical errors in these predictions at $\beta = 6.0$ reflects the 20% reduction in the errors in the data if the light quark mass is increased from the chiral limit to the strange quark mass.

There is a large shortfall between experiment and the lattice predictions. Furthermore, there is a large dependence on the lattice spacing for the static quark mass predictions of the splitting. Considering $\bar{m}_{Q1} \sim \bar{m}_{Q2}$ around the charm quark mass at $\beta = 6.2$, the predictions derived using the dynamical quark mass indicate there is a similar sensitivity to the value of a using this quark mass. However, the systematic errors are due to the uncertainty in m_Q are large; if the splittings are recalculated using the quark masses obtained from quarkonia, the central values in the splittings for the D and B mesons increase by approximately 20% and 10% respectively at $\beta = 6.0$. Combining this uncertainty with the statistical errors, the $D^* - D$ splitting obtained at $\beta = 6.2$ is still significantly below experiment.

Part of the discrepancy between prediction and experiment may be due to the use of the quenched approximation. The fact that the fits to the $\beta = 6.0$ data produce intercepts which are consistent with the origin suggests any effects arising from the absence of sea quarks appear in the slope of the hyperfine splitting with $1/\bar{m}_Q$. The ratio $D^* - D/B^* - B \sim 3$ is consistent with $m_b/m_c = 5.3/1.9 \sim 3$, but the statistical and systematic errors are too large for this to be significant.

4.4.2 The s-d Splittings

Figure 4.6 shows the $s - d$ spin-averaged and pseudoscalar mass splittings plotted against $1/\bar{m}_{Q_1}$ for the clover action at $\beta = 6.0$ and 6.2. Linear, correlated fits were performed on each data set and the fit parameters obtained are detailed in table 4.6. The correlated fit to the clover data at $\beta = 6.0$ illustrates further the problem of large correlations existing between data points. The pseudoscalar and vector masses used to calculate the splittings were all obtained using the same fitting range at $\beta = 6.0$ but not at $\beta = 6.2$ (see §(3.3)).

A striking feature of the figure is the the removal of the dependence on the heavy-quark mass using the spin-average of meson masses in the $\beta = 6.0$ data, in agreement with the predictions of chiral-HQET (equation (4.14)). There is a remaining dependence on $1/\bar{m}_{Q_1}$ at $\beta = 6.2$, however table 4.6 shows this is significantly reduced compared to the naïve $s - d$ splitting. Thus, this is a quantity which is less dependent on uncertainties in the mass scale; although as mentioned in §(4.1.1) the naïve and spin-averaged $s - d$ splittings are not expected to depend on the dynamical mass. Furthermore, the results for the naïve splitting are in rough agreement with the experimental value of 100 MeV at the charm quark mass; the splitting decreases with increasing quark mass, consistent with the lower experimental measurements of the splitting in the B meson.

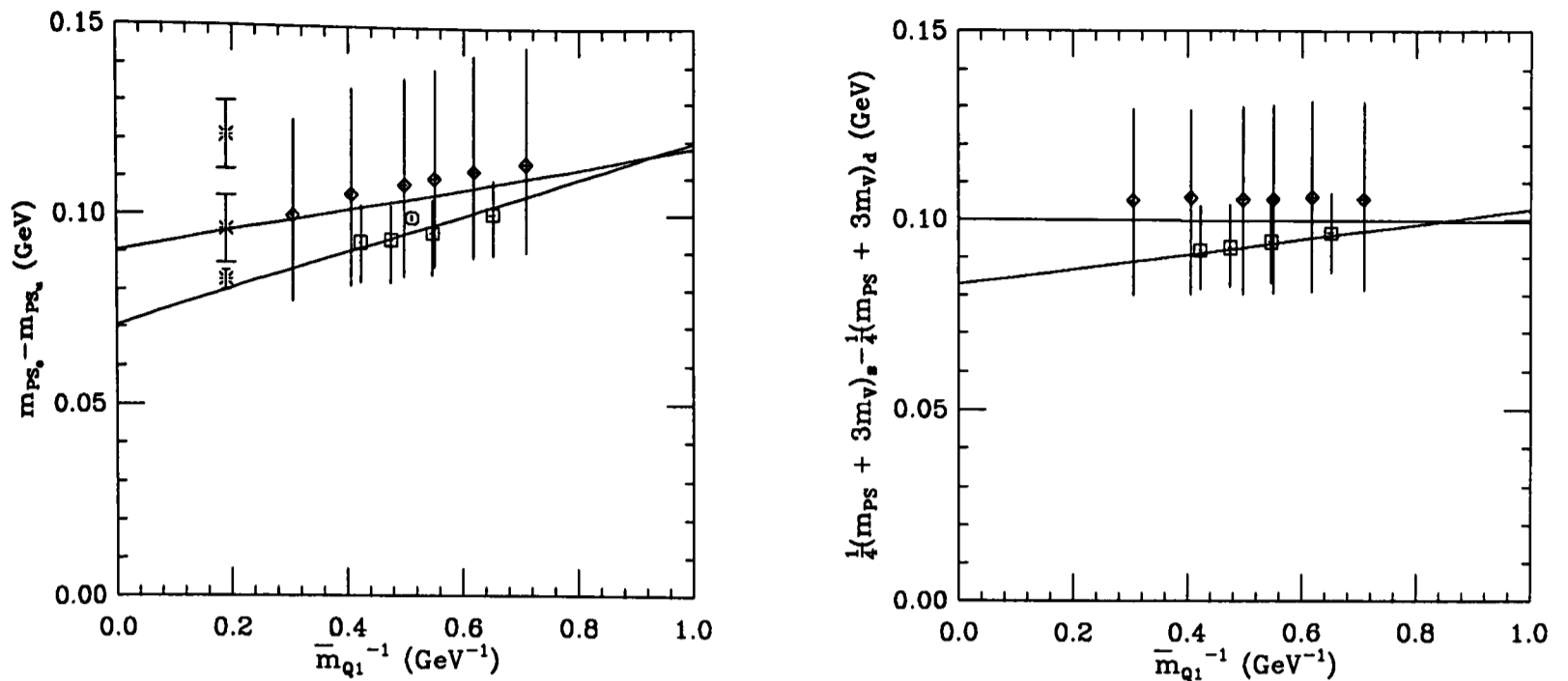


Figure 4.6: The naive and spin-averaged $s - d$ splittings versus $1/\bar{m}_{Q_1}$, for the clover action at $\beta = 6.0$ (diamonds) and $\beta = 6.2$ (squares). The experimental values for the $s - d$ naive splitting in the D meson (circle) and the B meson (bursts) are also shown.

Clover, $\beta = 6.0$, $\kappa_s = 0.1437$, $\kappa_d = 0.14553$			
\vec{a}	$\Delta_{s-d}(m_{PS})$	$\Delta_{s-d}[\frac{1}{4}(m_{PS} + 3m_V)]$	$\Delta_{s-d}(m_V - m_{PS})$
a_1	0.090^{+27}_{-28}	0.10^{+3}_{-3}	-
a_2	0.029^{+38}_{-19}	0.00^{+3}_{-3}	-
χ^2/dof	0.3/4	0.7/4	-
Clover, $\beta = 6.2$, $\kappa_s = 0.1416$, $\kappa_d = 0.14313$			
a_1	0.071^{+14}_{-15}	0.083^{+17}_{-13}	0.011^{+4}_{-3}
a_2	0.049^{+17}_{-16}	0.020^{+14}_{-16}	-0.036^{+7}_{-9}
χ^2/dof	2.3/2	0.2/2	1.7/2

Table 4.6: Linear fit parameters for $s - d$ mass splittings, in GeV, obtained using the static quark mass.

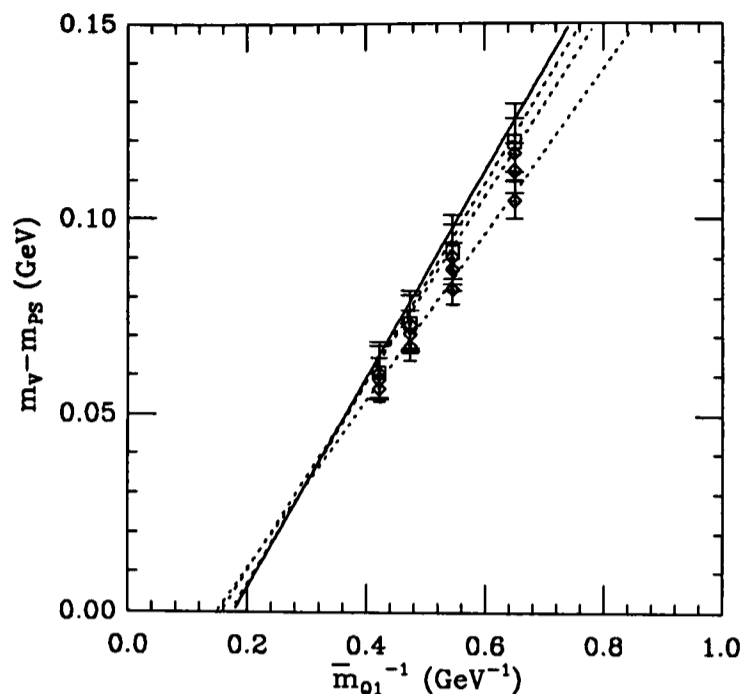


Figure 4.7: $m_V - m_{PS}$ versus $1/\bar{m}_{Q1}$, in physical units, for three values of the light quark mass (diamonds) and the chiral extrapolation (squares) using the clover action at $\beta = 6.2$. The solid lines show a linear fit to the data.

4.4.3 The $s - d$ Hyperfine Splitting

For a study of the effect of finite light quark mass on the hyperfine splitting, only the clover data at $\beta = 6.2$, using \bar{m}_{Q1} , is suitable; the statistical errors are small enough for differences of > 10 MeV to be significant. The meson masses available are below a^{-1} . In this region $\bar{m}_{Q1} \sim \bar{m}_{Q2} \sim \bar{m}_{Q3}$ and the light and heavy-quark mass dependence of the hyperfine splitting should be reproduced fairly reliably using \bar{m}_{Q1} for the heavy-quark mass. However the extrapolation of the data with $m_q = 0$ to infinite quark mass does not agree with the theoretical prediction, nor intuitive expectation, and the slope of the $m_V - m_{PS}$ versus $1/\bar{m}_{Q1}$ is not likely to be correct. Hence the value of Δ_0 , the constant term in the expansion of $\Delta(Ql)$ in m_q and $1/\bar{m}_Q$ (equation (4.5)), and the value of $\Delta(Ql)$ in the chiral limit, cannot be determined.

Figure 4.7 shows the dependence of the hyperfine splitting on \bar{m}_{Q1} for three light quark masses and the chiral extrapolation, for the clover action at $\beta = 6.2$. The

hyperfine splitting decreases with increasing light quark mass. Linear, correlated fits were performed for each value of the light quark mass; the fit parameters obtained are given in table 4.7. The correlated fits lie above the data points for each data set, however, as for the chirally extrapolated data, the χ^2 indicates this effect is not statistically significant.

κ_l	a_1	a_2	χ^2
0.14144	-0.031^{+3}_{-4}	0.21^{+1}_{-1}	2.4/2
0.14226	-0.037^{+3}_{-6}	0.24^{+2}_{-1}	2.7/2
0.14262	-0.043^{+5}_{-7}	0.25^{+2}_{-1}	2./2
κ_d	-0.047^{+7}_{-8}	0.26^{+2}_{-2}	3./2

Table 4.7: The parameters obtained from fitting to the hyperfine splitting for each value of the light quark mass and the chiral extrapolation, at $\beta = 6.2$ using the clover action and the static quark mass.

As the heavy-quark mass increases, figure 4.7 shows the splitting becomes independent of the light degree of freedom and consistent with value in the chiral limit. Any deviation from this behaviour at smaller values of \bar{m}_{Q1} and finite m_l necessitates the inclusion of higher order terms in $1/\bar{m}_{Q1}$. However smaller values of the heavy-quark mass or larger values of m_q are needed to see this in the data.

The light quark mass dependence can be explored further by considering the $s - d$ splitting, shown in figure 4.8. The parameters of a linear correlated fit to the data are included in table 4.6. The linear dependence on $1/\bar{m}_{Q1}$ is in agreement with the behaviour predicted in equation (4.7). Around the charm quark mass this splitting is approximately -5 MeV. The experimental results, (4.9), show the $s - d$ splitting is of this order of magnitude, but are not accurate enough

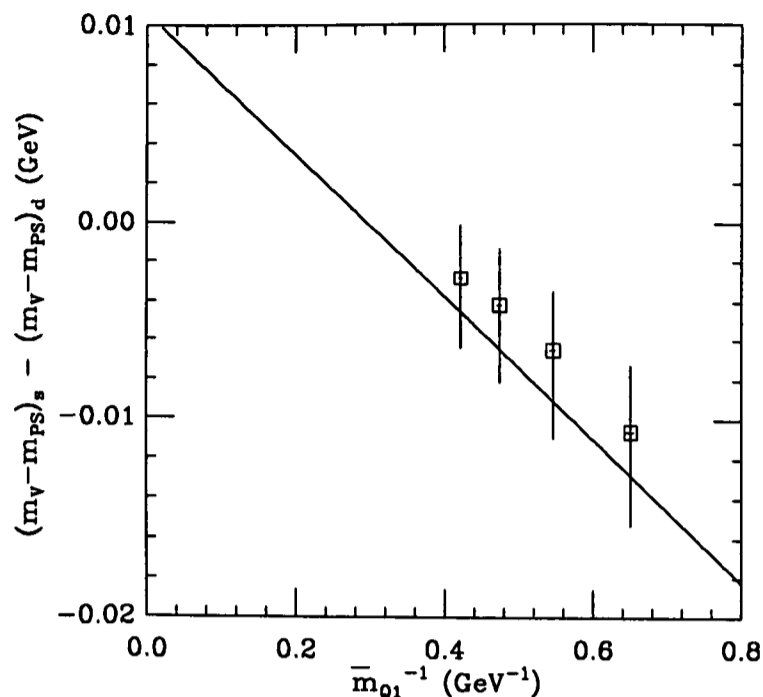


Figure 4.8: The $s - d$ hyperfine splitting for the clover action at $\beta = 6.2$ (squares).

to determine the sign of the splitting. A discrepancy between experiment and prediction is likely in a splitting of this size, since at this level the omission of electromagnetic effects in the lattice calculation will introduce a significant error.

4.5 Conclusions

The results presented in this chapter for the mass splittings in the $\bar{q}Q$ mesons are encouraging. For both the Wilson and clover data at $\beta = 6.0$ and 6.2 , the hyperfine splitting was found to be linearly dependent on $1/\bar{m}_{Q_1}$, in agreement with the expectations of chiral HQET. However, the hyperfine splittings were found to vanish at a finite value of the static quark mass, instead of the predicted value of $\bar{m}_Q = \infty$, suggesting that the splitting is determined by a different mass scale. In contrast, if the dynamical quark mass is used, at $\beta = 6.0$, the splittings are consistent with prediction. This is the first hint of \bar{m}_{Q_2} being a good approximation of the hyperfine quark mass. However, at $\beta = 6.2$, no improvement

was found in the behaviour of the splitting for large values of the quark mass using the dynamical quark mass, and it is possible there is a significant discretisation error in this or the hyperfine mass parameter. A comparison of the results from the Wilson and clover action at $\beta = 6.0$, showed the hyperfine splitting to be sensitive to the value of the clover coefficient, and hence to the value of a .

Since $\bar{m}_{Q_2} \sim \bar{m}_{Q_1}$ around the charm quark mass, the value for $D^* - D$ obtained using the dynamical quark mass to fix m_c , was found to be consistent with that obtained using the static quark mass, and $\sim 1\sigma$ below the result at $\beta = 6.2$. However, the dependence on the lattice spacing, combined with the statistical errors and the uncertainty in the physical quark mass, is not sufficient to account for the discrepancy found with experiment.

The behaviour of the $s - d$ spin splittings with the heavy quark mass is also in agreement with predictions of chiral HQET. A significant reduction in the dependence on \bar{m}_{Q_1} was found in the spin-averaged $s - d$ splitting compared to the naïve $s - d$ splitting. The value of the naïve $s - d$ splitting obtained at a quark mass corresponding to charm is roughly consistent with the experimental result, while at the bottom quark mass this splitting is consistent with the lower experimental measurements.

For the hyperfine splitting in quarkonia, the results are less clear cut. Assuming that the leptonic width is also determined by m_{Q_3} , the results of §(3.10.4) suggest the dynamical mass is a fair approximation of the hyperfine mass at $\beta = 6.0$, but it is unclear whether this is also true for $\beta = 6.2$. The lack of a firm theoretical prediction for the behaviour of the hyperfine splitting with the heavy quark mass prevents any test of this through the functional dependence of the splitting on \bar{m}_{Q_1} and \bar{m}_{Q_2} . In addition, the results of §(3.5.2)) show the dynamical meson mass is not determined by the quark mass; hence, if $\bar{m}_{Q_2} \sim \bar{m}_{Q_3}$ for $\bar{q}Q$ mesons, this is not necessarily true for $\bar{Q}Q$ mesons. The magnitude of lattice spacing dependence

differed between the quark mass parameters used, and this showed it is possible to over or under estimate the size of the discretisation errors if the wrong quark mass scale is used.

The predictions obtained for the hyperfine splitting in charmonium lie significantly below experiment, although those extracted using the dynamical quark mass are significantly larger than the corresponding values from the static quark mass. Considering the uncertainty in the value of the charm quark mass the results are consistent with the estimated $\sim 40\%$ reduction in the $J/\psi - \eta_c$ splitting due to quenching. However, a comparison of the results using the tree level value of the clover coefficient, with those from using a mean-field value, showed the hyperfine splitting to be very sensitive to the value of c . The splitting obtained using the latter value of c with the dynamical quark mass, was found to be slightly higher, though consistent with, the quenched corrected value, and also consistent with the results from the Fermilab group. A study is needed of the hyperfine splitting calculated using the tree level and mean-field value of c at a variety of β values, to test for a reduction in the dependence on the lattice spacing using the latter value of the clover coefficient and the dynamical mass; with greater confidence in the magnitude of this uncertainty, a clearer understanding of the effects of quenching can be obtained.

Chapter 5

Summary, Conclusions and Future Prospects

The main aim of this study of $\bar{Q}Q$ and $\bar{q}Q$ mesons has been to test the claim that the general Wilson action is valid for lattice masses at which the discretisation errors are conventionally expected to diverge, i.e. $M \gg 1$, providing it is reinterpreted as a nonrelativistic effective theory. The firmest evidence of this was found in the excellent agreement of the dispersion behaviour of the pseudoscalar mesons with a continuum nonrelativistic dispersion relation containing two mass parameters.

However, in taking the next vital step and identifying the dynamical mass rather than the static mass as the physical mass, the results are encouraging, but as yet not convincing. A particular difficulty lay in the quantities studied, which, apart from the pseudoscalar decay constant, were identified as being determined by the hyperfine mass rather than the dynamical mass. A test of whether the hyperfine mass leads to accurate predictions for the mass splittings, through the approximation that $M_{Q3} \sim M_{Q2}$, is not ideal. Furthermore, the terms dependent on M_{Q3} are sensitive to short distance effects and possibly involve a significant uncertainty due to quenching in addition to discretisation errors, and comparison with experiment is muddled. Despite this, notable successes were found using the

dynamical mass in preference to the static mass; in particular, the improvement in the predictions for the $J/\psi - \eta_c$ splitting and the $\bar{q}Q$ splitting in the infinite quark limit. Similar calculations for the $\bar{Q}Q$ mesons involving the dynamical mass are being performed by the Fermilab group [68] and will provide an important check of these results.

In general, for the $\bar{q}Q$ mesons, testing for the correct mass parameter and whether the general Wilson action is valid for $M \gg 1$ is difficult, since for the β values used here (currently fairly popular choices) the dynamical mass is approximately equal to the static mass around the region of the charm quark mass, where most experimental data exists. However, it is clear that using the dynamical mass has a significant effect on predictions extrapolated to the region of the bottom quark mass, and more significantly, in the case of the pseudoscalar decay constant, the functional dependence on the mass parameter. A comparison of f_{PS} obtained from NRQCD around the bottom quark region [69] may prove decisive in determining whether or not the dynamical mass is the mass parameter corresponding to the physical mass. In addition, a measurement of the dispersion behaviour from, for example, $f_{PS}E^{phys}(\vec{p})$, provides a further test for the correct mass parameter which avoids the difficulties involved in comparison with experiment.

For the $\bar{Q}Q$ mesons, the dynamical mass does have a significant effect on the predictions for charmonium, and a comparison of the results for the leptonic decay amplitude with experimental showed a feature general to all quantities considered here; the improvement found using the dynamical mass, which in this case provided consistency with experiment, was more clearly seen in the results at $\beta = 6.0$ than at $\beta = 6.2$. This suggests there are possibly significant discretisation errors in the dynamical mass; however, in order to judge the significance of this a range of quark masses comparable to those available at $\beta = 6.0$ is needed, particularly in the case of the $\bar{q}Q$ mesons.

There are many questions left unanswered, but this is a characteristic of an exploratory study. The significant differences in the results found between fixing the physical mass using the static mass and the dynamical mass (and the general improvement found using the latter) in the region of the bottom quark for both the $\bar{Q}Q$ and $\bar{q}Q$ mesons, and the charm quark region for $\bar{Q}Q$, provides motivation for further research if the general Wilson action is to be continued to used for $M > 1$. Not least, a study must be made of whether the theory is spoilt by renormalisation.

Bibliography

- [1] A. S. Kronfeld, lectures presented at the TASI summer school, *Perspectives in the Standard Model*, Boulder, Colorado, USA, (1991)
- [2] R. D. Kenway, *Rep. Prog. Phys.* **52** (1989) 1475
- [3] H. J. Rothe, *Lattice Gauge Theories: An Introduction*, World Scientific, (1992)
- [4] K. G. Wilson, *Phys. Rev.* **D10** (1974) 2445
- [5] K. G. Wilson, *Adv. Math.* **16** (1975) 176
- [6] G. Heatlie et al., *Nucl. Phys.* **B352** (1991) 266
- [7] B. Sheikholeslami et al., *Nucl. Phys.* **B259** (1985) 572
- [8] G. P. Lepage et al., *On the Viability of Lattice Perturbation Theory*, Fermilab preprint:91-355-T-Rev
- [9] P. M. Mackenzie, *Nuc. Phys. B (Proc. Suppl.)* **30** (1993) 36
- [10] P. Lepage, *Nuc. Phys. B (Proc. Suppl.)* **26** (1993) 45
- [11] J. N. Simone, *Nucl. Phys. B(Proc. Suppl.)* **30** (1993) 461
- [12] C. Bernard et al., *A lattice computation of the decay constants of the B and D mesons*, UW/PT-93-06 (1993)

- [13] UKQCD Collaboration C. Allton et al., *Phys. Lett.* **B284** (1992) 377
- [14] A. D. Simpson, *Algorithms for Lattice QCD*, Ph. D Thesis (1991)
- [15] K. C. Bowler et al., *Nuc. Phys.* **B220** (1983) 137
- [16] W. H. Press et al., *Numerical Recipes in C* Cambridge (1988)
- [17] R. M. Baxter, *Private communication*
- [18] B. Efron, *S. I. A. M. Review* **21** (1979) 460
- [19] M. Fukugita et al., *Phys. Rev. Lett.* **57** (1986) 953
- [20] D. Weingarten, *Nucl. Phys.* **B215** (1983) 1
- [21] G. Martinelli, *European Sympos.* (1982) 284
- [22] G. Rajan, *Nucl. Phys.* **B226** (1983) 152
- [23] A. Ukawa, Plenary talk *Nuc. Phys. B (Proc. Suppl.)* **30** (1993) 3
- [24] M. Guagnelli et al., *Nuc. Phys. B* **378** (1992) 616
- [25] Y. Iwasaki et al., *Nucl. Phys. B(Proc. Suppl.)* **30** (1993) 397
- [26] M. Lüscher and U. Wolff, *Nuc. Phys. B* **339** (1990) 222
- [27] S. Güsken, *Nuc. Phys. B (Proc. Suppl.)* **17** (1990) 361
- [28] UKQCD Collaboration C. Allton et al., *Phys. Rev. D* **47** (1993) 5128
- [29] D. Daniel et al., *Phys. Rev. D* **46** (1992) 3130
- [30] K. C. Bowler, *Private communication*
- [31] UKQCD Collaboration, *The Light Hadron Spectrum and Decay Constants with Non-degenerate Quarks in Quenched Lattice QCD*, Southampton preprint:SHEP 91/92-15 (1992)

- [32] Particle Data Group, *Phys. Rev. D* **45** (1992) 11
- [33] A. S. Kronfeld, *Nuc. Phys. B (Proc. Suppl.)* **30** (1993) 445
- [34] M. B. Wise, Lectures presented at the Lake Louise Winter Institute, *New Symmetries of the strong interaction*
- [35] C. Bernard et al., *Nuc. Phys. B (Proc. Suppl.)* **30** (1993) 465
- [36] A. Abada et al., *Nucl. Phys. B* **376** (1992) 172
- [37] E. Eichten, *Nucl. Phys. B (Proc. Suppl.)* **accirac 4** (1988) 170
- [38] E. Eichten et al., *Phys. Rev. Lett.* **43** (1979) 1205
- [39] J. D. Bjorken and S. D. Drell, *Relativistic Quantum fields* Mc Graw-Hill Vol. 1 (1965)
- [40] C. T. H. Davies et al., *Phys. Rev D* **45** (1992) 915
- [41] G. P. Lepage et al., *Seillac Sympos.* (1987) 199
- [42] B. A. Thacker et al., *Phys. Rev. D* **43** (1991) 196
- [43] C. Bernard et al., *Phys. Rev. D* **38** (1988) 3540
- [44] D. S. Henty et al., *Phys. Lett. B* **289** (1992) 109
- [45] R. M. Baxter, *New Approaches to Particle Spectra in Lattice QCD*, Ph. D Thesis (1993)
- [46] G. Martinelli et al., *Phys. Lett. B* **311** (1993) 241
- [47] UKQCD Collaboration C. Allton et al., *Quenched Light Hadron Mass Spectrum and Decay Constants: the effects of $O(a)$ -Improvement at $\beta = 6.2$* , Edinburgh preprint 92/507, (1993).
- [48] J. N. Simone, *Private communication.*

- [49] WA75 Collaboration, S Aoki et al., CERN preprint:PPE/92-157 (1992)
- [50] R. M. Baxter et al., *Quenched Heavy-Light Decay Constants*, Edinburgh preprint:93/526
- [51] R. van Royen et al., *Nuovo Cim.* **50** (1967) 617
- [52] A. X. El-Khadra, *Nuc. Phys. B (Proc. Suppl.)* **30** (1992) 449
- [53] J. L. Richardson, *Phys. Lett.* **B82** (1979) 272
- [54] M. B. Wise, *Phys. Rev* **D45** (1992) 2188
- [55] G. Burdman et al., *Phys. Lett.* **B280** (1992) 558
- [56] T. M. Yan et al., *Phys. Rev* **D46** (1992) 1148
- [57] U. Aglietti, *Phys. Lett.* **B281** (1992) 341
- [58] E. Jenkins, *Heavy Meson Masses in Chiral Perturbation Theory with Heavy Quark Symmetry*, CERN preprint:CERN-TH.6765/92, (1992)
- [59] H. Georgi, *Weak Interactions and Modern Particle Theory*, (Benjamin-Cummings) (1984) 80
- [60] Cleo Collaboration D. Bortoletto et al., *Phys. Rev. Lett.* **69** (1992) 2046
- [61] CUSB-II Collaboration J. Lee-Franzini et al., *Phys. Rev. Lett.* **65** (1990) 2947
- [62] Cleo II Collaboration D.S. Akerib et al., *Phys. Rev. Lett.* **67** (1991) 1692
- [63] ALEPH Collaboration V. Sharma et al., talk presented at 28th Recontres de Moriond, March 1993
- [64] W. Lucha et al., *Physics Reports* **200** (1991) 127
- [65] H. Krasemann et al., *Nuc. Phys.* **B154** (1979) 283

- [66] A. X. El-Khadra et al., *Phys. Rev. Lett.* **69** (1992) 729
- [67] D. Seibert, *Undesirable Effects of Covariance Techniques for Error Analysis*, CERN preprint:CERN-TH.6892/93 (1993)
- [68] A. El Khadra, *Private communication*
- [69] C. T. R. Davies, *Work in Progress*